AD-A044 812 ADVISORY GROUP FOR AEROSPACE RESEARCH AND DEVELOPMENT--ETC F/G 1/3
PHYSICAL VULNERABILITY OF AIRCRAFT DUE TO FLUID DYNAMIC EFFECTS--ETC(U)
JUL 77 D B ANKENEY

UNCLASSIFIED AGARD-AR-106 NL

1 OF 1
ADA
044812

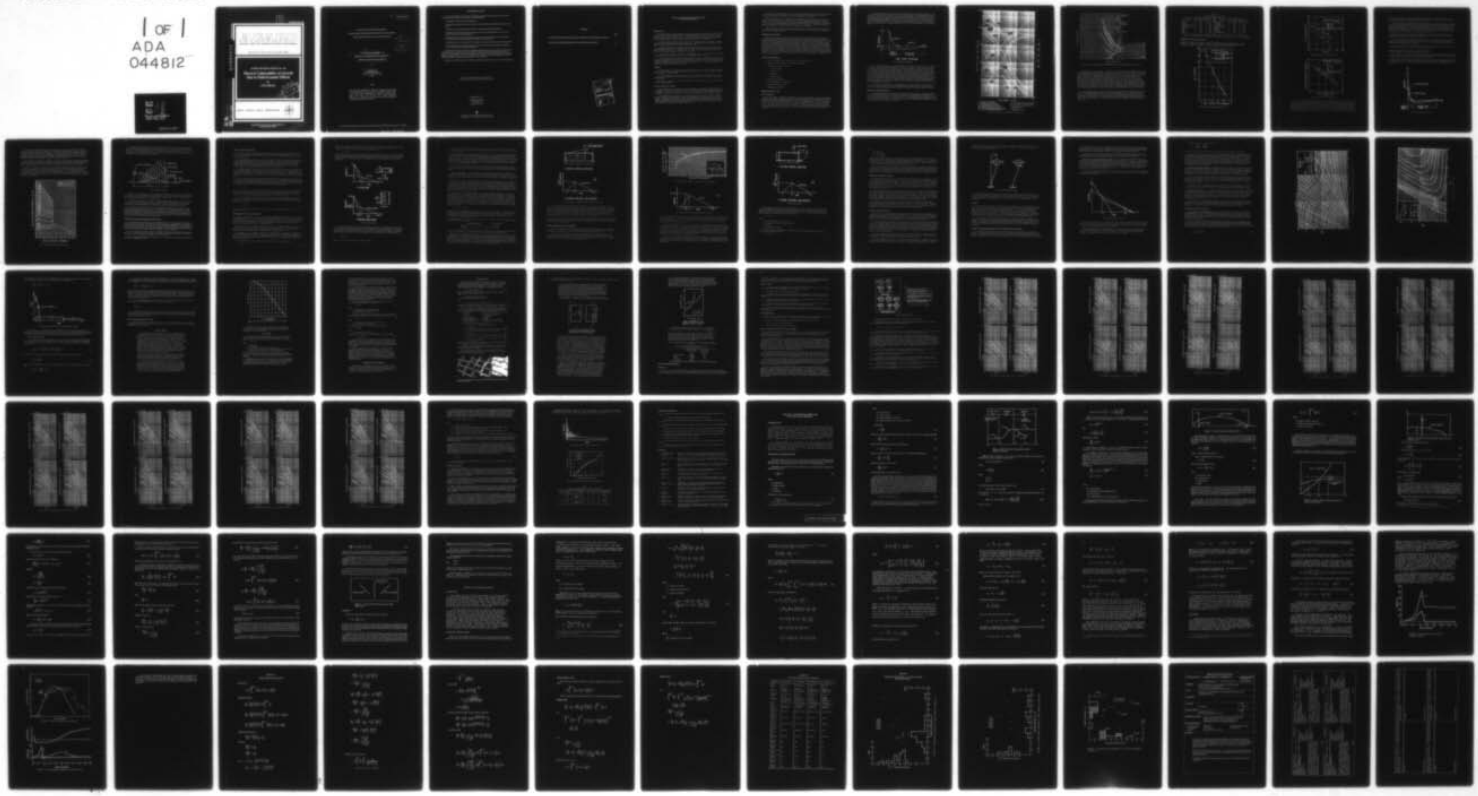

END
DATE FILMED
10-77
DDC

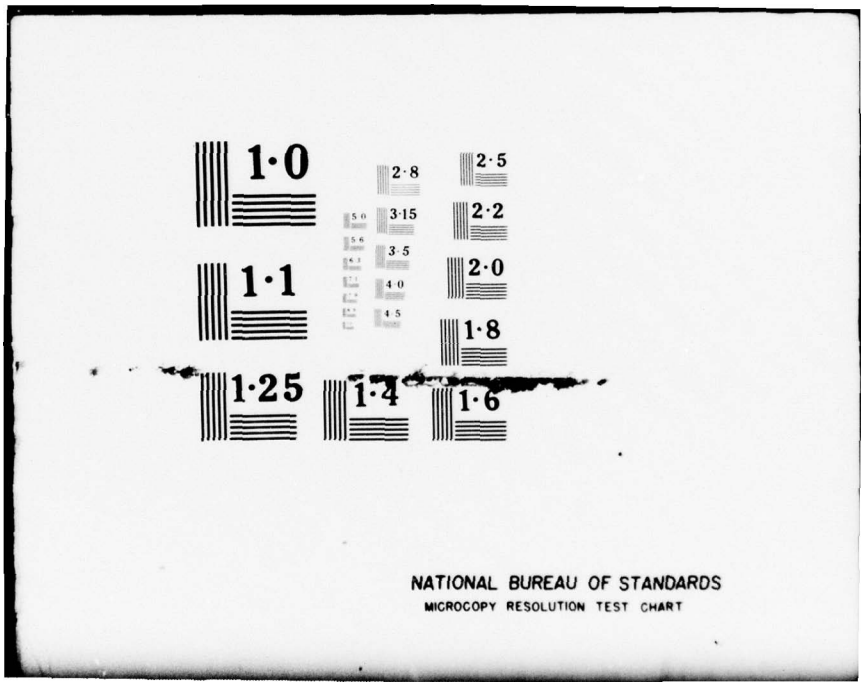
1·0
1·1
1·25
1·4
1·6
1·8
2·0
2·2
2·5
2·8
3·15
3·5
4·0
4·5
5·0
5·6
NATIONAL BUREAU OF STANDARDS
MICROCOPY RESOLUTION TEST CHART

AGARD-AR-106

AGARD-AR-106

AGARD

ADVISORY GROUP FOR AEROSPACE RESEARCH & DEVELOPMENT

7 RUE ANCELLE 92200 NEUILLY SUR SEINE FRANCE

AGARD ADVISORY REPORT No. 106

Physical Vulnerability of Aircraft Due to Fluid Dynamic Effects

by

D.B.Ankeney

NORTH ATLANTIC TREATY ORGANIZATION

DISTRIBUTION AND AVAILABILITY
ON BACK COVER

AGARD-AR-106

NORTH ATLANTIC TREATY ORGANIZATION

ADVISORY GROUP FOR AEROSPACE RESEARCH AND DEVELOPMENT

(ORGANISATION DU TRAITE DE L'ATLANTIQUE NORD)

Jul 77

83 p.

AGARD Advisory Report No. 106

PHYSICAL VULNERABILITY OF AIRCRAFT DUE TO FLUID DYNAMIC EFFECTS

by

D.B. Ankeney
Naval Weapons Center
China Lake, California 93555
USA

NOTE

The material in this Report is intended to supplement and provide a more detailed fluid dynamic input to AGARD Advisory Report No. 47, *The Physical Vulnerability of Aircraft*, (3 volumes, September 1972, May 1973 and May 1973, NATO Classified). Readers with a general interest in the subject of aircraft physical vulnerability are referred to AR-47.

This Advisory Report has been prepared at the request of the Fluid Dynamics Panel of AGARD.

THE MISSION OF AGARD

The mission of AGARD is to bring together the leading personalities of the NATO nations in the fields of science and technology relating to aerospace for the following purposes:

- Exchanging of scientific and technical information;
- Continuously stimulating advances in the aerospace sciences relevant to strengthening the common defence posture;
- Improving the co-operation among member nations in aerospace research and development;
- Providing scientific and technical advice and assistance to the North Atlantic Military Committee in the field of aerospace research and development;
- Rendering scientific and technical assistance, as requested, to other NATO bodies and to member nations in connection with research and development problems in the aerospace field;
- Providing assistance to member nations for the purpose of increasing their scientific and technical potential;
- Recommending effective ways for the member nations to use their research and development capabilities for the common benefit of the NATO community.

The highest authority within AGARD is the National Delegates Board consisting of officially appointed senior representatives from each member nation. The mission of AGARD is carried out through the Panels which are composed of experts appointed by the National Delegates, the Consultant and Exchange Program and the Aerospace Applications Studies Program. The results of AGARD work are reported to the member nations and the NATO Authorities through the AGARD series of publications of which this is one.

Participation in AGARD activities is by invitation only and is normally limited to citizens of the NATO nations.

Published July 1977

ISBN 92-835-1249-9

Printed by Technical Editing and Reproduction Ltd
Harford House, 7–9 Charlotte St, London, W1P 1HD

CONTENTS

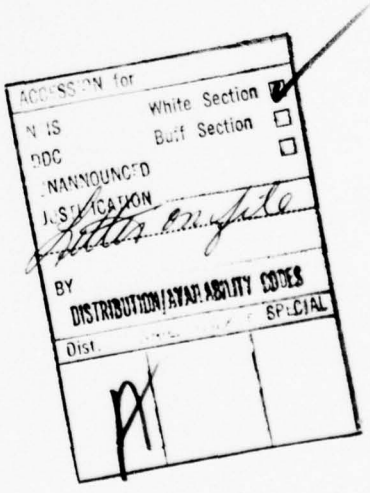

TECHNIQUES FOR PREDICTING STRUCTURAL RESPONSE DUE TO EXPLOSIVE AIR BLAST

INTRODUCTION

The problem of predicting the response of an aircraft structure to external blast is difficult for the simple reason that the aircraft designer has never been required to design aircraft that would survive the blast wave of a warhead. Since the aircraft designer has never been requested to design aircraft that could survive a blast wave, the aircraft stress analyst has never had to develop the tools for predicting the response of aircraft skin and structure to a free air blast.

On the other hand, the vulnerability analyst and the warhead designer are continually consulted about the size of warhead needed to defeat enemy aircraft. They are prevented from taking a rational approach and really settling the problem by at least three factors:

1. Construction details of new enemy aircraft are obviously unavailable to them. Usually, only some photographs of the external configuration are available. Hence, a rational structural response model from first principles (i.e., Newton's laws, etc.) cannot be developed since they do not have access to the necessary details to complete a rational model.

2. The main kill mechanism of warheads is usually fragmentation, with air blast being a secondary kill mechanism. Hence, most work has been done on fragmentation effects modeling.

3. The vulnerability analyst and the warhead designer are usually quite unfamiliar with the basic "nuts and bolts" approach of the aircraft stress analyst and, therefore, they never adopt the form of engineering language that the aircraft designer and stress analyst use. This is also compounded by the fact that the aircraft designer has never had to consider warhead effects and has no familiarity with warheads and structural response to blast loading.

APPROACH

The approach that will be taken to the problem of predicting the structural response to external blast is that of adapting and summarizing the most important details of a spherical charge in free air as it interacts with rigid surfaces.

The use of impulse momentum for calculating structural response and the approximation of a uniformly distributed impulse on the surface in question are approximations that appear to be experimentally justified.

Also listed is a technique by Sewell and Kinney (*Critical Impulse Within a Critical Time*), which has been used by designers.

SAFETY FACTOR AND ACCURACY

Certain simplifications have been made in the development of the design procedures presented in this manual. As a result, an analysis of a structure using these procedures will generally result in a conservative estimate of the structure's capacity and, consequently, structures designed using these procedures will generally be adequate for the blast load exceeding the assumed loading conditions.

Certain unknown factors can result in an over-estimate of the protective structure's capability to resist the effects of an explosion. These factors, reflections of the shock waves, structural response, construction methods, quality of construction materials, workmanship, etc., vary for each design. To compensate for weaknesses resulting from these factors, it is recommended that the "effective charge weight" or the actual charge weight, depending upon the method used to determine the TNT equivalent, be increased by 20% for design purposes.

The effects of the warhead shape (which can increase the impulse and peak pressure) are neglected. The effects created when the warhead is in direct contact with the structure are also neglected (neglected here because at the present time, they are impossible to calculate).

Another directional effect is sometimes found in high-velocity munitions (such as 23-mm high-explosive incendiary (HEI), etc.), particularly in contact or close-in proximity fuzing. Here, the forward velocity of the munitions will be felt in an increased damage capability in the forward direction. Use of impulse momentum structural response technique infers that the momentum of fragment and gas cloud be added to the blast wave impulse. This effect, to the writer's knowledge, has only been observed qualitatively, and has received little quantitative verification.

Another effect which has received little attention is that of warhead-aircraft closing velocity. This has been discussed at length, but no hard and fast rules as to how to include it in warhead air blast effects have been formulated.

COMMENTS ON DATA SOURCE

The data source listed in Reference 1 was selected because the approach taken was a rational one and the theoretical predictions were experimentally verified. Although the results quoted in the reference were obtained with concrete walls, the writer used the same technique on walls built of steel and obtained good agreement between theory and experiment. In terms of pure blast loading of structures, the civil engineering profession has had the most demands for rational and useful design procedures for calculating the effects of air blast loading on structures. The advent of nuclear weapons has forced the civil engineer to deal with the design of a building to resist air blast. The problems of designing explosive storage and loading facilities so that catastrophic incidents would not occur has also forced the civil engineer to be able to rationally design structural walls that can withstand blast loads. The closest approach in the field of damage to aircraft structures has been the "critical impulse in a critical time" technique. Other characterization such as the generic kill damage contours is of little value to the aircraft designer since it does not relate improvements in design in their ability to resist attack.

OUTLINE OF FUNDAMENTALS

1. Spherical charges in air, Hopkinson and Sachs' scaling relations
2. Reflected pressure coefficient versus angle of incidence
3. External blast loads on structures
   a. Reflected pressure
   b. Clearing time
   c. Drag phase
   d. Geometric effects
4. Impulse momentum approach
5. Critical impulse in a critical time
6. Closed compartment estimates
7. Summary and limitations

SPHERICAL CHARGES IN AIR

Blast Wave Phenomena

The violent release of energy from a detonation in a gaseous medium gives rise to a sudden pressure increase in that medium. The pressure disturbance, termed the blast wave, is characterized by an almost instantaneous rise from the ambient pressure to a peak incident pressure P_{so}. This pressure increase or shock front travels radially from the burst point with a diminishing velocity U, which is always in excess of the sonic velocity of the medium. Gas molecules, making up the front, move at lower velocities u. This latter particle velocity is associated with a dynamic pressure or the pressure formed by the winds produced by the shock fronts. As the shock front expands into increasingly larger volumes of the medium, the peak incident pressure at the front decreases and the duration of the pressures increases.

At any point away from the burst, the pressure disturbance has the shape shown in Figure 1. The shock front arrives at time t_A and, after the rise to the peak value, the incident pressure decays to the ambient value in the time t_o which is the positive phase duration. This is followed by a negative phase with a duration t_o^- longer than the positive phase and characterized by a pressure below the pre-shot ambient pressure (maximum value of P_{so}^-) and a reversal of the particle flow. The negative phase is usually less important in a design than is the positive phase. The incident impulse density (hereafter referred to as unit incident impulse) associated with the blast wave is the integrated area under the pressure-time curve and is denoted as i_s for the positive phase and i_s^- for the negative phase.

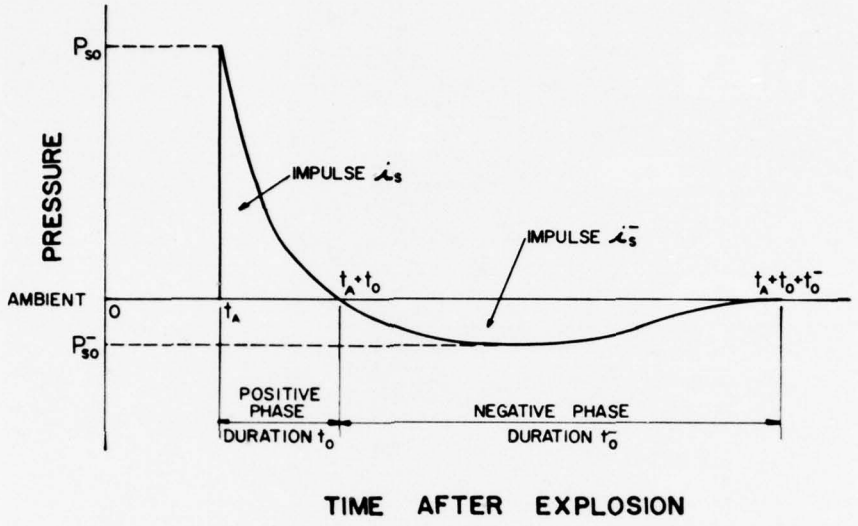

Fig.1 Free field pressure time variation

If the shock wave impinges on a rigid surface oriented at an angle to the direction of propagation of the wave, a reflected pressure is instantly developed on the surface, and the pressure is raised to a value in excess of the incident pressure. The reflected pressure is a function of the pressure in the incident wave and the angle formed between the rigid surface and the plane of the shock front. For a reflector, where flow around an edge or edges occurs, the duration of the reflected pressures is controlled by the size of the reflecting surface. The high reflected pressure seeks relief toward the lower pressure regions, and this tendency is satisfied by the propagation of rarefaction waves from the low- to the high-pressure region. These waves, traveling at the velocity of sound in the reflected pressure region, reduce the reflected pressures to the stagnation pressure which is the value that is in equilibrium with the high-velocity air stream associated with the incident pressure wave. When such a relief is not possible (for example, when an incident wave strikes an infinite surface), the incident pressure at every point in the wave will be reflected, and these reflected pressures will last for the duration of the wave.

The peak positive reflected pressure is designated P_r, the peak negative reflected pressure P_r^-, and the unit impulses associated with a completely reflected incident wave are i_r for the positive phase and i_r^- for the negative phase (Figure 2 lists the behavior of a spherical charge at sea level.)

Departures From Spherical Charge Behavior

For warheads other than spherical shapes, the blast wave produced may not be spherically symmetrical. Figure 3 (from Reference 2) illustrates the variation of the peak pressure (and impulse) of a point-initiated cylindrical charge. The pressure and impulse may be influenced to a much greater extent by the use of multiple detonators, focusing jacket, etc. It is recommended that the designer very carefully inquire as to the extent of the nonspherical behavior of the threat warhead before he attempts a blast-induced structural response calculation.

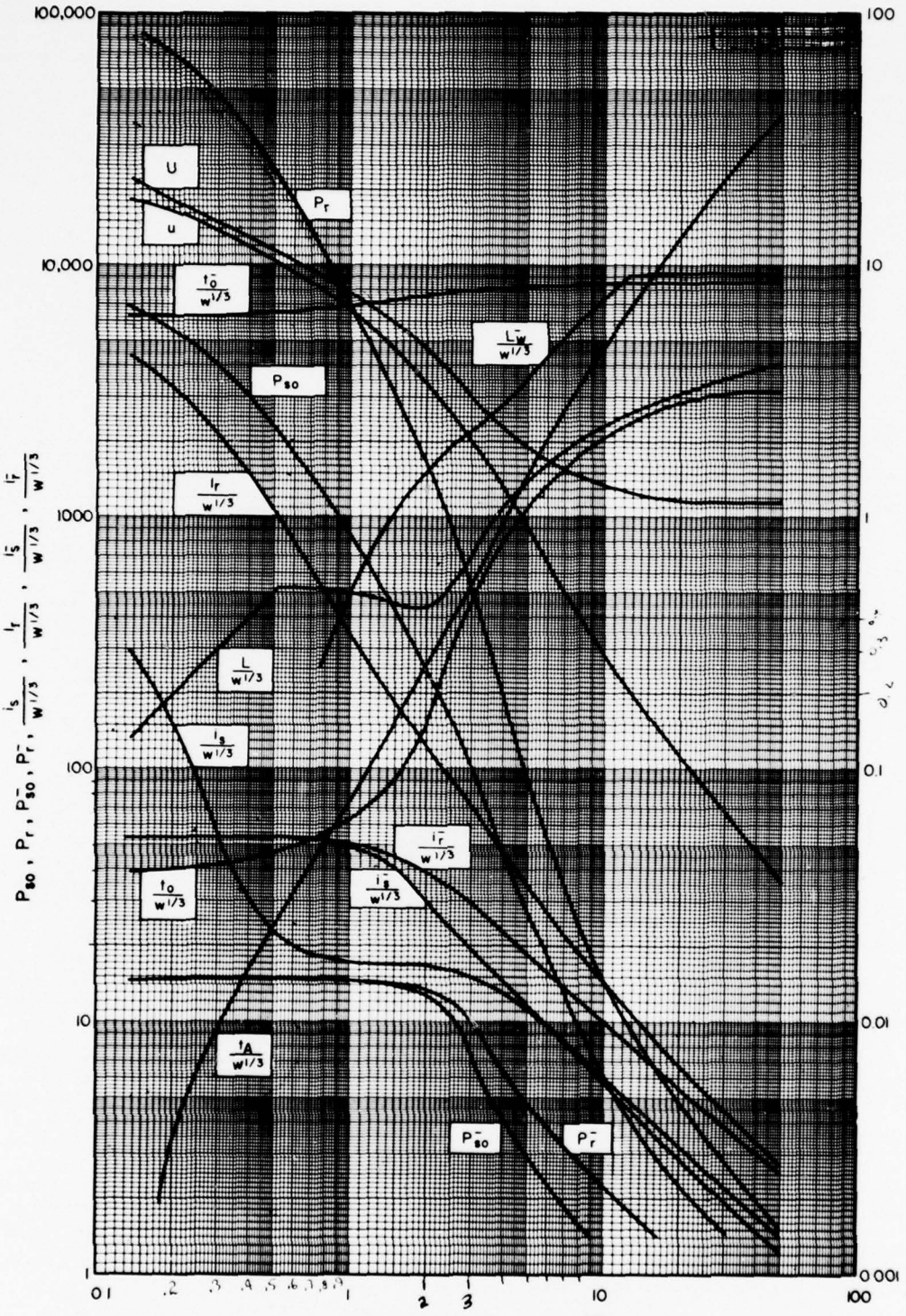

P_{so} = PEAK POSITIVE INCIDENT PRESSURE, PSI
P_{so}^- = PEAK NEGATIVE INCIDENT PRESSURE, PSI
P_r = PEAK POSITIVE NORMAL REFLECTED PRESSURE, PSI
P_r^- = PEAK NEGATIVE NORMAL REFLECTED PRESSURE, PSI
$i_s/W^{1/3}$ = SCALED UNIT POSITIVE INCIDENT IMPULSE, PSI-MS/LB$^{1/3}$
$i_s^-/W^{1/3}$ = SCALED UNIT NEGATIVE INCIDENT IMPULSE, PSI-MS/LB$^{1/3}$
$i_r/W^{1/3}$ = SCALED UNIT POSITIVE NORMAL REFLECTED IMPULSE, PSI-MS/LB$^{1/3}$
$i_r^-/W^{1/3}$ = SCALED UNIT NEGATIVE NORMAL REFLECTED IMPULSE, PSI-MS/LB$^{1/3}$
$t_A/W^{1/3}$ = SCALED TIME OF ARRIVAL OF BLAST WAVE, MS/LB$^{1/3}$
$t_o/W^{1/3}$ = SCALED POSITIVE DURATION OF POSITIVE PHASE, MS/LB$^{1/3}$
$t_o^-/W^{1/3}$ = SCALED NEGATIVE DURATION OF POSITIVE PHASE, MS/LB$^{1/3}$
$L_w/W^{1/3}$ = SCALED WAVE LENGTH OF POSITIVE PHASE, FT/LB$^{1/3}$
$L_w^-/W^{1/3}$ = SCALED WAVE LENGTH OF NEGATIVE PHASE, FT/LB$^{1/3}$
U = SHOCK FRONT VELOCITY, FT/MS
u = PARTICLE VELOCITY, FT/MS
W = CHARGE WEIGHT, LB
R = RADIAL DISTANCE FROM CHARGE, FT
Z = SCALED DISTANCE, FT/LB$^{1/3}$

Fig.2 Shock-wave parameters for spherical TNT explosion in free air at sea level

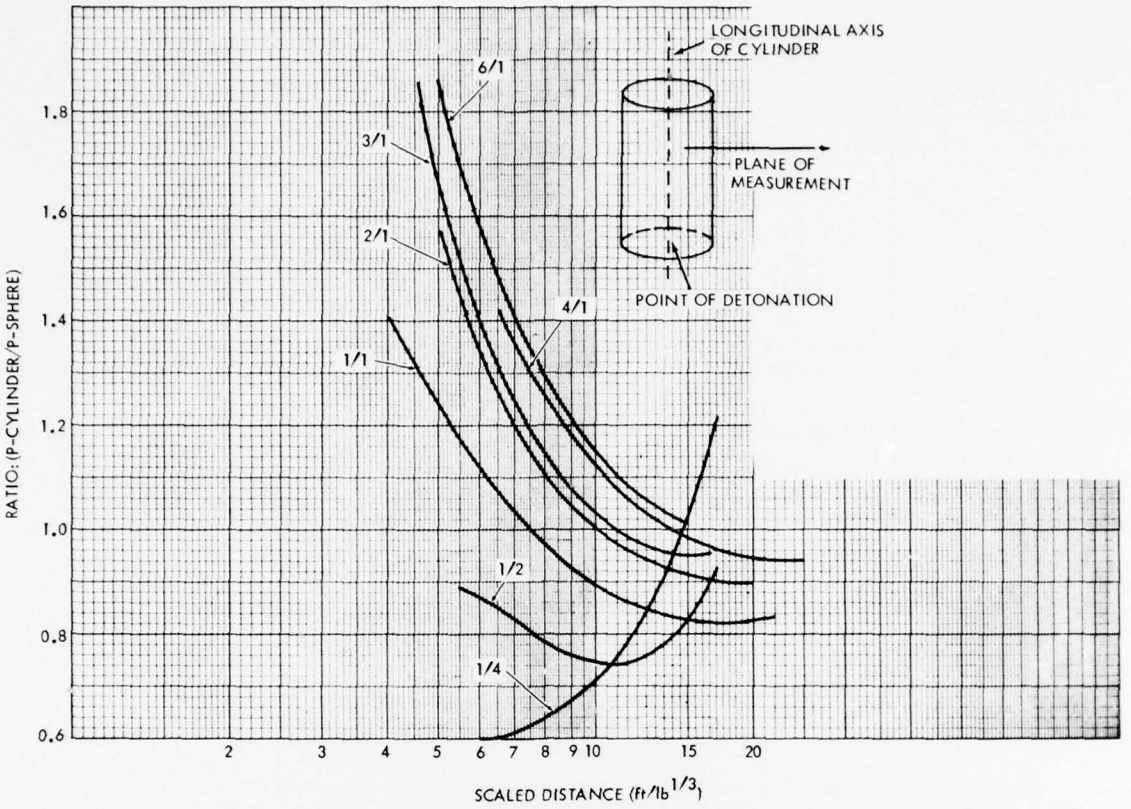

Fig.3 Ratio of free air peak overpressure (P-cylinder/P-sphere) versus distance for cylinders with differing aspect ratios (ℓ/d)

TNT Equivalent. The major quantity of blast effects data presented in this manual pertains to the blast pressure output of TNT explosions. These data can be extended to include other potentially mass-detonating materials and explosives whose shapes differ from those considered by relating the explosive energy of the effective charge weight of these materials to that of an equivalent weight of TNT. The explosive energy of the effective charge weight is also equal to that of the total mass of the material. No clear-cut, high-explosive equivalent may be utilized to define the blast effects of explosive materials other than high explosives themselves. The blast effects of other materials in the anticipated environments must be analyzed and then related to the blast effects produced by the TNT explosion at the range of interest to obtain their equivalencies. To illustrate a typical analysis, explosive tests of certain propellant liquids and hydrocarbon mixtures have indicated that the explosive equivalent of these materials, which relate both the peak blast pressures and impulse, is constant over the entire intermediate- and low-pressure ranges. At higher pressures, the TNT equivalent will vary for each pressure level and will be different than the TNT equivalent which relates the impulse.

For blast-resistant design in general, the TNT equivalent should be based upon a pressure and/or impulse relationship depending upon the anticipated pressure-design range. In addition to being a function of the comparable blast effects themselves, the equivalent will also be dependent upon the anticipated structural response. For the lower pressure ranges where structures respond to either the peak pressure or pressure pulse of the shock wave, the ratio of the weights of given explosives to that of TNT is given in Table 1 for both peak pressure and impulse in pressure levels varying between 2 and 50 psi.

TABLE 1

Equivalent Weight Ratios for Free-Air Effects

Material	Peak pressure, P_{so}	Impulse, i_s	Material	Peak pressure, P_{so}	Impulse, i_s
Comp A-3	1.09	1.07	Pentolite	1.17	1.15
Comp B	1.10	1.06	Picratol	0.90	0.93
Comp B/TiH_2 (70/30)	1.13	1.13	RDX/Wax (98/2)	1.19	1.16
Cyclotol (70/30)	1.14	1.09	RDX/Wax (95/5)	1.19	1.16
Explosive D	0.85	0.81	TNT	1.00	1.00
HBX-1	1.21	1.21	TNETB	1.13	0.96
HBX-3	1.16	1.25	Torpex II	1.24	1.20
H-6	1.27	1.38	Tritonal (80/20)	1/07	1.11
Minol II	1.19	1.17			

NOTE: Data are applicable for pressure levels between 2- and 50-psi range for shock overpressure.

HOPKINSON AND SACHS' SCALING LAWS

The data in Figure 2 are scaled for sea level conditions according to Hopkinson's law. Another scaling law is Sachs' law. Figures 4, 5, and 6 (from Reference 3) show peak pressure and scaled impulse for a range of conditions. Of interest is the size of experimental error.

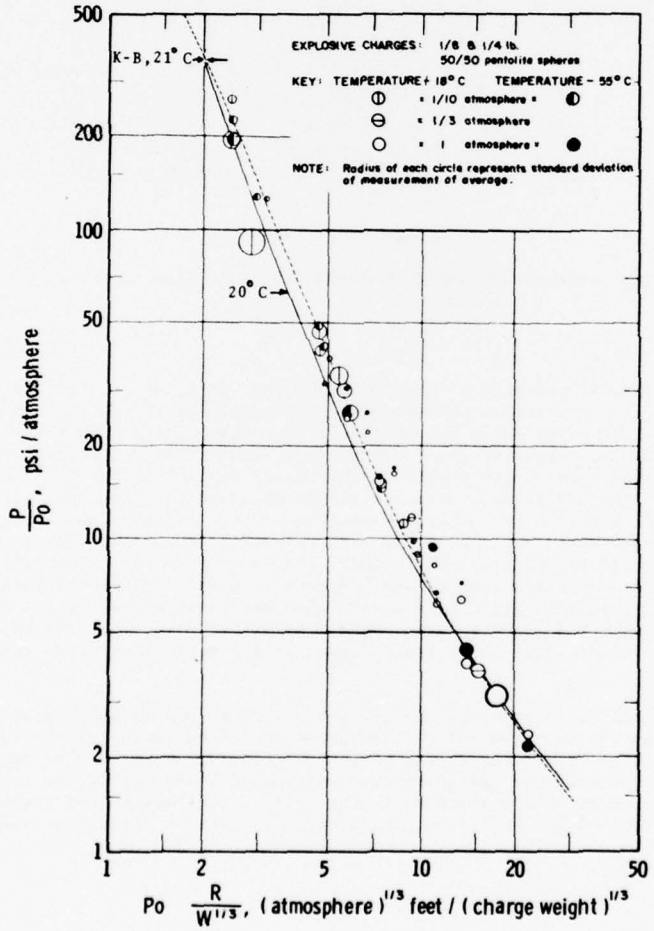

Fig.4 Peak overpressure versus Sachs-scaled distance (Ref. 4)

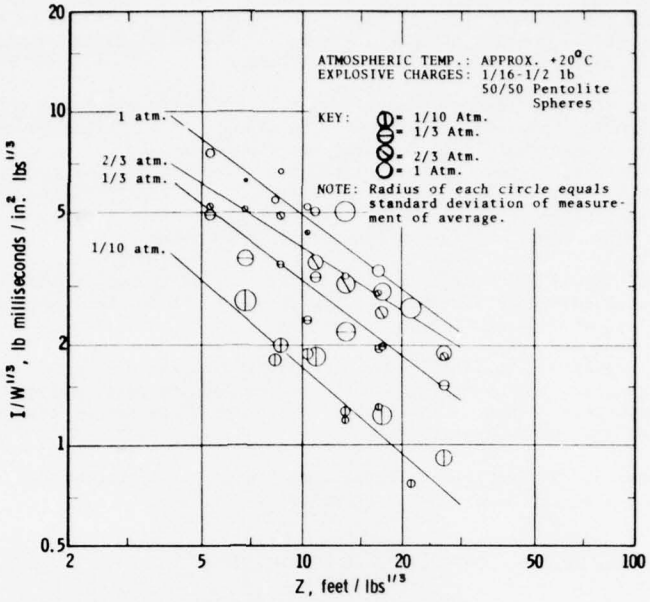

Fig.5 Hopkinson-scaled impulse versus distance (Ref. 4)

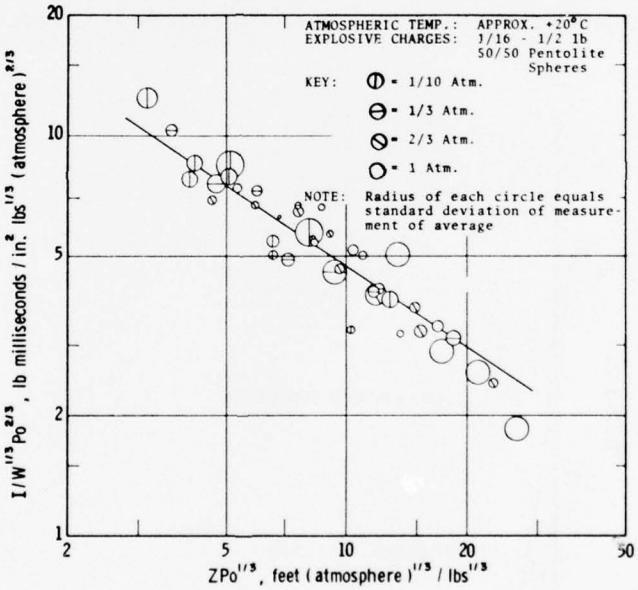

Fig.6 Sachs-scaled impulse versus distance (Ref. 4)

Sachs' law has been confirmed by experiments of Dewey and Sperrazza,[4] Ericsson and Edin,[5] and of Olson, et al.,[6] with by far the most extensive series of model-prototype comparisons being the first. Dewey and Sperrazza[4] conducted their tests with several sizes of bare Pentolite spheres in an altitude-simulating chamber in which both the ambient pressure and temperature could be varied. Arrays of side-on blast pressure transducers were mounted at various distances from the explosive spheres, and time histories of pressure were recorded. The two primary blast parameters reported were peak overpressure P and positive impulse I. A number of repeat tests were conducted for any given condition and distance. Figure 4 shows their data for peak overpressure, scaled according to

Sachs' law. Their data for impulse with Hopkinson scaling applied are shown in Figure 5, and with Sachs' scaling, in Figure 6. One can see that, within the limits of scaled distance covered by Dewey and Sperrazza,[4] Sachs' law is indeed verified by their tests.

In experiments for scaled distances close to explosive sources and under very low ambient pressure conditions, Jack and Armendt[7] showed that the entire character of the blast wave changes at altitude from sea level conditions, and that Sachs' scaling for pressures does not apply--the assumption of air behaving as a perfect gas is, of course, invalidated for these tests close to the blast source. An anomaly observed by both Olson, et al.[6] and Jack and Armendt[7] is that this law apparently *does* apply for the *reflected impulse* parameter, even very close to the explosive source. We note here that this agreement is strictly fortuitous, and an explanation is given later.

Sachs' law is used almost universally to predict effects of change in the condition on blast parameters. Most authors correctly identify the law as due to Sachs, but some, such as Brode[8] and Glasstone,[9] simply use it with no mention of its author.

Inherent in both Hopkinson and Sachs' laws, in addition to the assumption in Sachs' law that air behaves as a perfect gas, are the assumptions that gravity and viscosity effects are negligible. Sachs' law includes Hopkinson scaling as a special case, when there are no changes in ambient conditions between model and prototype experiments.

For worst case design, the sea level relations in Figure 2 are recommended. In particular, the Z values ranging from 0.1 to 1.0 have some experimental verification.

REFLECTED PRESSURE COEFFICIENT VERSUS ANGLE OF INCIDENCE

When a detonation occurs adjacent to and above a protective structure so that no amplification of the initial shock wave occurs between the explosion source and the protective structure, then the blast loadings acting on the structure are free-air-burst blast pressures.

As the incident pressure wave moves radially away from the center of the explosion, it will come in contact with the structure and, upon contact, the initial wave pressures and impulse are reinforced and reflected (Figure 7). The reflected pressure pulse of Figure 7 is typical for infinite plane reflectors.

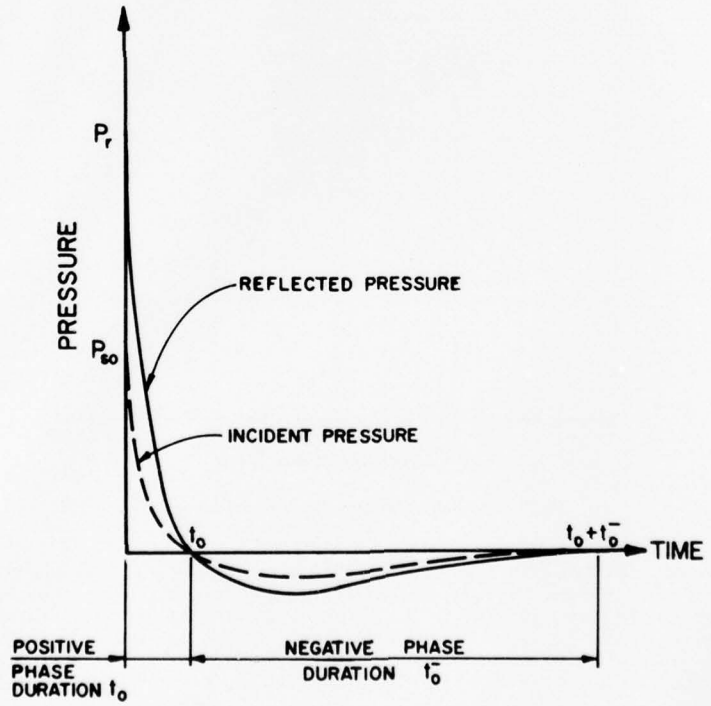

Fig.7 Pressure-time variation for free air burst

When the shock wave impinges on a surface oriented so that a line which describes the path of travel of the wave is normal to the surface, then the point of initial contact is said to sustain the maximum (normal reflected) pressure and impulse. The positive phase pressure and impulse patterns on the structure vary with distance from a maximum at this normal distance R_A to a minimum (incident pressure) where the plane of the structure's surface is perpendicular to the shock front. The peak pressures, impulses, velocities, and other parameters of this shock environment for a spherical TNT explosion versus the scaled distance ($Z = R_A/W^{1/3}$) are given in Figure 2.

The variation of the pressure and impulse patterns on the surface between the maximum and minimum values is a function of the angle of incidence α. This angle is formed by the line which defines the normal distance R_A between the point of detonation, and the structure and the line R which defines the path of shock propagation between the center of the explosion and any other point in question.

The effect of the angle of incidence on the peak reflected pressures is shown in Figure 8, which is a plot of the angle of incidence versus the peak reflected pressure coefficient as a function of the peak incident pressure. The peak reflected pressure $P_{r\alpha}$ is obtained by multiplying the peak reflected pressure coefficient $C_{r\alpha}$ by the peak incident pressure P_{so}. For design purposes, the other blast parameters except the duration of the wave may be taken as those corresponding to the reflected pressure $P_{r\alpha}$ and are obtained from Figure 2. The duration of the blast wave corresponds to the duration of the free air pressures.

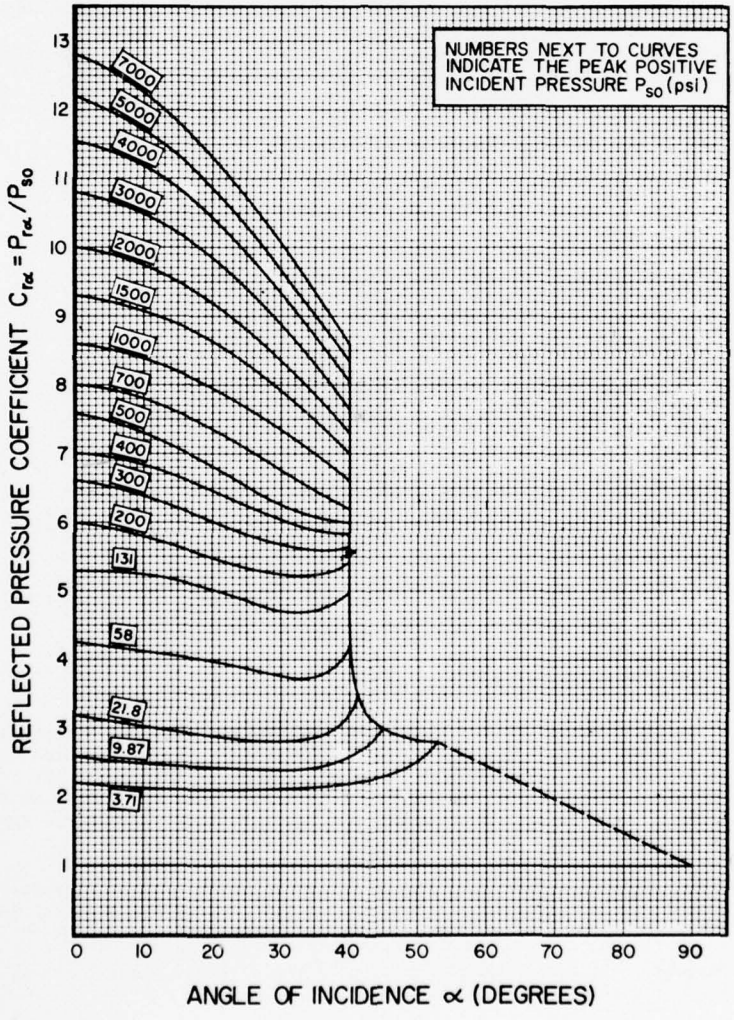

Fig.8 Reflected pressure coefficient versus angle of incidence

The air-burst blast environment is produced by detonations which occur above the ground surface and at some distance away from the protective structure so that the initial shock wave, propagating away from the explosion, impinges on the ground surface prior to arrival at the structure. As the blast wave continues to propagate outward, a front known as the Mach front (Figure 9) is formed by the interaction of the initial wave (incident wave) and the reflected wave, which is the result of the reinforcement of the incident wave by the ground.

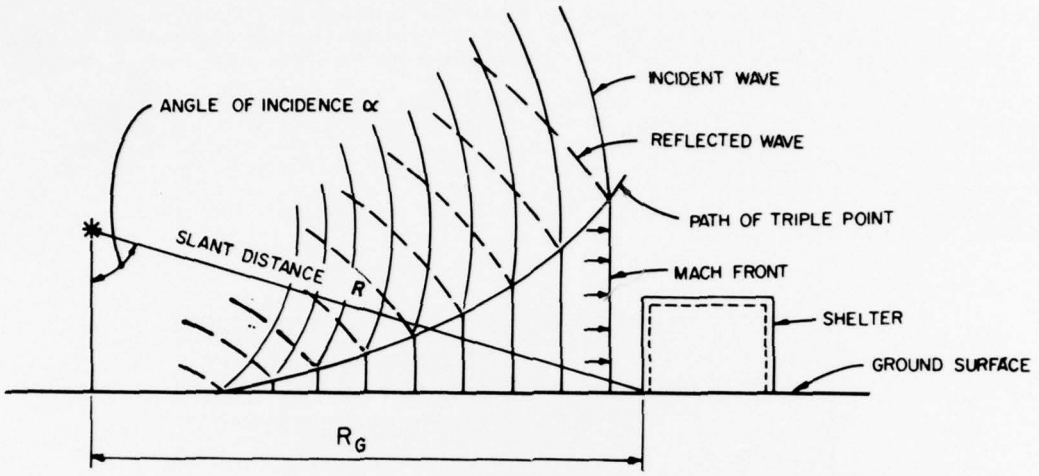

Fig.9 Air burst blast environment

Some variation of the pressures over the height of the Mach front occurs but, for design purposes, this variation can be neglected and the shock considered as a plane wave over the full height of the front. The pressure-time variation of the Mach front is similar to that of the incident wave except that the magnitude of the pressure is somewhat larger.

The height of the Mach front increases as the wave propagates away from the center of the detonation. This increase in height is referred to as the path of the triple point and is formed by the intersection of the initial, reflected, and Mach waves. A structure is subjected to a plane wave (uniform pressure) when the height of the triple point exceeds the height of the structure.

If the height of the triple point does not extend above the height of the structure, then the magnitude of the applied loads will vary with the height of the point considered. Above the triple point, the pressure-time variation consists of an interaction of the incident and reflected incident wave pressures resulting in a pressure-time variation different from that of the Mach incident wave pressures. The magnitude of pressures above the triple point is smaller than that of the Mach front. In most practical design situations, the location of the detonation will be far enough away from the structure so as not to produce this pressure variation.

ESTIMATE OF EXTERNAL BLAST PRESSURES ON STRUCTURES

The techniques that will be described now were developed for the civil or structural engineer. Since the writer has never seen these techniques applied to aircraft, the explanation will be developed around a rectangular structure. The application to aircraft shapes is therefore left to the reader. One advantage of this approach will be that the reader, if he uses these approaches in estimating blast loads on aircraft, will have no false illusions concerning the extent to which these approximate relations have been applied and experimentally verified against aircraft structures.

The blast loading on a structure caused by a high-explosive detonation is dependent upon several factors: (1) the magnitude of the explosion, (2) location of the detonation relative to the structure in question, and (3) the geometrical configuration of the structure.

The procedures presented here for the determination of the external blast loads on structures are restricted to rectangular structures.

FORCES ACTING ON STRUCTURES

The forces acting on a structure associated with a plane shock wave are dependent upon both the peak values and the pressure-time variation of the incident and dynamic pressures acting in the free field. The peak values of the free-field incident pressures for the several blast-loading categories were treated previously.

For each pressure range, there is a particle or wind velocity associated with the blast wave that causes a dynamic pressure on objects in the path of the wave. In the free field, these dynamic pressures are essentially functions of the air density and particle velocity. For typical conditions, standard relationships have been established between the peak incident pressure P_{SO} and the peak dynamic pressure q_o. The magnitude of the peak dynamic pressure is solely a function of the peak incident pressure and, therefore, independent of the size of the explosion.

For design purposes, it is necessary to establish the variation or decay of both the incident and dynamic pressures with time since the effects on a structure subjected to a blast loading depend upon the intensity-time history of the loading as well as on the peak intensity. The idealized form of the incident blast wave (Figure 1) is characterized by an abrupt rise in pressure to a peak value, a period of decay to ambient pressure, and a period in which the pressure drops below ambient (negative pressure phase).

The rate of decay of the incident and dynamic pressures, after the passage of the shock front, is a function of the peak pressure and the size of the detonation. For design purposes, the actual decay of the incident pressure may be approximated by the use of an equivalent triangular pressure-time pulse. The actual duration of the positive pressure phase is replaced by a fictitious positive duration which is expressed as a function of the total positive impulse and the peak pressure:

$$t_{of} = \frac{2i}{P} \tag{1}$$

The above relationship for the equivalent triangular pulse is applicable to the incident pressures as well as the reflected blast pressures; however, in the case of the latter, the value of the impulse used with Eq. 1 is equivalent to that associated with the reflected wave. The fictitious duration of the dynamic pressures may be assumed to be equal to that of the incident pressures.

For determining the pressure-time data for the negative phase, a similar procedure as used in the evaluation of the positive phase may be utilized. The equivalent negative pressure-time curve will have a time of rise equal to 0.125 t_o^- whereas the fictitious duration t_{of}^- is given by the triangular equivalent pulse equation.

$$t_{of}^- = \frac{2i^-}{P^-} \tag{2}$$

where i^- and P^- are the total impulse and peak pressure of the negative phase and t_o^- is the actual negative phase duration.

ABOVEGROUND RECTANGULAR STRUCTURES

General. For any given set of free-field incident and dynamic pressure pulses, the forces imparted to an aboveground structure can be divided into three general components: (1) the force resulting from the incident pressure, (2) the force resulting from the dynamic pressure, and (3) the reflected pressure resulting from the shock impinging upon an interfering surface. The relative significance of each of these components is dependent upon the geometrical configuration and size of the structure, and the orientation of the structure relative to the shock wave.

The interaction of the incident blast wave with an object is a complicated process. To reduce the complex problem of blast to reasonable terms, it will be assumed here that: (1) the structure is generally rectangular in shape, (2) the incident pressure of interest is in the order of 200 psi or less, and (3) the object being loaded is in the region of the Mach reflection.

Front Surface. For a rectangular structure at low pressure ranges, the variation of pressure with time on the side facing the detonation is illustrated in Figure 10a. At the moment the incident shock front strikes the surface, the pressure is immediately raised from zero to the reflected pressure P_r, which is a function of the incident pressure and the angle of incidence between the shock front and the structure face (Figure 8).

The clearing time t_c required to relieve the reflected pressures is represented as

$$t_c = \frac{3s}{U} \tag{3}$$

where U is the velocity of the shock front and S is equal to the height of the structure H_S or one-half its width W_S, whichever is smaller. The pressure P acting on the front surface after time t_C is the algebraic sum of the incident pressure P_S and the drag pressure $C_D q$.

$$P = P_S + C_D q \tag{4}$$

The drag coefficient C_D gives the relationship between the dynamic pressure and the total translational pressure in the direction of the wind produced by the dynamic pressure, and varies with the Mach number (or with the Reynold's number at low incident pressures) and the relative geometry of the structure. A value of $C_D = 1$ for the front surface is considered adequate for the pressure ranges considered in this manual.

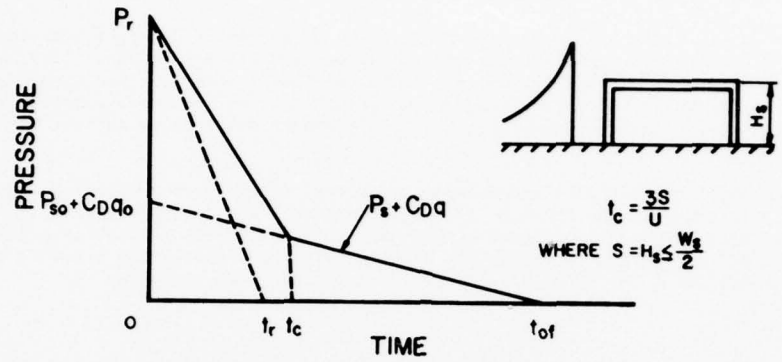

a) PLANE WAVE

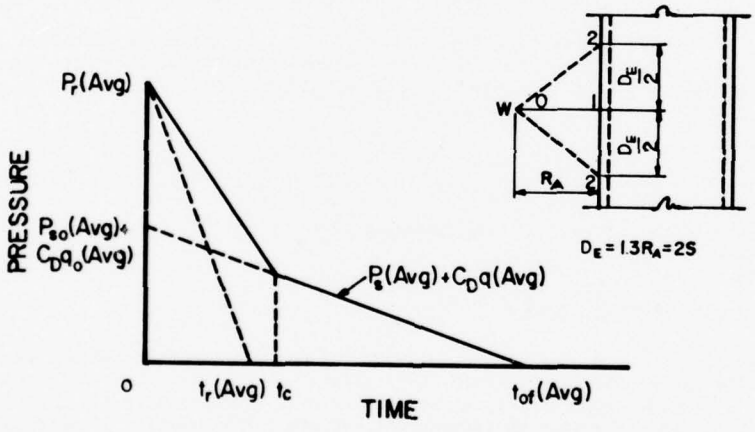

b) VARYING WAVE FRONT

Fig.10 Front surface loading

At higher pressure ranges, the above procedure may yield a fictitious pressure-time curve because of the extremely short pressure pulse durations involved. Therefore, the pressure-time curve construction must be checked to determine its accuracy. The comparison is made by constructing a second curve (dotted triangle as indicated in Figure 10a), using the total reflected pressure impulse i_r depending upon the shock environment. The fictitious duration t_r of the reflected wave is calculated from

$$t_r = \frac{2i_r}{P_r} \tag{5}$$

where P_r is the peak reflected pressure previously used.

Whichever curve gives the smallest value of the impulse (area under curve), use that curve in calculating the wall loading. The reflected pressure impulse includes the effects of both the incident and dynamic pressures.

The pressure-time curve assumes that the shock front of the blast wave is essentially parallel to the front surface of the structure (plane wave shock front). In those cases where the detonation is located relatively close to the structure, the pressure and impulse patterns acting across the wall surface will vary. In these cases an average pressure-time curve (Figure 10b) may be constructed using average values of the loading acting over a length D_E of the structure where D_E is equal to 1.3 R_A (R_A is the normal distance between the detonation and the front surface of the structure) but not greater than $2S$. In this solution, both the pressures and the duration are average values of the loading acting on the wall between points 1 and 2.

As in the case of the plane wave front, the calculations for the average loading on the front surface subjected to a varying shock wave front must consider the effect of extremely short pressure pulses. Here the values of P_r and t_r are taken as average values of the loading acting between points 1 and 2.

Roof and Side Surfaces. As the shock front traverses a structure, a pressure is imparted to the roof slab and side surfaces equal to the incident pressure at a given time at any specified point reduced by a negative drag pressure. The portion of the surface loaded at a particular time is dependent upon the location of the shock front and the wave lengths (L_w and L_w^-) of the positive and negative pulses.

To accurately determine the overall loading on a surface where the span direction is perpendicular to the shock front, a step-by-step analysis of the wave propagation should be made. This analysis would include a simultaneous dynamic analysis of the stresses produced in the element at any given time. To simplify this procedure, an approximate method of calculating the pressure-time history has been developed where the actual loading on the surface has been replaced by an equivalent uniform loading, which will produce stresses in the element similar to those produced by the actual loading as the blast wave crosses the surface. For this analysis to be valid, it is assumed that the reinforcement on both faces is continuous across the span length.

The peak value of the incident pressure decays and the wave length increases as the shock wave traverses the roof. As illustrated in Figure 11a, the maximum stress in the member occurs when the shock front is at point d although the point of maximum stress is located elsewhere. The equivalent uniform loading versus time is shown in Figure 11b and, to simplify the calculations, has been taken as a function of the blast wave parameters at point b, the back end of the element being considered. The equivalent load factor C_E and the blast wave location ratio D/L are obtained from Figure 12 as a function of the wave length-span ratio L_{wb}/L. The pressure builds up linearly from the time t_f when the blast wave reaches the beginning of the element (point f) to time t_d when the blast wave reaches point d. The peak value P_o of the pressure is the sum of the contributions of the equivalent incident and drag pressures.

$$P_o = C_E P_{sob} + C_D q_{ob} \tag{8}$$

where P_{sob} is the peak overpressure occurring at point b and q_{ob} corresponds to the value of $C_E P_{sob}$. Following the peak, the pressure decays linearly to zero at time $t_b + t_{of}$ where t_b is the time at which the blast wave reaches the end of the element (point b) and t_{of} is the fictitious duration of the positive phase. The negative phase of the equivalent uniform loading, if required, may be taken conservatively as that occurring at point b.

The drag coefficient C_D for the roof and side surfaces is a function of the peak dynamic pressure. Recommended values are as follows:

Peak dynamic pressure	Drag coefficient
0-25 psi	-0.40
25-50 psi	-0.30
50-130 psi	-0.20

If the span direction of the member is parallel to the shock front, the pressure-time curve shown in Figure 13 should be used where L is the width of the strip or element being considered.

Rear Surface. As the shock front moves past the rear edges of the roof and/or side surfaces, the pressure front will expand forming secondary waves which propagate over the rear wall. In the case of long buildings, this secondary wave enveloping the back surface essentially results from the spillover from the roof, while in short buildings, surface loads arise from the interaction of the spillover both from the roof and the side surfaces. In both cases, the secondary waves are reinforced due to their impingement with reflecting surfaces. Presently, little information is available on the overall effects on the rear surface loading produced by the reflections of the secondary waves.

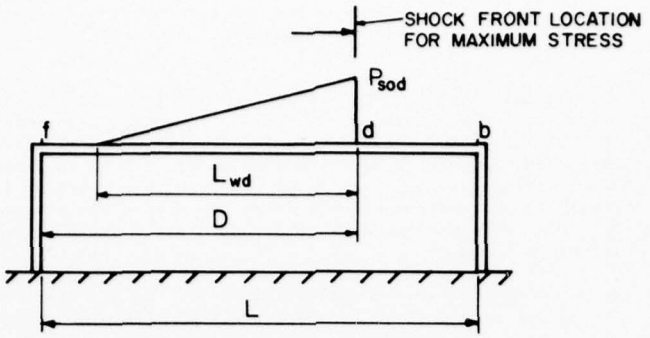

a) SECTION THROUGH STRUCTURE

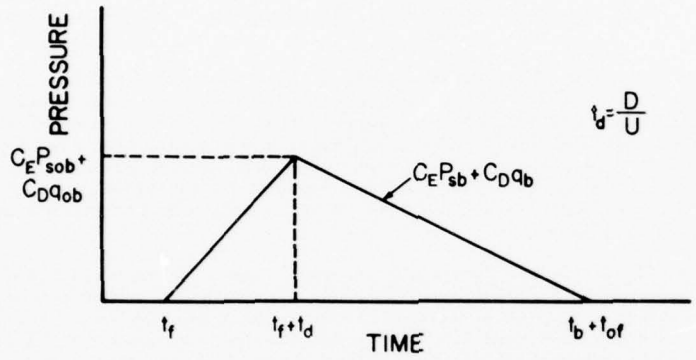

b) AVERAGE PRESSURE – TIME VARIATION

Fig.11 Roof and side surface loading (span direction perpendicular to shock front)

In most design cases, the primary reason for determining the blast loads acting on the rear surface is to determine the overall drag effects (both front and rear surface loadings) on the structure. For this purpose, a procedure may be used where the blast loading on the surface is calculated using the equivalent uniform method utilized for computing the blast loads on the roof and side surfaces. Here the peak pressure of the pressure-time curve (Figure 14b) is calculated using the peak pressure that would occur at distance H_S (point e on Figure 14a) past the rear edge of the roof slab. The equivalent load factor C_E is based on the wave length of the peak pressure above and the unsupported length of the rear surface, as are the time of rise and duration.

Like the roof and side surfaces, the blast loads acting on the rear surface are a function of the drag pressures in addition to the incident pressures. The dynamic pressure of the drag corresponds to that associated with the equivalent pressure, while the recommended drag coefficients are the same as used for the roof and side surfaces.

IMPULSE MOMENTUM STRUCTURAL RESPONSE

The classical approach to structural response for pressure loads that are of short time duration with respect to the lowest period of the responding structure is called impulse momentum technique. This approach is a rational one in that it utilizes Newton's equations of motion.

Before discussing the fundamental principles of dynamic analysis, the principles used in the analysis of structures under static load will be reviewed briefly. Two different methods are used either separately or concurrently in static analysis: one is based on the principle of equilibrium, and the other on work done and internal energy considerations.

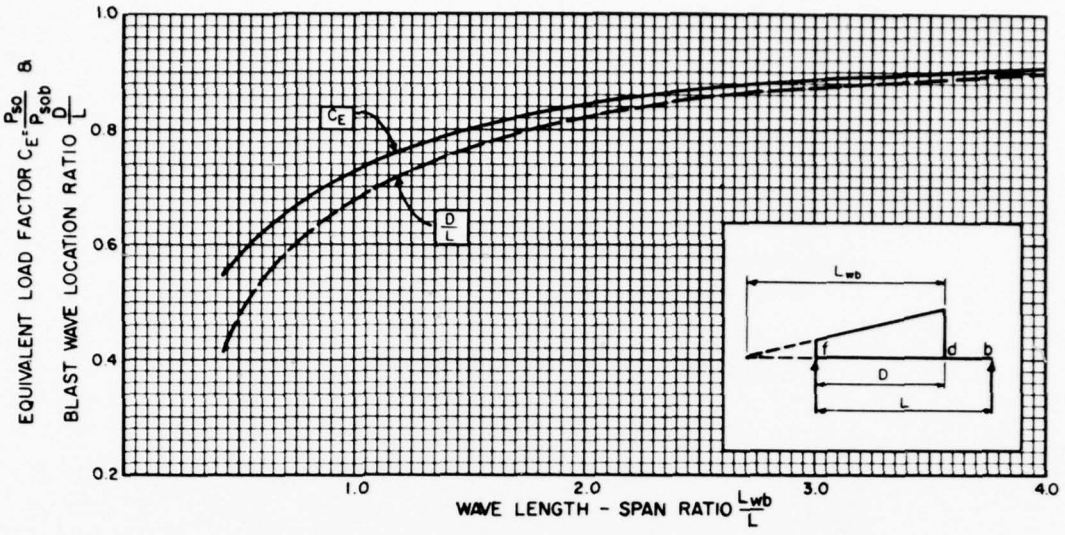

Fig.12 Equivalent load factor and blast wave location ratio versus wave length-span ratio

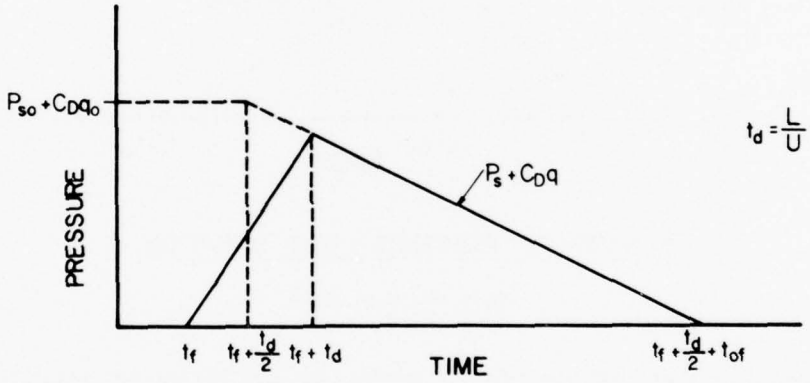

Fig.13 Roof and side surface loading (span direction parallel to shock front)

Under the application of external loads, a given structure is deformed and internal forces developed in its members. In order to satisfy static equilibrium, the vector sum of all the external and internal forces acting on any free body portion of the structure must be equal to zero. For the equilibrium of the structure as a whole, the vector sum of the external forces and the reactions of the foundation must also be equal to zero.

The method based on work done and energy considerations is sometimes used when it is necessary to determine the deformation of a structure. In this method, use is made of the fact that the deformation of the structure causes the point of application of the external load to be displaced. The force then does work on the structure. Meanwhile, because of the structural deformations, potential energy is stored in the structure in the form of strain energy. By the principle of conservation of energy, the work done by the external force and the energy stored in the members must be equal. In static analysis, simplified methods such as the method of virtual work, and the method of the unit load are derived from the general principle of energy conservation.

In the analysis of statically indeterminate structures, in addition to satisfying the equations of equilibrium, it is necessary to include a calculation of the deformation of the structure in order to arrive at a complete solution of the internal forces in the structure. The methods based on energy considerations, such as the method of least work and the method based on Castigliano's theorems, are generally used.

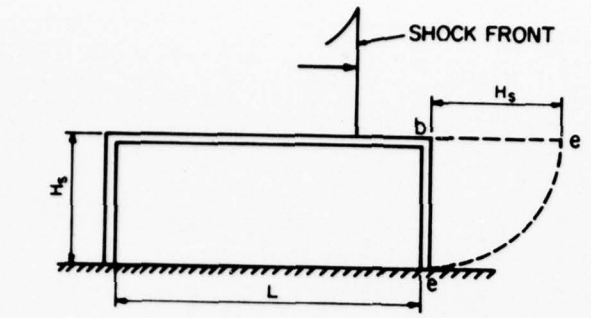

a) SECTION THROUGH STRUCTURE

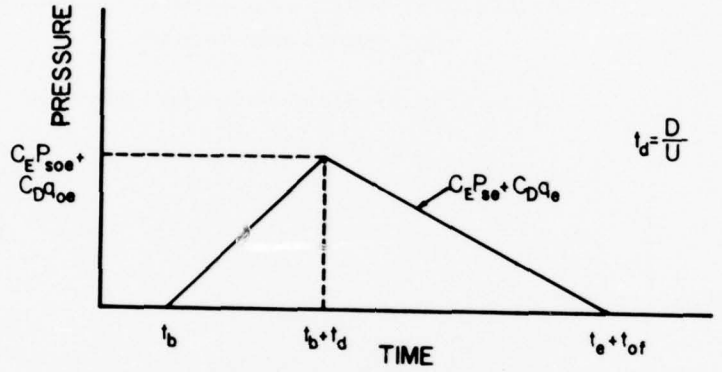

b) AVERAGE PRESSURE – TIME VARIATION

Fig.14 Rear surface loading

For the analysis of structures under dynamic loading, the same two methods basically are used, but the load changes rapidly with time, and the acceleration, velocity and, hence, the inertial force and kinetic energy are of magnitudes requiring consideration. Thus, in addition to the internal and external forces, the equation of equilibrium includes the inertial force, and the equation of dynamic equilibrium takes the form of Newton's equation of motion:

$$F - R = Ma \tag{7}$$

where

F = total external force as a function of time

R = total internal force as a function of time

M = total mass

a = acceleration of the mass.

As for the principle of conservation of energy, the work done must be equal to the sum of the kinetic energy and the strain energy:

$$WD = KE + SE \tag{8}$$

where

WD = work done

KE = kinetic energy

SE = strain energy

and the strain energy includes both the reversible elastic strain energy and the irreversible plastic strain energy. Thus the difference between structures under static and dynamic loads is the presence of inertial force (Ma) in the equation of dynamic equilibrium, and of kinetic energy in the equation of energy conservation. Both terms are related to the mass of the structure. Hence, the mass of the structure becomes an important consideration in dynamic analysis.

In the above discussion, the two methods of analysis are described as if they were independent of each other. This is not the case. The force and energy equations are interdependent and are derived from each other. Although these two methods are not independent, the conveniences of applying them to a given problem varies depending on the particular problem under consideration. Generally, the force equation is convenient for analysis of structures, and the energy equation is convenient for design.

DYNAMICALLY EQUIVALENT SYSTEMS

In dynamic analysis there are only three quantities to be considered: (1) the work done, (2) the strain energy, and (3) the kinetic energy. To evaluate the work done, the displacement at any point on the structure under external distributed or concentrated loads must be known. The strain energy is equal to the summation of the strain energies in all the structural elements, which may be in bending, compression, shear, or torsion. The kinetic energy involves the energy of translation and rotation of all the masses of the structure. The actual evaluation of these quantities for a given structure under dynamic load would be complicated. However, for practical problems this can be avoided by using appropriate assumptions.

In order to simplify the problem, a given structure is replaced by a dynamically equivalent system. The distributed masses of the given structure are lumped together into a number of concentrated masses. The strain energy is assumed to be stored in several weightless springs which do not have to behave elastically. Similarly, the distributed load is replaced by a number of concentrated loads acting on the concentrated masses. Therefore, the equivalent system consists merely of a number of concentrated masses joined together by weightless springs and subjected to concentrated loads which vary with time. This concentrated mass-spring-load system is defined as an equivalent dynamic system.

The reduction of a given structure to an equivalent dynamic system involves the principle of dynamic similarity which is the requirement that the work done, strain energy, and kinetic energy of the equivalent system must be identical, respectively, with those of the given structure. Any given structure, a multistory building or an individual structural element such as a beam or column, can be approximated by an equivalent dynamic system for the purpose of dynamic analysis.

DYNAMIC ANALYSIS AND DESIGN

The analysis of a structural member under applied dynamic loads consists of the determination of the deflection of the member using Newton's equation of motion. Analysis is a direct procedure while design is a verification by analysis. The acceleration, velocity, and displacement versus time relationships are obtainable from the mathematical solution of the equation of motion of the structural system. But the solution also requires expression of the load and structural parameters.

In the typical design problem, the load-time relationship is known while the structural parameters are not and, therefore, must be assumed. The displacement of the structural element at certain critical points can be related to moments or stresses at these same points. Solution of the equation of motion will give the maximum deflection of the system which can be compared to acceptable or limit values and, if adequate, the structural properties originally assumed are satisfactory for the loading parameters. If not, the assumption of a new set of structural properties will give a new equation of motion which, in turn, can be solved. The process of structural design is a trial-and-error procedure--a series of analyses to verify assumed designs.

It can be seen that the writing and solution of the equation of motion for a structure are essential, but usually mechanical, steps in the design process. They are not always readily apparent in the equations and charts presented here, but they are nevertheless there.

The simplest dynamic system consists of a concentrated mass supported by a weightless spring and subjected to a concentrated load as shown in Figure 15. A single displacement variable X is sufficient to describe its motion; hence this system is called a single-degree-of-freedom system. The degree of

freedom of a dynamic system is defined as the number of independent displacement variables needed to specify completely the configuration of the system. This manual is restricted to consideration of single-degree-of-freedom systems only.

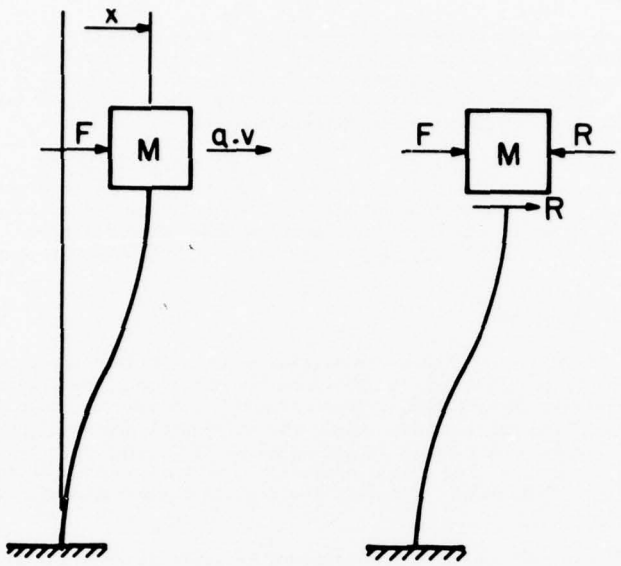

Fig.15 Typical single-degree-of-freedom system

Two fundamental methods are available for treating simple systems subjected to dynamic forces. The first of these methods is concerned with solving the differential equations of the system by either classical, numerical, or graphical means. The second method of analysis, a chart solution, depends on solutions that have been determined by use of the first method and is an approximate solution to the problem.

GENERAL

Structural elements must develop an internal resistance sufficient to stop all motion within the limits of deflection prescribed for the particular design; flexural design is the determination of this required resistance. The load capacity of the member depends on the peak strength developed by the member and on the ability of the member to sustain its resistance for a specific though relatively short period of time. This section describes the methods used for flexural design of structural elements and is divided into two parts: (1) elements that respond to the pressure only, and pressure-time relationship that corresponds to the low- and intermediate-pressure design ranges, respectively, and (2) elements that respond to the impulse which fall into the high-pressure design range.

Both the method of analysis and the maximum deflection criteria are different. Elements that respond to the pressure only and pressure-time relationship are designed using a response chart, while elements that respond to the impulse are designed using either impulse charts for large deflection designs or an impulse method for designs with limited deflections. Maximum allowable deflections for the first case are based on the ductility ratio, and in the second case, on the angle of rotation at the supports.

ELEMENTS THAT RESPOND TO PRESSURE ONLY AND PRESSURE-TIME RELATIONSHIP

These elements were previously shown to be those where the true magnitudes of the pressure and duration of the applied blast loads must be known. The determination of the dynamic response of these systems is accomplished using a response chart which relates the dynamic properties of the blast loads (pressure and duration) to those of the element (natural period of vibration, resistance, and deflection).

The maximum allowable deflection is expressed in terms of the ductility ratio or the ratio of the maximum deflection X_m to the equivalent maximum elastic deflection X_E of the element. Maximum deflections associated with the analysis of elements that respond to pressure only and elements that respond to pressure-time relationship usually conform to those designated as limited deflections.

In order to utilize these response charts, both the blast load (pressure-time history) and the resistance-deflection curve are idealized to linear or bilinear functions. The idealization of these functions consists of replacing the true functions by one or a series of straight lines.

Idealization of Load and Resistance Functions. The most commonly used idealized pressure-time function is an initially peaked triangle defined by a peak pressure B and a duration T. This simplified loading function has been studied extensively. The basic consideration in replacing the given loading by an idealized loading shape is that the maximum displacement produced by each must be equal. No general rules can be given for the idealization; however, the following will serve as a guide. Since t_m is the time at which the maximum deflection X_m occurs, the idealized load and the given load should be very close to each other in the time interval from zero to t_m and have the same area under the respective curves in the same time interval.

For example, consider the solid loading curve shown in Figure 16. For a time t_{m1} to reach maximum deflection, the idealized loading curve is best defined by B_1 and T_1, while for a time t_{m2} the loading would be defined by B_2 and T_2.

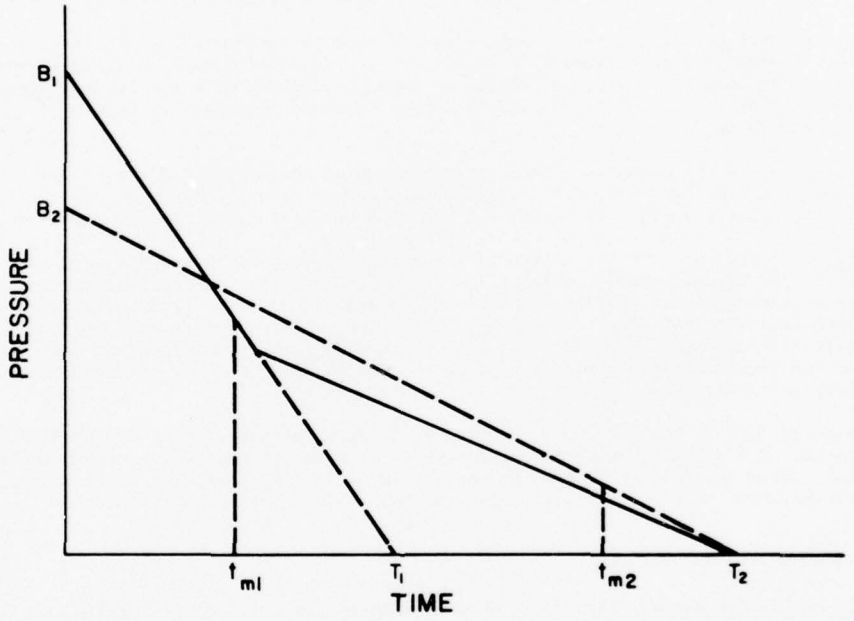

Fig.16 Idealization of pressure-time functions

The typical resistance function for limited deflection design consists of elastic, elasto-plastic, and plastic ranges, and for the large majority of problems, can be adequately idealized to a bilinear form. For the particular case where the structural element exhibits only elastic and plastic behavior, idealization of the resistance function is not necessary.

Natural Period of Vibration. When designing for limited deflections using the response chart, the effective natural period of vibration is required. This effective period of vibration, when related to the duration of a blast loading of given intensity and a given structural resistance, determines the maximum transient deflection X_m of the structural element.

The effective natural period of vibration is

$$T_N = 2\pi \sqrt{\frac{m_e}{K_E}} = 2\pi \sqrt{\frac{K_{LM} m}{K_E}} \tag{9}$$

where m_e is the effective unit mass and K_E is the equivalent unit stiffness of the system.

The values used for m_e and K_E for a particular element depend upon the allowable maximum deflections permitted. For example, when designing for completely elastic behavior, the elastic values of the effective unit mass and unit stiffness would be used; for elasto-plastic action, the effective unit mass is the average of the elastic and elasto-plastic values and the stiffness is the equivalent unit stiffness K_E. For design in the plastic range, a weighted value of the effective unit mass is used with the equivalent unit stiffness K_E. When plastic deformations less than those specified by the limited deflection criteria are used, the use of the average value of the average elastic and elasto-plastic effective unit masses and the plastic effective unit mass will suffice for most structural elements considered in this manual.

Determination of Maximum Response. The maximum response of a pressure or pressure-time sensitive system with an elasto-plastic resistance function subjected to a triangular loading pulse is shown in Figure 17. This nondimensional chart is a convenient plot of solutions made by numerical integration of the equation of motion using a digital computer. If any two of the four parameters are known, the remaining two can be found. It should be noted that since the blast load is expressed in terms of pressure (force/unit area), unit values are used for the resistance and stiffness of an element.

In the typical design example, the pressure-time loading is calculated, and this curve is then idealized to the triangular form defined by B and T. If a structural member is assumed, the idealized resistance function defined by r_u, X_E, and K_E can be determined along with the natural period T_N. Then, knowing the ratios B/r_u and T/T_N, X_m and t_m can be obtained readily from Figure 17 by reading the ratios X_m/X_E and t_m/T_N.

The deflection X_m is the maximum deflection corresponding to the assumed parameters. The value of t_m is the time at which the maximum deflection occurs and is used to check the adequacy of the idealization of the loading curve. If either t_m or X_m are unsatisfactory, the procedure is repeated.

Determination of Rebound. In the design of elements that respond to the pressure only and pressure-time relationship, the element must be designed to resist the negative deflection or rebound which can occur after the maximum positive deflection has been reached. The ratio of the required unit rebound resistance to the ultimate unit resistance r^-/r_u, so that the element will remain elastic during rebound, is obtained from Figure 18. Entering with the ratios X_m/X_E and T/T_N previously determined for the design, the required unit rebound resistance r^- can be read in terms of the originally designed ultimate unit resistance r_u.

It may be noted that if the loading is applied in a relatively short time compared to the natural period of vibration, the required rebound resistance can be equal to the resistance in the initial design direction. When the loading is applied for a relatively long time, the maximum deflection is reached when the positive forces are still large, and the rebound resistance is reduced.

ELEMENTS THAT RESPOND TO IMPULSE

General Equations for Maximum Response. When an element responds to the impulse, the maximum response depends upon the area under the pressure-time curve (impulse of the blast loading). The magnitude and time variation of the pressure are not important. Response charts based on pressure-time relationships are therefore not applicable to these problems. Instead, the element resistance required to limit the maximum deflection to a specified value is obtained through the use of a semi-graphical method of analysis.

Consider the pressure- and resistance-time curves shown in Figure 19. The resistance curve depicted is for a two-way element with a resistance-deflection function having a post-ultimate range. From Newton's equation of motion it can be shown that the summation of the areas (considering area A as positive and area B as negative) under the time curves up to any time t_a divided by the corresponding effective masses is equal to the instantaneous velocity at that time:

$$v_a = \int_0^{t_a} \frac{(f - r)}{m_e} \, dt \tag{10}$$

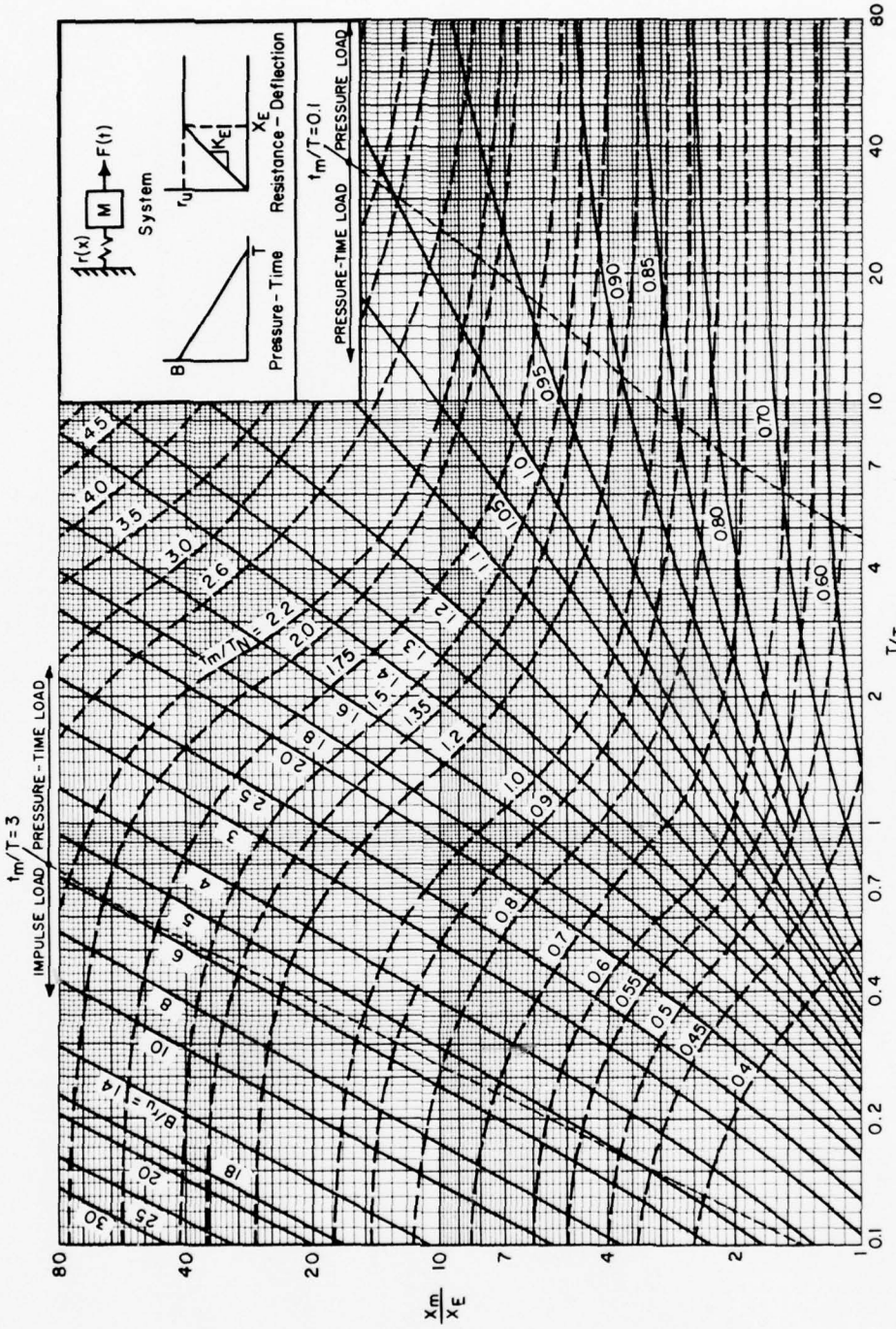

Fig.17 Maximum response of simple spring-mass system to initially peaked triangular pressure pulse

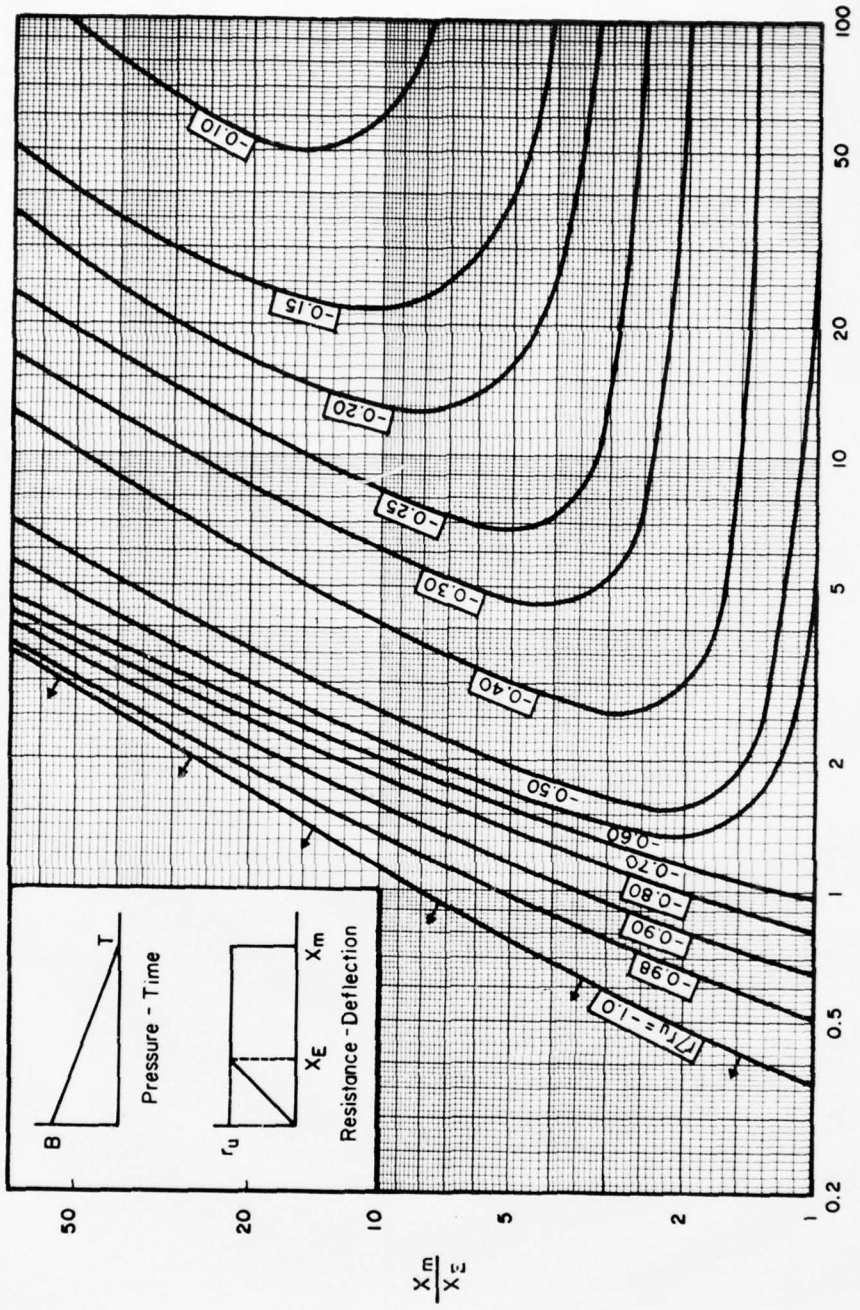

Fig.18 Elastic rebound of simple spring-mass system

The displacement at time t_a is found by multiplying each differential area divided by the appropriate effective mass by its distance to t_a and summing the values algebraically:

$$X_a = \int_0^{t_a} \frac{(f - r)}{m_a} \left(t_a - t\right) dt \tag{11}$$

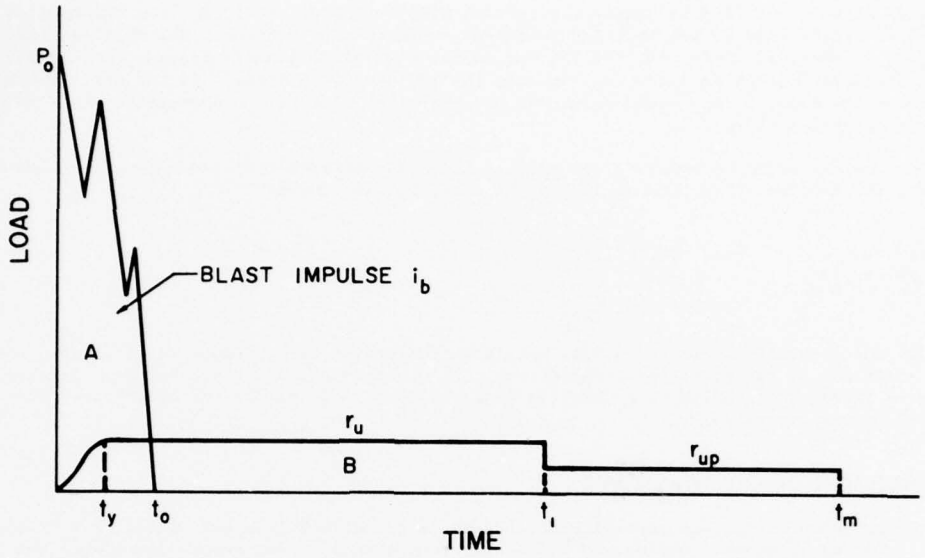

Fig.19 Pressure time and resistance-time curves for elements that respond to impulse

For an element to be in equilibrium at its maximum deflection, its impulse capacity must be numberically equal to the impulse of the applied blast load. With the use of the foregoing equations, the expressions, which define the motion and capacity of elements subjected to impulse type loads, can be defined. These expressions are presented for both large and limited deflection criteria.

Case 1--Large Deflections.

1. Utilizing Eq. 11 and by taking moments of the areas under the pressure- and resistance-time curves (Figure 19) about time t_m, assuming that the unit blast impulse i_b is applied instantaneously at $t = 0$, and that the time to reach yield t_y is also close to zero, the expression for the maximum deflection X_m is

$$X_m = \frac{i_b t_m}{m_u} - \frac{r_u t_1 \left(t_m - \frac{t_1}{2}\right)}{m_u} - \frac{r_{up}\left(t_m - t_1\right)\left(t_m - t_1\right)}{2m_{up}} \tag{12}$$

If moments of the areas are taken about t_1, then the deflection at partial failure X_1, is

$$X_1 = \frac{i_b t_1}{m_u} - \frac{r_u t_1^2}{2m_u} \tag{13}$$

Using Eq. 10 and summing the areas to t_m and recognizing that the instantaneous velocity at t_m equals zero

$$\frac{i_b}{m_u} - \frac{r_u t_1}{m_u} - \frac{r_{up}\left(t_m - t_1\right)}{m_{up}} = 0 \tag{14}$$

2. Solution of the above three simultaneous equations is accomplished by solving Eq. 14 for t_m and substituting this expression into Eq. 12, and solving Eq. 13 for t_1 and substituting this expression into the modified Eq. 12. After combining and rearranging terms, the general response equation becomes

$$\frac{i_b^2}{2m_u} = r_u X_1 + \frac{m_u}{m_{up}} r_{up}\left(X_m - X_1\right) \tag{15}$$

The left side of this equation is simply the initial kinetic energy resulting from the applied blast impulse and the right side is the modified potential energy of the element. The modification is required since the above analysis requires the use of two equivalent dynamic systems (before and after time t_1). The modification factor m_u/m_{up} equates the two dynamic systems. If the effective mass in each range was the same, m_u/m_{up} would equal one and the right side of the expression would be ΣrX which is the potential energy.

3. For one-way elements which do not exhibit the post-ultimate resistance range, or for two-way panels where the maximum deflection X_m is less than X_1, Eq. 15 becomes

$$\frac{i_b^2}{2m_u} = r_u X_m \tag{16}$$

5. The above solutions are valid only for large deflection design (support rotations >5 degrees) since the variation of resistance with deflection in the elasto-plastic range has been ignored. This limitation is based on the assumption that the time to reach yield t_y and the duration of the impulse t_0 are small in comparison to t_m.

CRITICAL IMPULSE WITHIN CRITICAL TIME

Another technique which has received limited use is the critical impulse within a critical time. An excerpt from two references (Reference 10 and 11) is herein included which illustrates the method. From Reference 10, the following.

CRITICAL IMPULSE

The identification and selection of the critical time within which an impulse must be received by a target in order to have damage inflicted is essentially empirical. However, there are available some theoretical guidelines. Thus, for a simple system at rest but capable of harmonic motion, a maximum velocity and maximum amplitude of swing are given by an impulse of very short duration. Increasing the duration of the given impulse results in a decrease in achieved velocity and amplitude. However, this decrease is relatively small until the duration of the impulse becomes about one-quarter of the natural period of oscillation, when further increases give marked decreases in amplitude. These observations have been amply confirmed by analog computer studies as illustrated in FIGURE 2. In addition, it may be noted that a simple harmonic oscillator travels from zero to maximum displacement in one-quarter of its natural period and that the enforced motion of a structural member leading to damage effects should not be greatly different.

On a basis of these considerations, it appears that a time equal to one-quarter of the natural period of oscillation should for any structural element represent a rough sort of cut-off time for impulse effectiveness. Representative calculations based on the determination of such natural periods are discussed in the following section.

In addition to structural deformations as a form of blast damage, there is also the situation where an object such as a truck or a body is physically displaced and hurled from its original position. The forces giving rise to such a hurling action must at least be sufficiently great to override the forces of gravity, and they are arbitrarily taken to be those forces which by acting for one second can produce the corresponding free-fall velocity. A time in the order of one second thus becomes the critical time for blast damage received by this hurling mechanism.

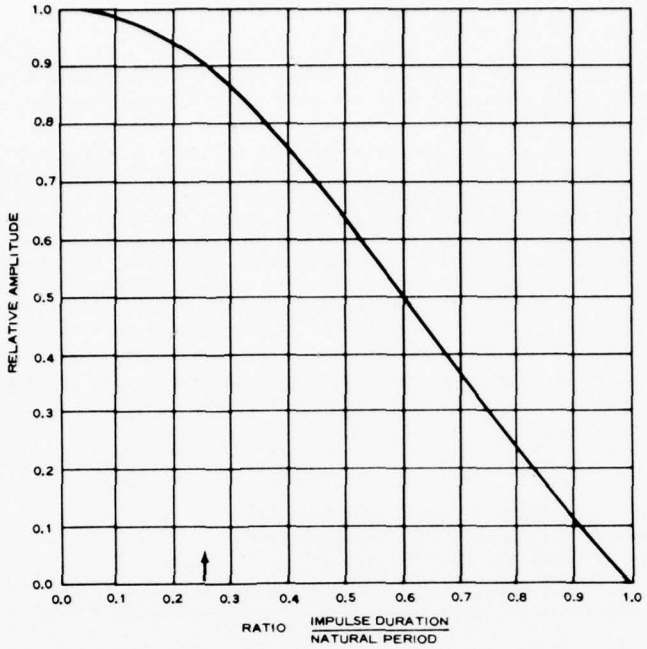

FIGURE 2. Relative amplitude of undamped harmonic motion versus duration of applied impulse.

To summarize, the critical times for explosive blast damage are arbitrarily but reasonably taken as one-quarter of the natural period for structures and structural members, and one second for destructive hurling away for nonattached objects.

Critical Impulse

Structural damage inflicted by explosive blast is the result of an impulsive load that exceeds the resistance of a material. In ordinary impulsive loading, a stress wave moves through the material such that

$$\sigma = \rho C V, \tag{7}$$

where

- σ is the stress,
- ρ is the density,
- C is the velocity of sound in the material, and
- V is the relative particle velocity associated with the stress wave (the product ρC is known as the "acoustic impedance")

For the limiting situation where the stresses developed are equal to the dynamic yield strength, there also is a limiting or critical particle velocity, V_C, which if exceeded causes permanent displacement within the material.

Experimental values for this critical particle velocity are available for the tensile failure of some of the common metals. For other materials, the critical particle velocity can in principle be found from the dynamic yield strength when such dynamic yield values are known (they are appreciably greater than the conventional static values). However,

blast produced failures are seldom ones in simple tension. Hence, the critical particle velocity applicable in the disruption of a target by blast is not so simply described, but it should be at least closely related to the critical particle velocity for failure in simple tension. For purposes here, these two critical particle velocities will be considered as being identical.

For blast damage, the critical particle velocity is actually a differential velocity referenced to a part of the system at rest. Consider, for example, a structural system where a skin is stretched between two rigid support members. When an impulsive load is applied, the inertia of the support members keeps them from moving significantly, while the thinner skin is accelerated to a velocity that may exceed the critical velocity, in which case tearing of the skin results. Similar considerations apply in systems that cantilever out from a massive inertial reference system, such as the empennage or the wing of an aircraft cantilevered out from the fuselage.

The critical impulse per unit area associated with the critical velocity is given by elementary considerations as

$$I_c = \rho \delta V_c \tag{8}$$

where

ρ is the density of the target material,
δ is the thickness of the material, and
V_c is the critical velocity.

The critical impulse may also be expressed in terms of the dynamic yield strength for the material by combining the above relations to give

$$I_c = \delta \sigma_y / C \tag{9}$$

where

C is the velocity of sound in the material, and
σ_y is the dynamic yield strength.

The velocity of sound, C, can be replaced by its equivalent

$$C = \sqrt{E/\rho}$$

where

E is the modulus of elasticity

and this gives a third form for the expression for critical impulse

$$I_c = (\rho/E)^{1/2} \delta \sigma_y \tag{10}$$

These three forms of the expression for critical impulse are all expressed in coherent units and are all equivalent. The first of these would appeal to those who have worked with impulsive loads and shock waves in metals, but the others may on occasion be preferred since they contain items directly related to the ordinary strength characteristics of a material.

The above expressions apply as part of the criterion for blast damage when the damage occurs by deformations of a structure or a structural member. For the important situation where a target is damaged by hurling it bodily from its original position, the critical impulse is arbitrarily taken to be that which could cause the entire object to reach free-fall velocity in one second. This is convenient mathematically, and also is in accord with the observation that the corresponding fall of about 16 feet is ordinarily very damaging to most targets of interest.

REPRESENTATIVE CALCULATIONS

Values for the blast damage criterion, critical impulse within a critical time, were computed both for a parked aircraft and for a light industrial building. For the aircraft, three types of damage were considered: (1) tearing the skin, (2) breaking off a wing section, and (3) physical displacement by hurling the entire plane.

Aircraft Skin Failure

For damage by the mechanism of tearing the skin, the critical time is taken from a computed value for the resonant frequency of this structural member. The skin was assumed to be of 1/16-inch-thick aluminum, clamped to stringers on 8-inch separation. For clamped panels of infinite length, the resonant frequency, f, is given by the relation

$$f = 217{,}600 \times 0.985 \times \delta/b^2 \qquad (11)$$

where the factor 217,600 pertains to this type of structure, and the factor 0.985 is for the type of metal.
Here

δ is the skin thickness in inches, and
b the distance of spacing in inches.

Thus,

$$f = 217{,}600 \times 0.985 \times (1/16)(8)^2 = 212 \text{ cps} \qquad (12)$$

This resonant frequency corresponds to a natural period of vibration of 1,000/212 = 4.70 milliseconds (ms), and to a critical time of 4.70/4 = 1.2 ms.

The critical impulse required for tearing the skin is computed in any one of three separate ways, depending on the primary data available. Data on the aluminum skin, as obtained from various sources are as follows.

δ	(thickness)	= 1/16 inch = 0.0052 feet
ρ	(density)	= 2.7 g/cm^3 = 2.7 x 62.4/32.2 = 5.22 slugs/ft^3
C	(speed of sound)	= 16,470 fps
V_c	(critical velocity)	= 240 fps
σ_Y	(dynamic yield strength)	= 140,000 psi = 2.02 x 10^7 psf
E	(elastic modulus)	= 11 x 10^6 psi = 1.58 x 10^9 psf

1. Critical impulse from critical velocity:

$$I_c = \rho\delta V_c = 5.22 \times 0.0052 \times 240 = 6.5 \text{ psf-sec}$$
$$= 45 \text{ psi-ms} \qquad (13)$$

2. Critical impulse from dynamic yield strength and speed of sound:

$$I_c = \delta\sigma_y/C = 0.0052 \times 2.02 \times 10^7/16{,}470 = 6.4 \text{ psf-sec}$$
$$= 44 \text{ psi-ms} \qquad (14)$$

3. Critical impulse from elastic modulus and dynamic yield strength:

$$I_c = (\rho/E)^{1/2}\delta\sigma y = (5.22/1.58 \times 10^9)^{1/2} \times 0.0052 \times 2.02 \times 10^7$$
$$= 6.0 \text{ psf-sec} = 42 \text{ psi-ms} \qquad (15)$$

Differences in the calculated results, which in this instance are minor, are caused by disparities in the original data.

A diagram illustrating skin rupture as caused by a blast impulse that exceeds the critical impulse for the skin within the critical time is shown schematically in FIGURE 3.

The computed minimum overpressure for this damage becomes 43/1.2 = 36 psi, which must persist for at least as long as 1.2 ms in order to provide the necessary minimum impulse.

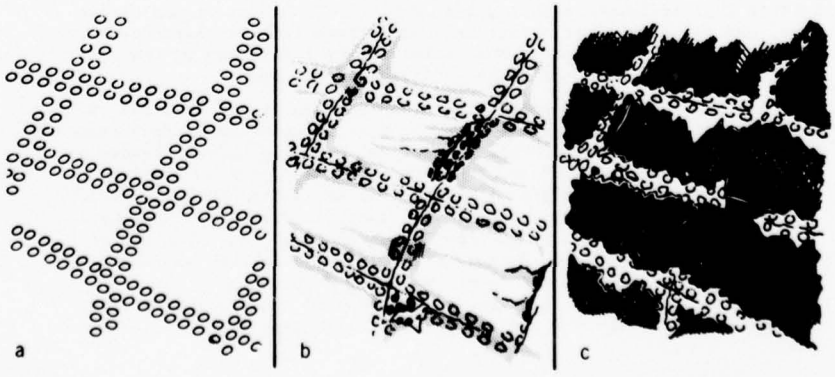

FIGURE 3. Rupture of structural skin panel. Computed critical impulse, 43 psi-ms; computed critical time, 1.2 ms.

An excerpt from Reference 11 gives background to support the ability to estimate critical fracture stress and critical impact velocity.

> *Scabbing*--When the primary longitudinal wave, which is one of compression, strikes the lower edge of the plate it is reflected and comes back as a wave of tension. If the wave is decaying in intensity, interference between the incident and reflected waves will cause a tensile stress to be built up a short distance from the bottom of the plate. The tension may reach a high enough value to cause the plate to fracture. When a fracture of this type occurs, the plate is said to have scabbed. Fracturing of this type was first described by Hopkinson many years ago and is sometimes known as a Hopkinson fracture.
>
> The mechanics of scabbing can be treated qualitatively in a fairly elementary fashion. Consider a laterally infinite slab of finite thickness

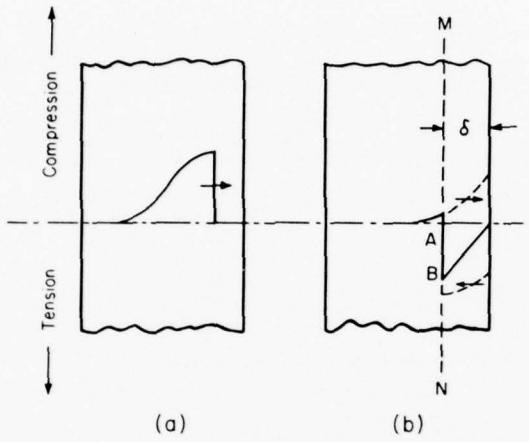

Fig. 9-3—Stress Distribution Near Free Surface of Plate of Finite Thickness and Infinite Lateral Extent. (a) Before reflection and (b) shortly after reflection of transient disturbance.

and assume a perfectly elastic plate material. Suppose that the pressure pulse is of the form shown in Fig. 9-3A; that is, the pressure rises instantaneously and then begins to decay. When the disturbance strikes the free (right) boundary of the plate, it will be reflected as a tension wave. The incident compression wave and its reflected tension counterpart will interfere. The resultant distribution of stress within the plate at a particular time during reflection of the wave will be that shown in Fig. 9-3b. The tension AB will increase as the reflected wave moves to the left. If at some point the metal can no longer support the tension, it will fracture and a scab will fly off. For a body with a definite critical normal fracture stress, the thickness δ of the scab will be equal to one-half the distance within the wave that corresponds to a decrease in stress equal to the critical normal fracture stress.

Studies of the scabbing of metal plates have shown that the two factors that influence scabbing most are, (a) the *shape* of the stress wave, and (b) a critical normal fracture stress that is characteristic of the material acted upon. The latter may be influenced by the conditions of loading and the state of stress in the body.

The very strong dependence that the location of the scab has on the shape of the stress wave is perhaps best illustrated by some examples of scabbing of flat, mild steel plates that were explosively loaded in the manner shown in Fig. 5-3c of Chapter 5. The plates in the test ranged in thickness from 1/4 to 2 inch; the explosive charges were 1/8 and 1/4 inch in thickness. Results are shown in Fig. 9-4. The most interesting things shown by the two curves are that the thickness of scab increases rather than decreases with plate thickness and that, under some conditions, a 1/8 inch layer of explosive can produce a thicker scab than a 1/4 inch layer. The general qualitative aspects of the curves of Fig. 9-4 are in agreement with expected behavior,

i.e., flattening and elongation, of the pulse as it moves through the plate. Decrease in steepness of the stress-time curve behind the wave front with increasing plate thickness will cause increasingly thicker scabs to form. The pulse will be more sustained and the initial pressure somewhat higher for the thicker charge; hence, the thickness of the scab generated by the 1/4 inch layer of explosive will be greater than that generated by the 1/8 inch layer when the plate is thin.

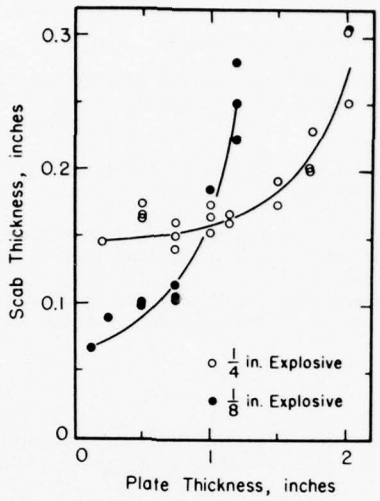

Fig. 9-4—Dependence of Scab Thickness on Plate Thickness for Two Thicknesses of Explosive. Plates were mild steel and loaded in manner of Fig. 5-3c.

Experimentally determined values of the critical normal fracture stresses for five metals are listed in Table 9-1. The relationship

$$\sigma = \rho\, cv \qquad \text{Equation (9-1)}$$

can be used to associate a critical differential particle velocity with each critical normal fracture stress. Values of critical particle velocities obtained in this way are also listed in the same table. There is some, but not conclusive, evidence that indicates that the state of stress that exists in the region of the fracture at the time the fracture occurs may affect the value of σ_c.

Table 9-1

Critical Normal Fracture Stresses and Associated Critical Impact Velocities

	Critical normal fracture stress σ_c psi	Associated critical impact velocity (ft/sec)
24S-T4 Aluminum	140,000	202
Copper	410,000	264
Brass	310,000	216
1020 Steel	160,000	84
4130 Steel	440,000	235

AIR BLAST INSIDE COMPARTMENTS

Warhead Effect

The subject of air blast inside the various compartments of the aircraft such as the wing box, fuselage fuel tanks, and the various fuselage compartments is usually restricted to the smaller warheads. A rule of thumb sometimes used is that a 2-pound-weight charge placed inside an aircraft will destroy

the aircraft. This rule, of course, has been found experimentally to have exceptions for certain aircraft compartments where the local geometry by shielding, angle of incidence effects, and venting can increase the amount of explosive required to kill the aircraft by almost a factor of 10.

Effects to Consider

1. The warhead length-to-diameter ratio will have a very pronounced effect for the close-scaled distances in many aircraft compartments. It can be highly directional.

2. Momentum as well as impulse must be considered.

3. The fragmentation can be quite different within five diameters of the warhead. (This can produce a fragment hole pattern which the wounded structure must respond to in its maximum structural deflection.)

4. Nothing is available to predict the effects of a contact burst (where the warhead is in contact, or partially through the structure, at detonation).

5. Detonator location, multiple detonators, possible jacket focusing effect, etc., can have a pronounced influence on effective explosive yield in various angular directions.

6. Data on the ability of aircraft fasteners to resist tension created by blast loads are nonexistent. Hence, predictions of amount of aircraft skin removal (due to internal blast) is difficult if not impossible.

Best Method of Procedure

Despite all the uncertainties previously listed, we must proceed and do the best we can if we are ever to arrive at a rational approach. The following approach is tentatively suggested:

1. Consider reflection from adjacent walls (using weight of explosive (WE) + 20%).

2. Check to see whether volume is vented.

3. Proceed with structural response calculation.

Reflections From Adjacent Walls of Closed Vented Compartments

In confined areas, amplification of the initial shock front (free-air pressures) due to reflections within the structure will occur. At any given point on a particular reflecting surface, the total impulse loading is a combination of the contributions from the initial shock and from the shock reflected from adjacent surfaces.

An approximate method for the calculation of the total impulse in a fully vented cubicle has been developed in connection with the Safety Design Criteria Program. The total reflected impulse acting on various points of each surface of the cubicle have been calculated and then integrated to obtain the total impulse loads. In order to simplify the calculation of the response of a cubicle wall to these applied loads, the total impulse is assumed to be distributed uniformly, giving an average value of the impulse acting on any one surface. The actual distribution of the blast impulses is highly irregular due to the multiple reflections and time phasing, and results in localized high shear stresses in the elements. When designing, the use of average impulse loads is predicted on the ability of the element to transfer these localized loads to regions of lower stress.

The method of calculating the average blast impulses was developed using a theoretical procedure based on semiempirical blast data and on the results of response tests of reinforced concrete slabs. The calculated average impulse loads have been compared with those obtained from the results of tests of a scale-model steel cubicle and have shown good agreement for a wide range of cubicle arrangements.

The parameters which are necessary to determine the average impulse loads are structure configuration and size, charge weight, and charge location. Surfaces depicted are not frangible for determining the shock loadings but could be frangible when considering gas pressure buildup. For the four-wall cubicle with roof, one of the surfaces shown must be frangible or vented for such gas pressures. Figure 20 shows the definition of a four-wall cubicle.

Because of the wide range of required parameters, the procedure for the determination of the impulse loads was programmed for solution on a digital computer. The results of these calculations, presented in Figures 21 through 29, give the scaled average unit blast impulse $\bar{i}_b$ as a function of the parameters defining the configurations presented in Figure 20. Each illustration is for a particular combination of values of h/H, l/L, and the number N of reflecting surfaces adjacent to the surface for which the impulses are being calculated. The wall (if any) parallel to the surface in question was found to have a negligible contribution to the impulse for the range of parameters used and was therefore not considered.

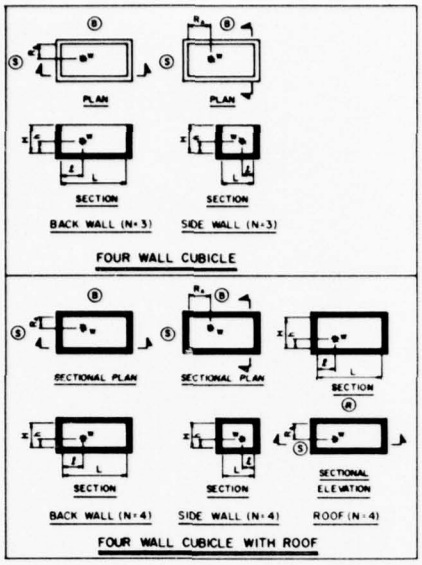

NOTES:

1. B DENOTES BACK WALL, S SIDE WALL AND R ROOF
2. NUMBERS IN PARENTHESES INDICATE NUMBER N OF REFLECTING SURFACES ADJACENT TO SURFACE IN QUESTION
3. h IS ALWAYS MEASURED TO THE NEAREST REFLECTING SURFACE.
4. ℓ IS ALWAYS MEASURED TO THE NEAREST REFLECTING SURFACE EXCEPT FOR THE CANTILEVER WALL WHERE IT IS MEASURED TO THE NEAREST FREE EDGE.
5. FOR VALUES OF SCALED AVERAGE UNIT BLAST IMPULSE $\bar{i}_b$ FOR BARRIER AND CUBICLE ARRANGEMENTS SHOWN SEE FIGURES 21 THROUGH FIGURE 29. REQUIRED PARAMETERS ARE:

$$\frac{\ell}{L}, \quad \frac{h}{H}, \quad \frac{L}{H}, \quad \frac{L}{R_A}, \quad \text{AND} \quad Z_A = \frac{R_A}{W^{1/3}}$$

Fig.20 Four-wall cubicle with roof

The general procedure for use of the above illustrations is as follows:

1. Determine the values of the parameters indicated for the selected surface of the barrier or cubicle configuration and calculate the following quantities:

$$\frac{h}{H}, \quad \frac{l}{L}, \quad \frac{L}{H}, \quad \frac{L}{R_A}, \quad \text{and} \quad Z_A = R_A/W^{1/3}$$

2. *In most cases the above procedure will require* interpolation for one or more of the parameters which define a given situation, in order to obtain the correct average impulse load.

3. Because of the limitation in the range of the test data and the limited number of values of the parameters given in the above impulse charts, extrapolation of the data given in Figures 21 through 29 may be required for some of the parameters involved. On the other hand, the limiting values as given in the charts for other parameters will not require extrapolation. The values of the average impulse loads corresponding to the values of the parameters which exceed their limiting values (as defined by the charts), will be approximately equal to those corresponding to the limiting values. The following are recommended procedures that will be applicable in most cases for either extrapolation, or establishing the limits of impulse loads corresponding to values of the various parameters that exceed the limits of the charts:

(a) Plot curve of values of $\bar{i}_b$ versus Z_A for constant values of L/R_A, L/H, h/H, and l/L. Extrapolate curve to include value of $\bar{i}_b$ corresponding to the value of Z_A required.

(b) Extrapolate given curve for constant values of Z_A, L/H, h/H, and l/L, to include value of $\bar{i}_b$ corresponding to the value of L/R_A required.

(c) Values of $\bar{i}_b$ corresponding to values of L/H greater than 6 shall be taken as equal to those corresponding to $L/H = 6$ for actual values of Z_A, h/H, and l/L, but with a fictitious value of L/R_A in which R_A is the actual value and L is fictitious value equal to $6H$.

(d) Values of $\bar{i}_b$ corresponding to values of l/L less than 0.10 and greater than 0.75 shall be taken as equal to those corresponding to $l/L = 0.10$ and 0.75, respectively.

(e) Values of $\bar{i}_b$ corresponding to values of h/H less than 0.15 and greater than 0.75 shall be taken as equal to those corresponding to $h/H = 0.15$ and 0.75, respectively.

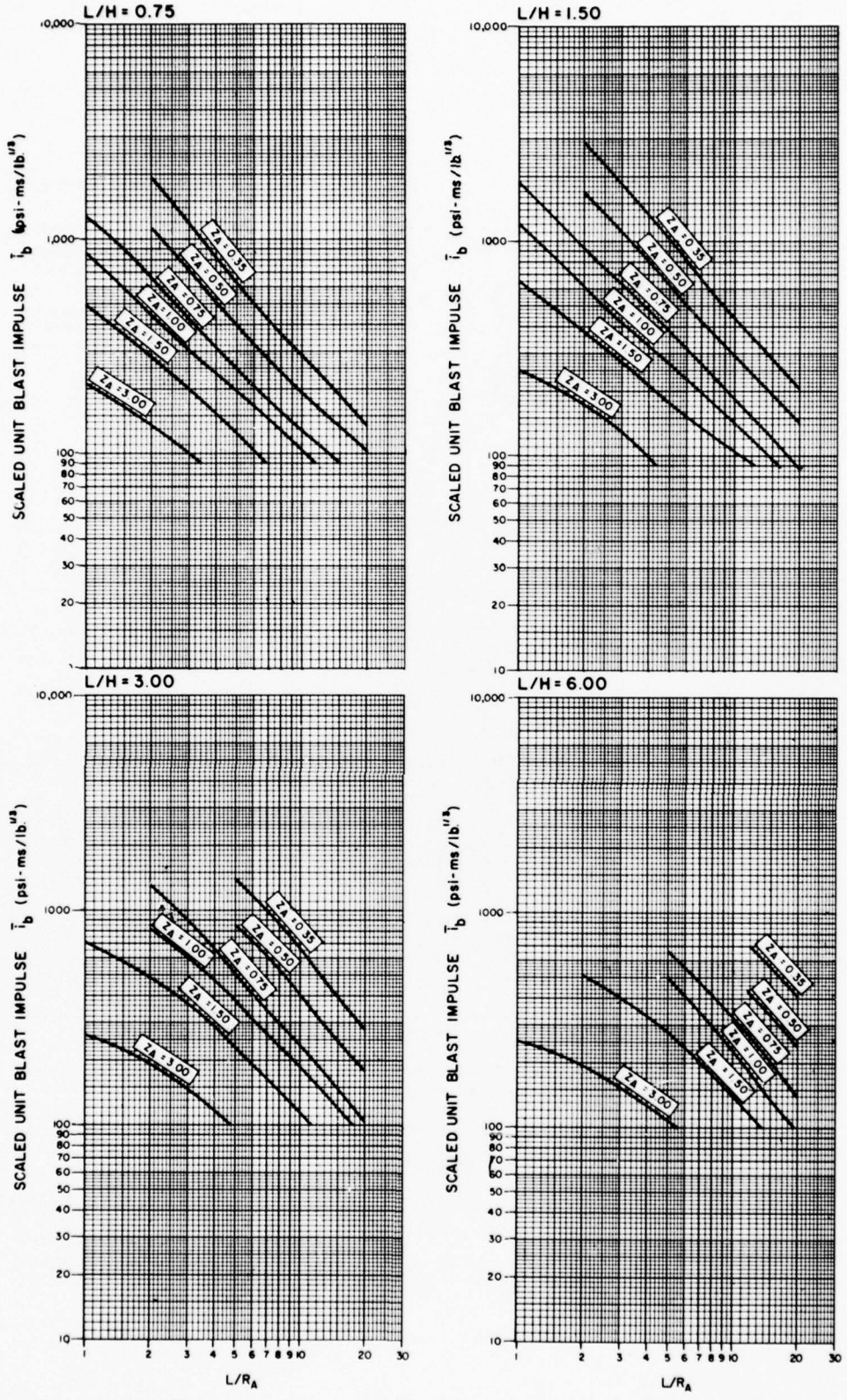

Fig.21 Scaled average unit blast impulse (N = 4, l/L = 0.10, h/H = 0.15)

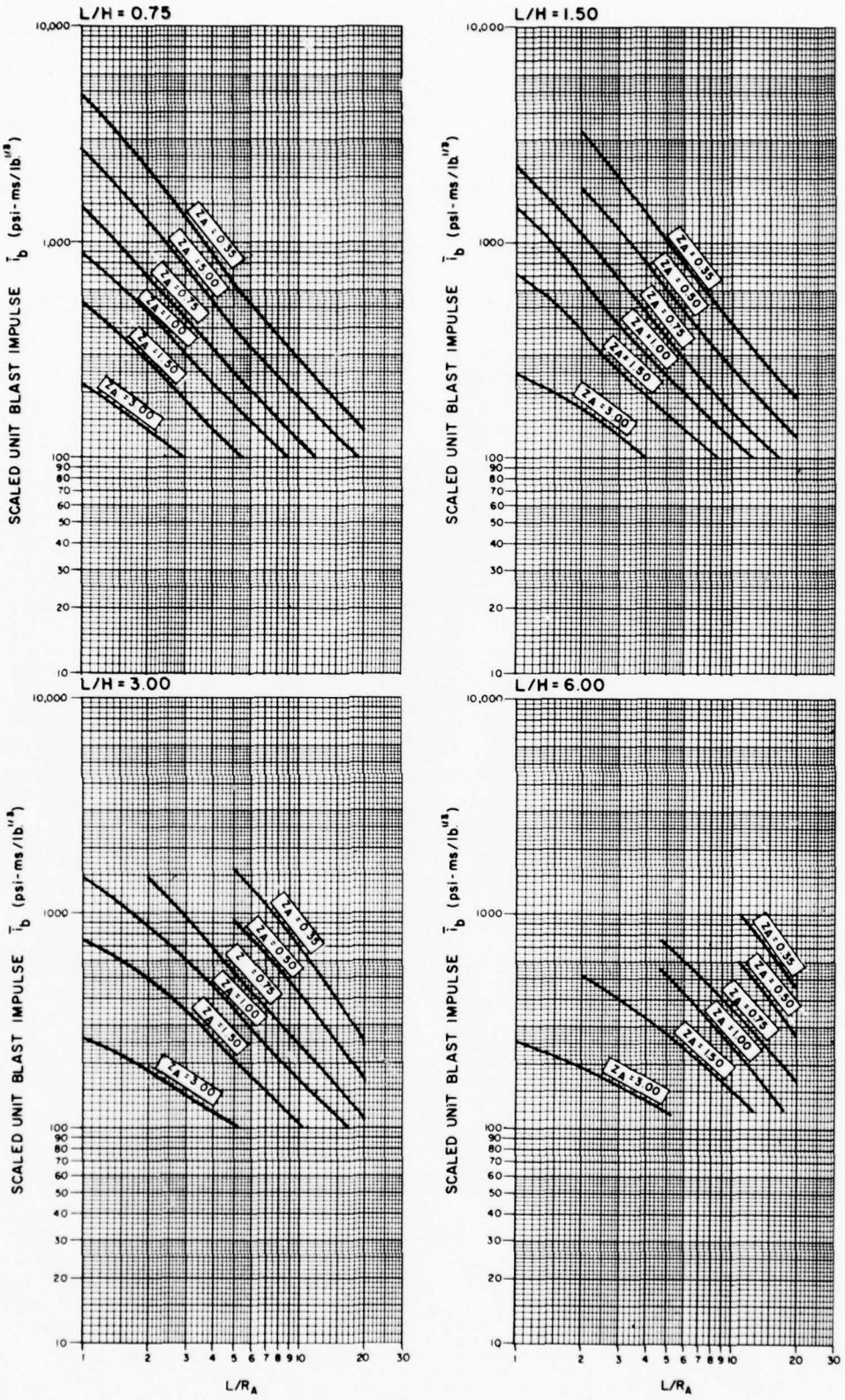

Fig.22 Scaled average unit blast impulse (N = 4, l/L = 0.25 and 0.75, h/H = 0.15)

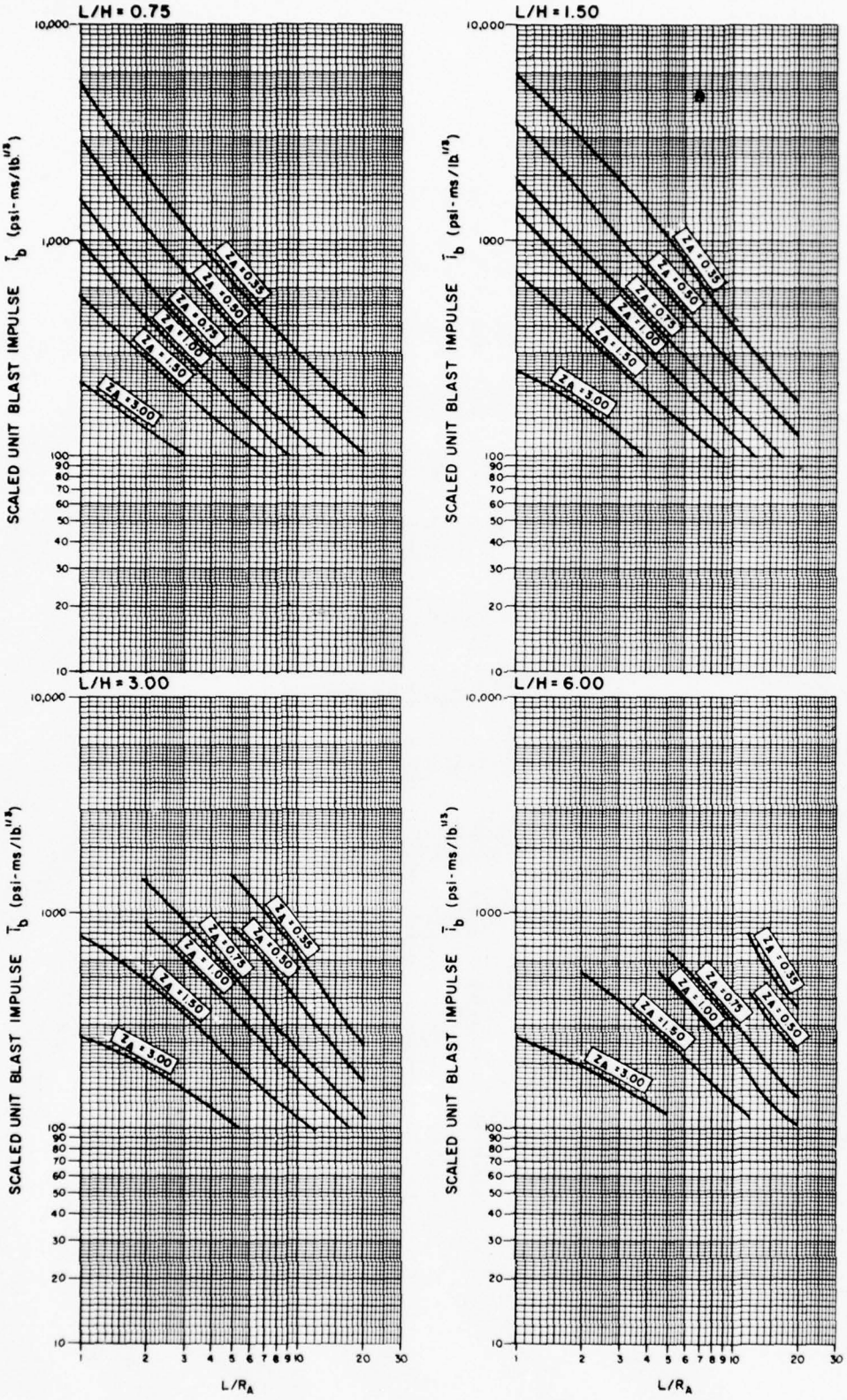

Fig.23 Scaled average unit blast impulse (N = 4, l/L = 0.50, h/H = 0.15)

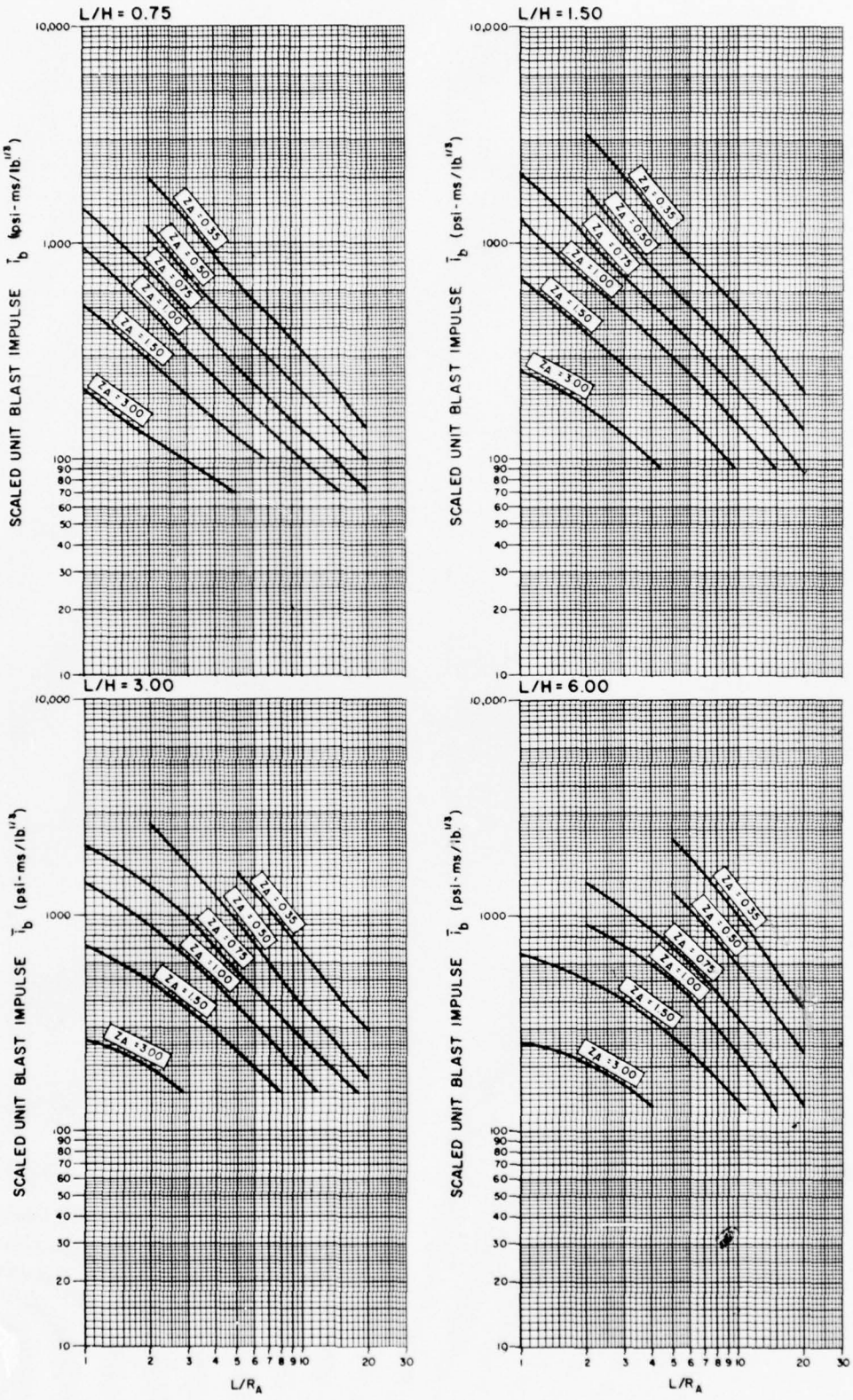

Fig.24 Scaled average unit blast impulse (N = 4, l/L = 0.10, h/H = 0.25 and 0.75)

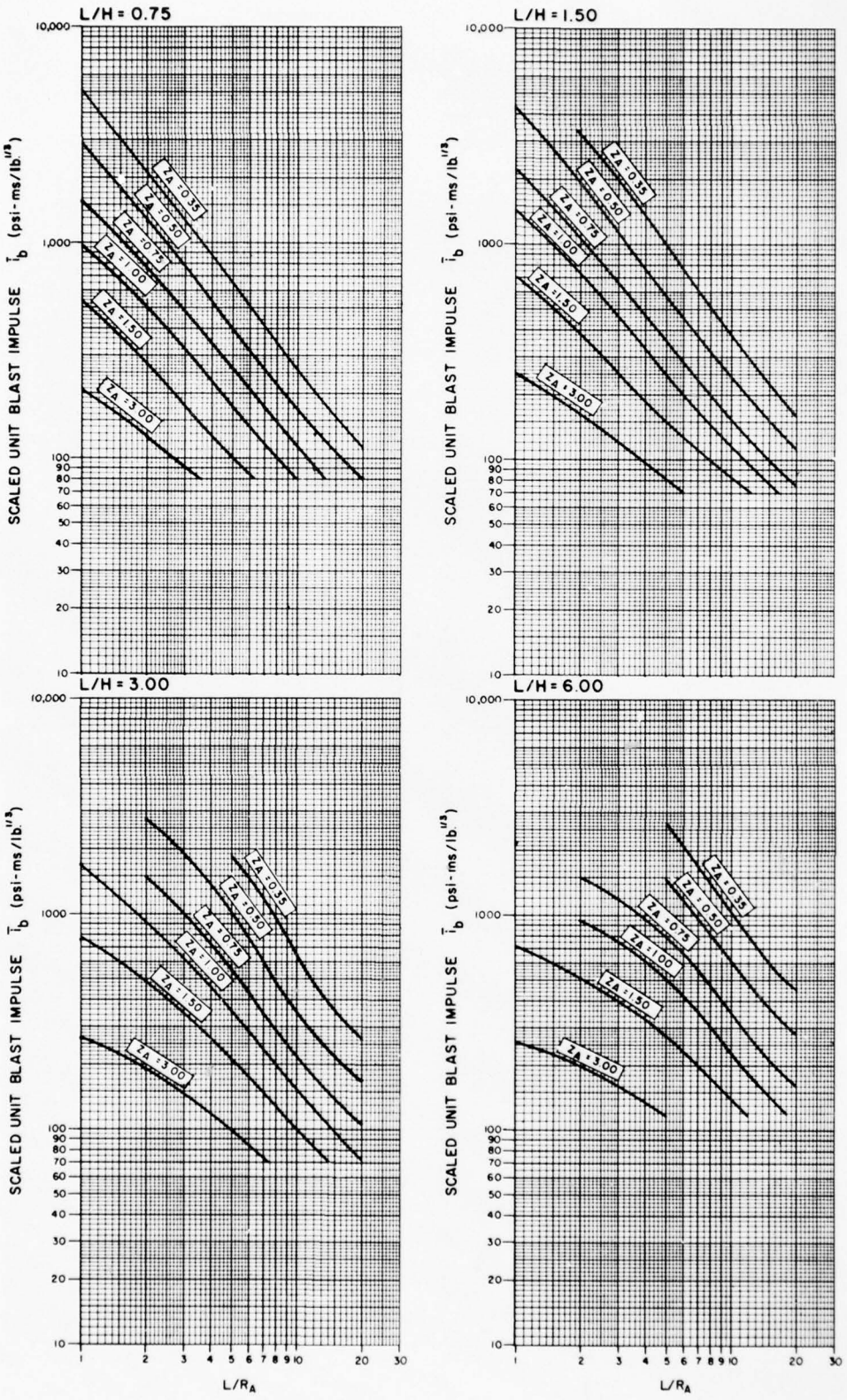

Fig.25 Scaled average unit blast impulse (N = 4, l/L = 0.25 and 0.75, h/H = 0.25 and 0.75)

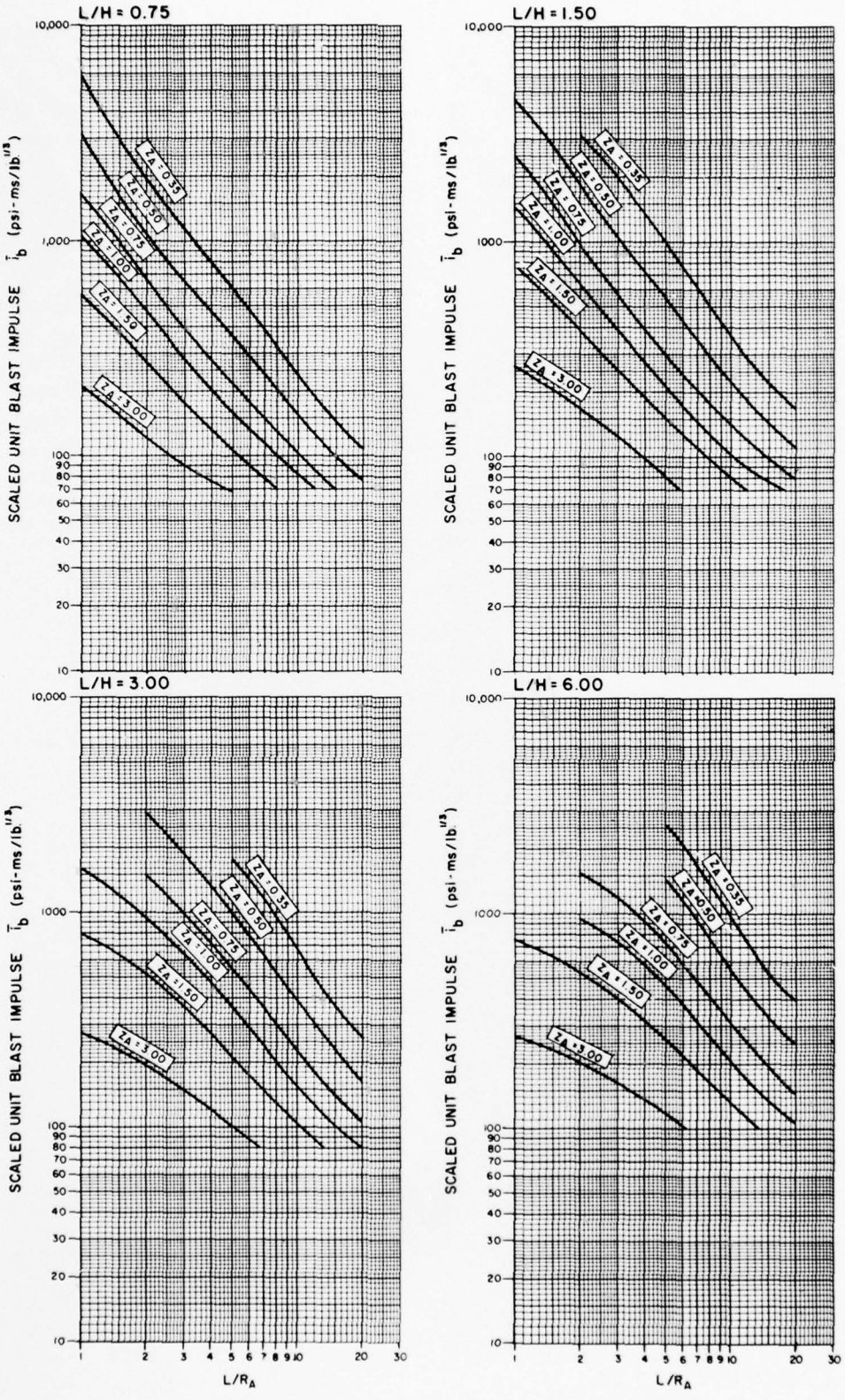

Fig.26 Scaled average unit blast impulse (N = 4, l/L = 0.50, h/H = 0.25 and 0.75)

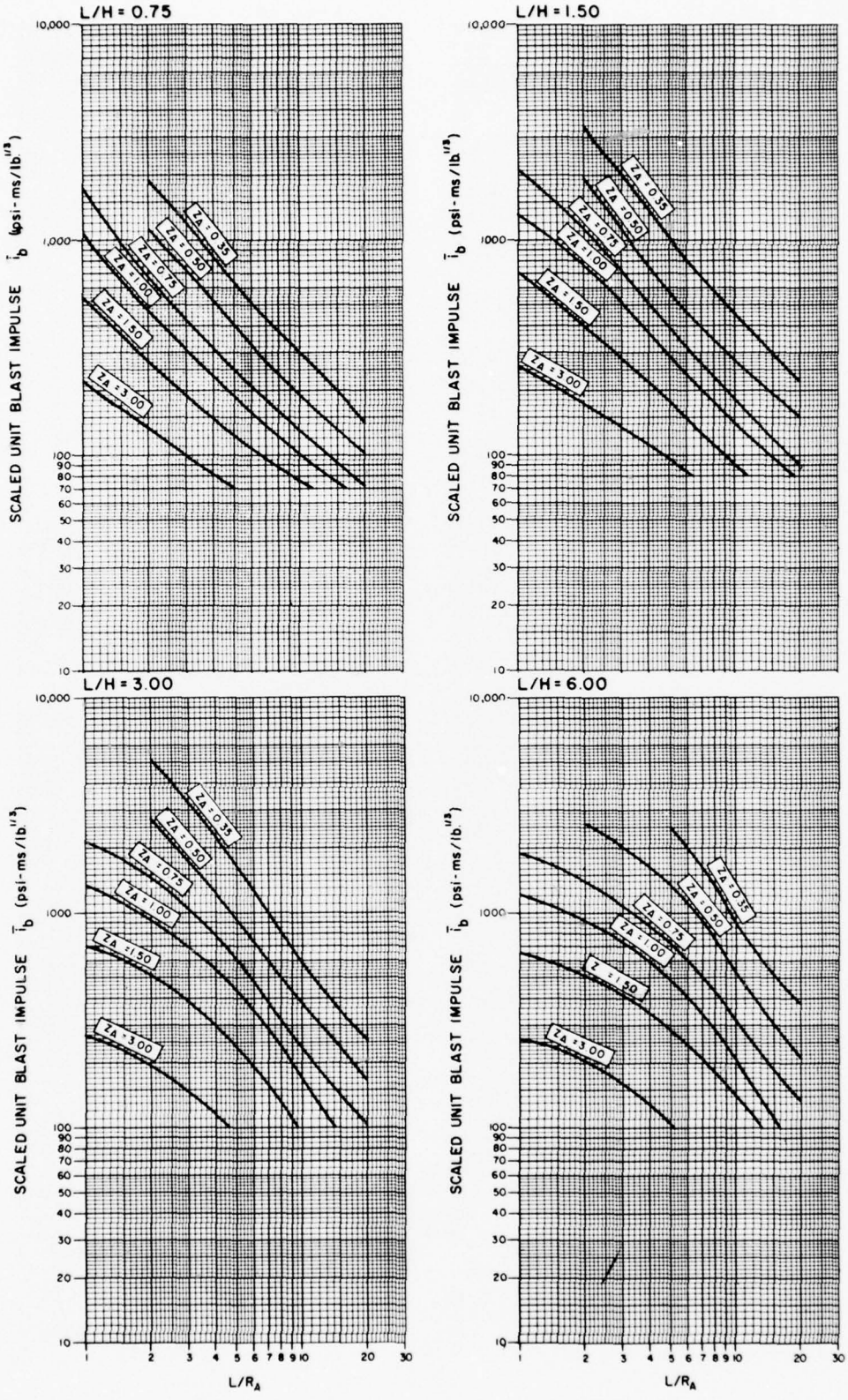

Fig.27 Scaled average unit blast impulse (N = 4, l/L = 0.10, h/H = 0.50)

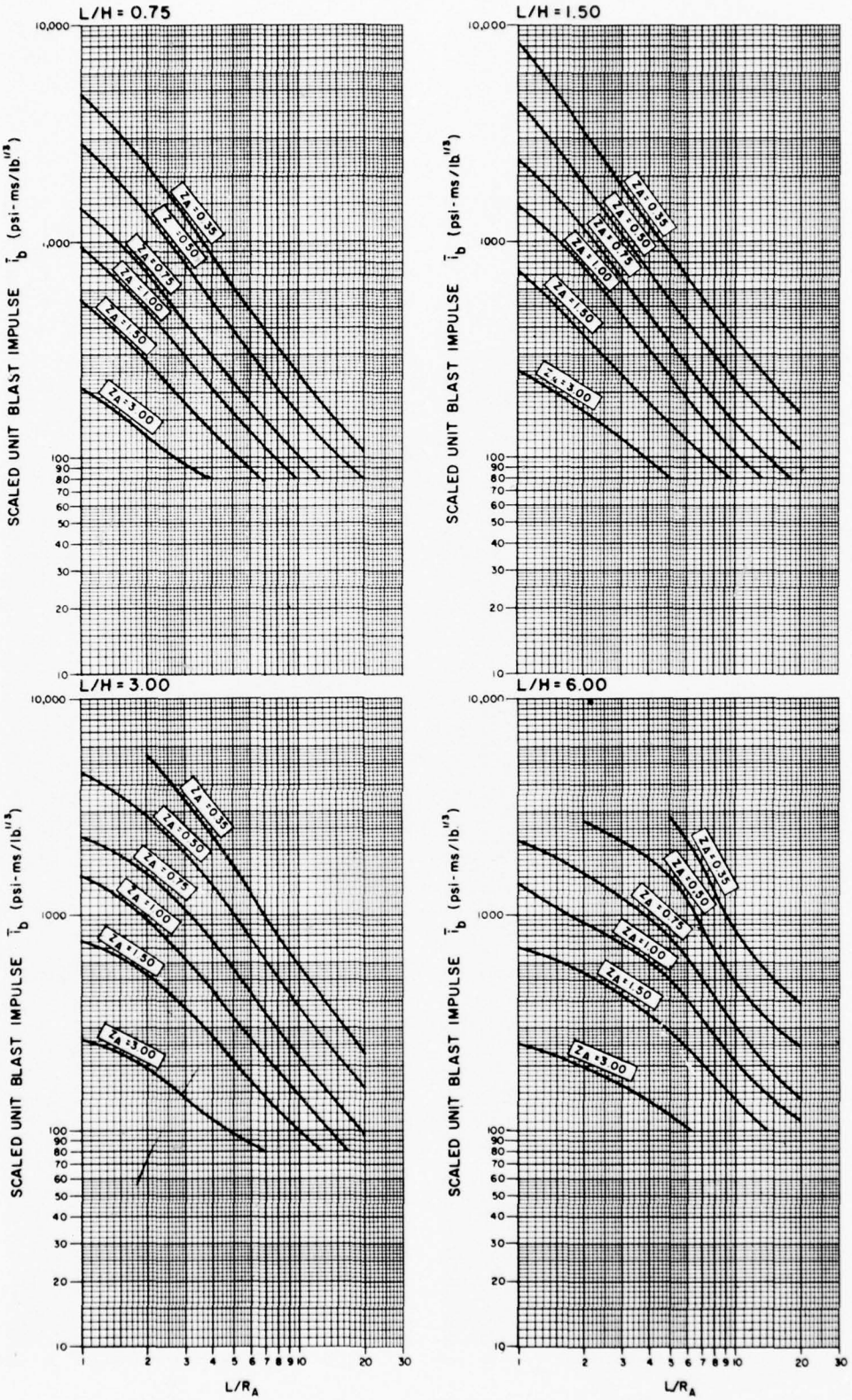

Fig.28 Scaled average unit blast impulse (N = 4, l/L = 0.25 and 0.75, h/H = 0.50)

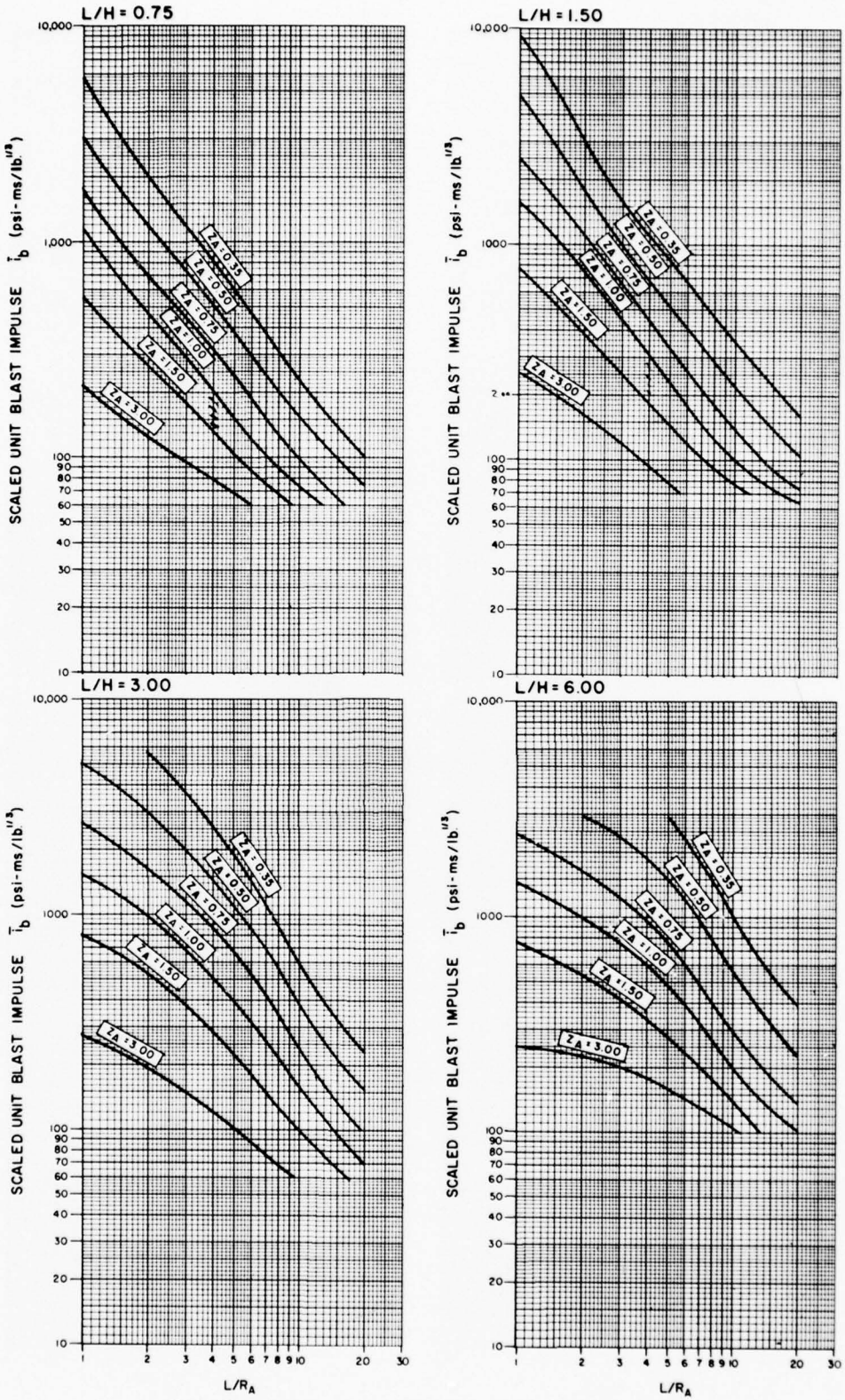

Fig.29 Scaled average unit blast impulse (N = 4, l/L = 0.50, h/H = 0.50)

As previously mentioned, a protective element subjected to the high-pressure range effects of an explosion may be designed for the impulse rather than for the pressure pulse only if the duration of the applied pressures acting on the entire element is short in comparison to its response time. An estimate of this duration may be obtained by adding the time increments corresponding to the time required for the blast wave to fully engulf the element and the duration of the blast load at the section of the element furthest removed from the explosion. This relationship is represented by:

$$t_o = (t_A)_F - (t_A)_A + 1.5(t_o)_F \tag{17}$$

where

t_o = duration of load (ms)

$(t_A)_F$ = time of arrival of the blast wave at the point on the element furthest from the explosion; defined by the largest slant distance.

$(t_A)_F$ = time of arrival of the blast wave at the point on the element nearest to the explosion; defined by the normal distance.

$(t_o)_F$ = duration of the blast pressure at the point on the element furthest from the explosion.

The time of arrival of the blast wave for the two points of interest as well as the duration of the load at the furthest point on the element are obtained from Figure 2. To account for the increased load duration due to the multiple reflections of the blast wave within the cubicle, the value of $(t_o)_F$ has been increased by 50%.

A protective element subjected to the high-pressure range effects of an explosion may have to be designed for the pressure pulse rather than for the impulse effects if the duration of the applied pressures acting on the entire element is long in comparison to the response time of the element (t_m less than $3t_o$). For these cases, the actual pressure-time relationship resulting from a pressure distribution on the element, which is highly irregular due to the multiple reflections and time phasing, may be approximated by a fictitious peaked triangular pressure pulse. The duration t_o of this pulse is obtained from Eq. 17 and a fictitious peak pressure P_f is established as a function of this duration and the average blast impulse i_b (Figures 21 through 29) acting on the element.

$$P_f = \frac{2i_b}{t_o} \tag{18}$$

The above solution for the average impulse load does not account for increased blast effects produced by contact charges.

Partially Vented Explosions

Interior Blast Loadings. When the openings in a cubicle-type structure are small compared to the total surface area, full venting of a contained explosion will not occur. The effect of the reduction of the venting areas from a fully vented configuration is an increase in the interior pressures, impulse, and duration. In addition to the initial shock wave and its reflections, the accumulation of gases from the explosion results in a pressure buildup, and since the venting area is limited, the duration of the pressure is prolonged.

A typical pressure-time record at a point on the surface of a partially vented chamber is shown in Figure 30. The high peaks are the multiple reflections of the initial shock wave. The mean pressure, denoted as P_m, has a long duration when compared to the duration of the shock wave pressures. The maximum mean pressure P_{mo} is used as the basis for design and is a function of the charge weight, contained volume of the chamber, and venting area.

Figure 31 shows an experimentally fitted curve based upon test results of partially vented chambers with small venting areas. The maximum mean pressure is plotted against the charge-volume ratio. The sizes of the venting areas used in the individual tests were relatively small compared to the volume of the chambers and the quantities of explosive, and had no noticeable influence on the maximum pressures recorded.

Since little data are available concerning the duration of these pressures, it is suggested that, for purposes of design, the pressures be assumed to have a very long duration and a constant magnitude insofar as the response of the structure is concerned. The total impulse used in the design of such a cubicle is a combination of the contributions from the initial shock wave, its reflections, and the pressures caused by the gas accumulations. Because of the long duration aspect of the gas accumulation pressures, the strength of the individual elements of the structure must be equal to, or greater than, the pressure P_{mo}, whereas the response of the elements to the initial blast wave and its reflections will be similar to the response of cubicles where full venting is achieved.

Leakage Pressure Loadings. Little data are currently available for the determination of leakage pressures from a partially vented explosion. Table 2 (from Reference 12) lists the experimental venting or "leak" areas. In most cases, rather small leakage areas will vent the structure.

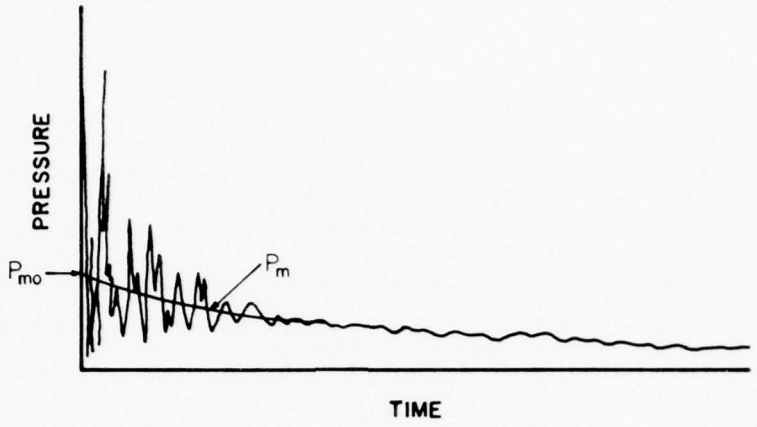

Fig.30 Pressure-time variation for a partially vented explosion

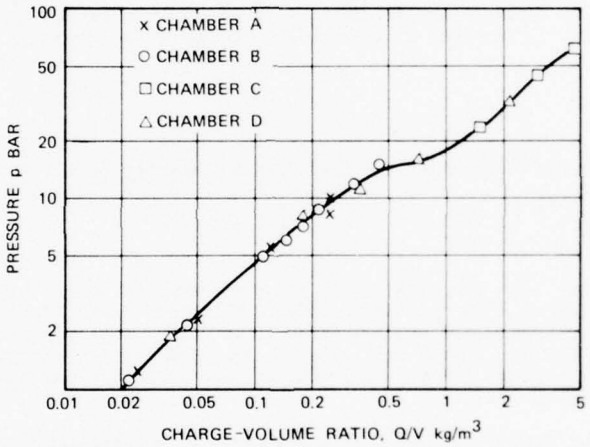

Fig.31 Test results from four chambers, pressure versus charge-volume ratio

TABLE 2

Dimensions of the Chambers Used in the Tests and Their Leak Areas

Mark	Form	Dimensions	Volume, m^3	Leak area, cm^2
A	Sphere	Diam = 0.92 m	0.41	15-80
B	Tube	Diam = 1.5 m Length = 2.5 m	4.5	30-400
C	"Cube"	2.5 x 2.3 x 2.3 m	13.2	25-200
D	Tube	Diam = 2.0 m Length = 8.5 m	28.2	7-2000

SUMMARY AND LIMITATIONS

1. The impulse, peak pressure, and durations of blast waves from spherical charges in air are listed.

(a) Cylindrical charge deviations from spherical behavior are covered.

(b) Momentum and traveling-charge effects are mentioned, although no quantitative effects are listed.

(c) Hopkinson versus Sachs' spherical charge scaling laws (to account for altitude variations) are discussed.

2. The effect of angle of blast wave incidence on lowering of reflected impulse is discussed.

3. Simple methods of computing external blast loads on rectangular structures are discussed.

4. A summary of the single-degree-of-freedom structural response is listed. Suggestions as to how to handle the elastic-plastic response range are included.

5. Critical impulse within a critical time is dicussed.

6. Techniques (assuming rigid surface reflections) used to estimate internal blast loads are covered.

7. Pressure buildup due to products of combustion in partially vented closed chambers is discussed. Limited experimental data are shown.

REFERENCES

1. Departments of the Army, Navy, and Air Force — *Structures to Resist the effects of Accidental Explosions*, Army Technical Manual TM 5-1300, Navy Publication NAVFAC P-397, Air Force Manual AFM 88-22, U.S. Government Printing Office, Washington, D.C., June 1969.

2. Swisdak, Michael M. — *Explosion Effects and Properties, Part 1. Explosion Effects in Air.* NSWC/WOL/TR 75-116, Naval Surface Weapons Center, White Oak, Silver Spring, Md., 6 October 1975.

3. Baker, W. E. et al. — *Similarity Methods in Engineering Dynamics: Theory and Practice of Scale Modeling*, Spartan Books, Hayden Book Company, Inc. Rochelle Park, N.J. 1973.

4. Dewey, Jane M. Sperrazza, J. — "The Effect of Atmospheric Pressure and Temperature on Air Shock," BRL Report No. 721, Aberdeen Proving Ground, Md., 1950.

5. Ericsson, V. Edin, K. — "On Complete Blast Scaling," *Jour. of the Physics of Fluids*, Vol. 3, No. 5, pp. 893-895, September-October 1960.

6. Olson, Jr., W. C. et al. — "The Effect of Atmospheric Pressure on the Reflected Impulse From Blast Waves," BRL Memo Report No. 1421, Aberdeen Proving Ground, Md., January 1960.

7. Jack, Jr., W. H. Armendt, Jr., B. F. — "Measurements of Normally Reflected Shock Parameters From Explosive Charges Under Simulated High Altitude Conditions," BRL Report No. 1280, Aberdeen Proving Ground, Md., April 1965.

8. Brode, H. L. — "Numerical Solutions of Spherical Blast Waves," *Jour. of Appl. Physics*, Vol. 26, No. 6, pp. 766-775, June 1955.

9. Glasstone, S. (Editor) — *The Effects of Nuclear Weapons*, U.S. Atomic Energy Commission, Rev. Ed., pp. 128-129, April 1962.

10. Sewell, R. G. S. Kenney, G. F. — *Response of Structures to Blast: A New Criteria*, Annals of the New York Academy of Sciences, Vol. 152, Art. 1, pp. 532-547, 28 October 1968.

11. Rinehart, J. S. Pearson, John — *Behavior of Metals Under Impulsive Loads*, Published by the American Society for Metals, Cleveland, Ohio, 1954.

12. Weibull, H. R. W. — *Pressures Recorded in Partially Closed Chambers at Explosion of TNT Charges*, Annals of the New York Academy of Sciences, Vol. 152, Art. 1, pp. 357-361, 28 October 1968.

HYDRAULIC RAM PRESSURE PREDICTION AND STRUCTURAL RESPONSE

INTRODUCTION

During penetration of an aircraft fuel cell, bullets and other high-speed projectiles generate intense pressure waves in the fuel. Response of the fuel cell walls to these pressure waves can be catastrophic failure due to severe fracturing of entrance and exit fuel cell walls. This failure is often accentuated, in brittle aluminum cell walls, by the bullet or high-speed projectile wound in the fuel cell wall, and a catastrophic brittle fracture failure at low stress levels, can occur. This phenomenon, termed "hydraulic ram," is of particular importance to the survivability of military aircraft.

A computer program was developed by the Naval Weapons Center which calculates the pressure waves generated by decelerating, tumbling projectiles in a fluid. The theory of hydraulic ram is given in Reference 1. The pressure prediction theory in this report is excerpted from Reference 1. The hydraulic ram structural response theory is described later in this report.

THEORETICAL CONSIDERATIONS

To calculate fluid pressures, it is necessary to know the velocity, rate of kinetic energy loss, and time of projectile arrival as functions of distance along the trajectory. Estimates of these quantities can be obtained by using a simple model of the bullet behavior.

The bullet is assumed to travel in a straight line, and its deceleration is described by Newton's Second Law.

$$m \frac{dV}{dt} = -D \tag{1}$$

where

m = bullet mass

V = bullet velocity

t = time

D = drag force

The drag force can be expressed as

$$D = \frac{1}{2} \rho V^2 A_o C_D \tag{2}$$

[1] Naval Weapons Center. *Fluid Dynamic Analysis of Hydraulic Ram IV*, by E. A. Lundstrom and W. K. Fung. China Lake, CA, NWC, October 1976. (JTCG/AS-74-T-018, publication UNCLASSIFIED.)

where

ρ = fluid density

V = bullet velocity

C_D = drag coefficient of the bullet

A_o = projected frontal area of an unyawed bullet

Noting that

$$V = \frac{dx_b}{dt} \tag{3}$$

where x_b = bullet position along the trajectory, equations 1 and 2 can be combined, yielding

$$\frac{dV}{dx_b} = -\beta V_b \tag{4}$$

Where the velocity decay coefficient, β, is defined as

$$\beta = \frac{1}{2m} \rho C_D A_o \tag{5}$$

the rate of kinetic energy loss, dE/dx_b, where $E = 1/2mV^2$ can be expressed as

$$\frac{dE}{dx_b} = -mV \frac{dV}{dx_b} \tag{6}$$

Combining equations 4 and 6 yields

$$\frac{dE}{dx_b} = m\beta V^2 \tag{7}$$

For tumbling bullets, β is a function of x_b.

In this model the bullet is presumed to enter the test cell with 0 degree yaw and continue in this attitude with a constant drag coefficient until it reaches a distance, x_1, where it begins to tumble. The bullet becomes fully tumbled at a distance, x_2, and continues in this attitude with a constant drag coefficient. However, as evidenced from experimental results,[2] the bullet will impact the cell with 0 degree yaw and continue to tumble along its trajectory for a number of cycles before assuming a stable attitude. The model has an option to include this continuous tumbling of the bullet. The coefficients, β_1 and β_2, are associated with the 0-degree yaw and tumbled attitudes, and the value β_3 is associated with the stern-first attitude. For simplicity it was assumed that the tumbling proceeds at a constant rate along the trajectory (Figure 1); that is

$$x_2 - x_1 = x_3 - x_2 = x_4 - x_3 = \ldots \tag{8}$$

---

[2]Naval Weapons Center. *Fluid Dynamic Analysis of Hydraulic Ram III* by E. A. Lundstrom and W. K. Fung. China Lake, CA, NWC, October 1974. (JTCG/AS-74-T-015, publication UNCLASSIFIED.)

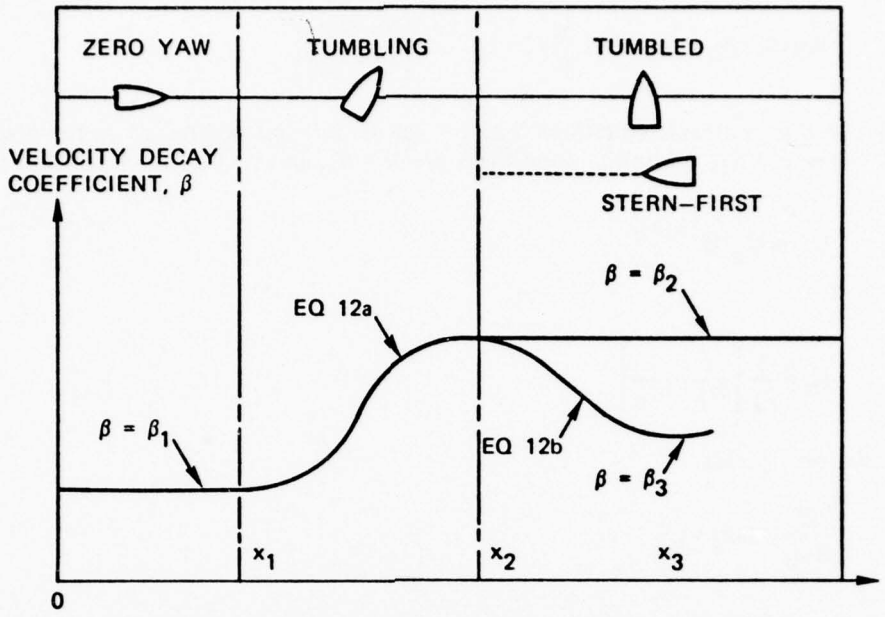

Figure 1. Bullet Orientation Versus Distance Along the Bullet Trajectory.

While the bullet is tumbling, i.e., $x_1, < x_b, < x_2$, β varies radically as a function of x_b. This variation can be expressed in general form as

$$\beta = \beta_1 + (\beta_2 - \beta_1)\, f(Y) \tag{9}$$

where

$$Y = \frac{x_b - x_1}{x_2 - x_1} \tag{10}$$

while

$$f(0) = 0$$

$$f(1) = 1$$

An empirical function of the following form was used.

$$f(Y) = \left[1/2 - 1/2 \cos (Y)\right]^n \tag{11}$$

The exponent, n = 3, is varied (see Footnote 2) yielding the following equations, for $x_1 < x_b < x_2$

$$\beta(x_b) = \beta_1 + (\beta_2 - \beta_1) \left\{1/2 - 1/2 \cos\left[\frac{x_b - x_1}{x_2 - x_1}\right]\right\}^3 \tag{12a}$$

for $x_2 < x_b < x_3$

$$\beta(x_b) = \beta_2 + (\beta_3 - \beta_2) \left\{1/2 - 1/2 \cos\left[\frac{x_b - x_2}{x_3 - x_2}\right]\right\}^3 \tag{12b}$$

When β is constant, equations 3 and 4 can be integrated directly. In the region $0 < x_b < x_1$, where $\beta = \beta_1$, the initial conditions are $V = V_o$ and $t = 0$. The integration then yields

$$V_b = V_o \, e^{-\beta_1 x_b} \tag{13}$$

and

$$t_b = \frac{1}{\beta_1}\left[\frac{1}{V_b} - \frac{1}{V_o}\right] \tag{14}$$

and equation 7 yields

$$\frac{dE}{dx_b} = m\beta_1 V_b^2 \tag{15}$$

In the region of tumbling, $x_1 < x_b < x_2$, algebraic expressions cannot be found; therefore, a numerical integration method is used for the model.

For stripping of bullet jackets from the AP (armor piercing) core of the API (armor-piercing incendiary) ammunition, a crude method for incorporating the jacket energy deposition was developed. The projectile penetrates the fluid for a distance, x_s, where the jacket strips. The kinetic energy of the jacket and incendiary material are calculated at that point. The energy deposition of the AP core is calculated in the normal manner except that values of β appropriate to the core must be used. The energy deposition of the jacket is assumed to be exponential and is added to that of the core. The equation for total energy deposition is

$$\frac{dE}{dx_b} = m_c\beta_c V_b^2 + a\frac{E_{js}}{\beta_j} e^{-\beta_j(x_b - x_s)} \tag{16}$$

$$E_{js} = 1/2 \, m_j \, V_s^2 \tag{17}$$

where

m_j = mass of jacket

V_s = velocity of bullet at stripping location

m_c = mass of core

a = a constant found to be 1/3 (Footnote 2)

Because of the mathematical difficulties introduced by the wall boundary conditions, a simple model (Figure 2) is used which neglects the wall effects.

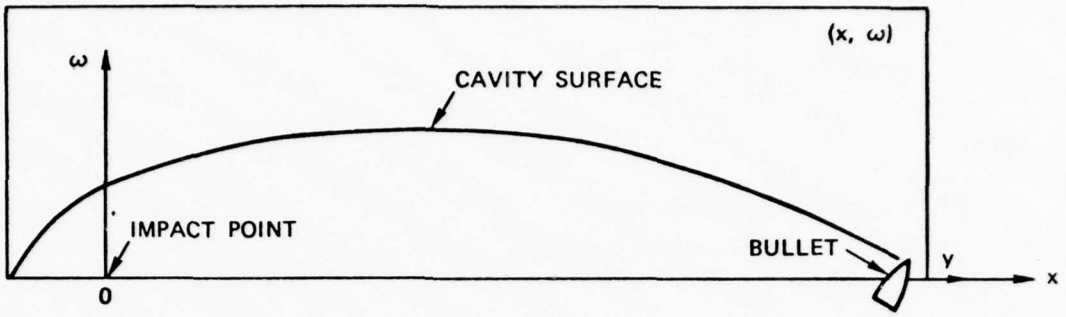

Figure 2. Model of Drag Phase of Hydraulic Ram.

The bullet shown in Figure 2 is initially stationary in an infinite body of fluid until $t = 0$. Then the bullet is impulsively accelerated to an initial velocity of V_o. At times, $t > 0$, the bullet moves with a velocity, V, in a straight line along the axis. It is assumed that the flow field can be described in terms of a potential function, ϕ, which satisfies the wave equation.

$$\nabla^2\phi = \frac{1}{c^2}\frac{\partial^2\phi}{\partial t^2} \tag{18}$$

where c = speed of sound in the fluid.

Then, the fluid velocity, $\vec{u}$, is expressed as

$$\vec{u} = \nabla\phi \tag{19}$$

and the Bernoulli equation yields

$$P = P_o - \rho\frac{\partial\phi}{\partial t} - 1/2\rho u^2 \tag{20}$$

where

P = total fluid pressure

P_o = ambient pressure

ρ = fluid density

$u = |\vec{u}|$

The boundary conditions for equation 18 are that the fluid velocity is tangential to the projectile surface and that $P = P_c$ on the cavity surface, where P_c denotes the pressure in the cavity. It is assumed that P_c is constant throughout the cavity; hence, the problem is to determine the pressure as a function of time at any arbitrary point (x,ω) where, as shown in Figure 2, ω is the perpendicular distance of this point from the x axis.

The problem is further simplified by ignoring the boundary conditions and then approximating the effect of the bullet and cavity on the fluid by the action of a line of sources distributed along the bullet trajectory. Then, the resulting flow field is symmetric about the x axis, and the potential due to these sources can be expressed as

$$\phi(x,\omega,t) = -\int_0^{X_b(\tau)} \frac{\zeta(\xi,\tau)}{r}\, d\xi \tag{21}$$

where

ξ = distance along the trajectory

r = distance between points ξ and (x,ω)

ζ = source strength at ξ

For the finite sound speed, the integral must be evaluated along the line $\tau + r/c$ = constant, where τ is the retarded time given by $\tau = t - r/c$. The integration path is included in the time space representation shown in Figure 3. Using equation 14, the time of bullet arrival, t_b, on the trajectory as a function of the bullet position, x_b, can be determined. However, the results of the theory are not considered to be valid during the cavity collapse; therefore, the lower limit in this integral can be taken as zero. The upper limit, X_b, denotes the projectile position when $\tau = t_b$.

The source strength, ζ, is estimated by a method based on the conservation of energy. It is assumed that the flow is confined to a section, dx, as shown in Figure 4.

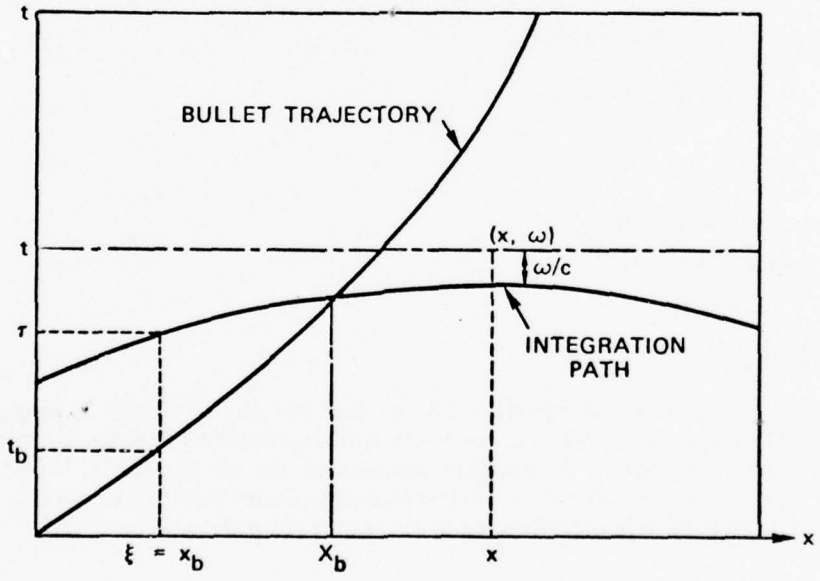

Figure 3. Integration Path of Integral in Equation 21 on the Time-Space Plane.

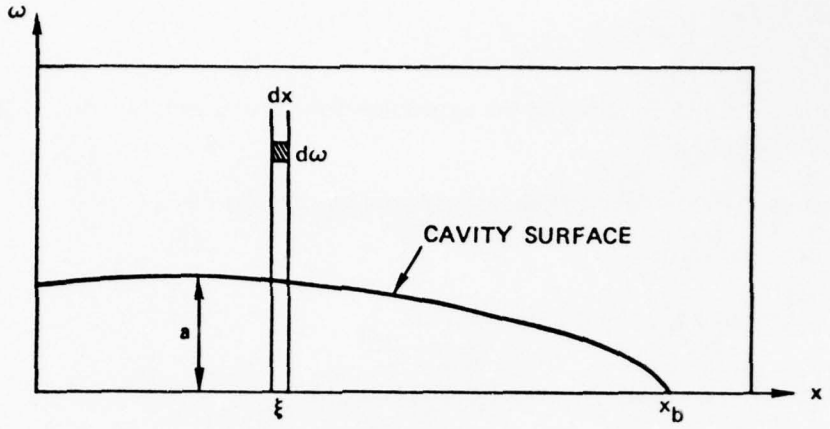

Figure 4. Flow Model for Estimating Cavity Growth and Source Strength Variation.

The fluid velocity in this section is then

$$u = \frac{2\zeta(\xi,t)}{\omega} \tag{22}$$

At the cavity radius, $\omega = a$ and $u = da/dt$ so

$$\zeta = 1/2a \frac{da}{dt} \tag{23}$$

Following Birkoff's theory,[3] the kinetic energy, dK, of the fluid in this section within a radius, Ω, is

$$dK = \left[\pi\rho \int_0^{\Omega} u^2 \omega d\omega\right] dx \tag{24}$$

with equation 22 and integrating

$$dK = 4\pi\rho N\zeta^2 dx \tag{25}$$

where

$$N = \ell n(\Omega/a)$$

Since the upper limit, Ω, cannot be infinite due to the physical impossibility of allowing dK to be infinite, Ω will be assumed to be finite. Because the value of N varies slowly as a function of Ω, it can be treated as a constant. This is justified for the special case in which a bullet is traveling with a constant velocity, since the correct cavity shape is obtained for constant values of the quantity Ω/a in the 15 to 30 range. Physically, this step can be rationalized by considering the neglected influence of the noncylindrical divergence of the flow.

The work, dW, done by the difference between the ambient and cavity pressure is

$$dW = \pi(P_o - P_c)a^2 dx \tag{26}$$

The energy, $d\epsilon$, deposited by the projectile in the fluid at dx is

---

[3] G. Birkoff and E. H. Zarantonello. *Jets, Wakes, and Cavities*. New York, Academic Press, 1957.

$$d\epsilon = \left(\frac{dE}{dx_b}\right)_\xi dx \tag{27}$$

with equations 15 and 16 showing the expression for dE/dx_b as a function of the distance along the trajectory.

The conservation of energy can be expressed by the relation

$$d\epsilon = dK + dW \tag{28}$$

and with equations 25, 26, and 27, it becomes

$$\left(\frac{dE}{dx_b}\right)_\xi dx = 4\pi\rho\zeta^2 N dx + \pi(P_o - P_c)a^2 dx \tag{29}$$

Defining

$$A^2 = \frac{\left(\frac{dE}{dx_b}\right)_\xi}{\pi(P_o - P_c)} \tag{30}$$

$$B^2 = \frac{P_o - P_c}{\rho N} \tag{31}$$

and simplifying, the energy balance yields the expression

$$\zeta = \pm 1/2 B\sqrt{A^2 - a^2} \tag{32}$$

Eliminating ζ from equation 32, with equation 23

$$a\frac{da}{dt} = \pm B\sqrt{A^2 - a^2} \tag{33}$$

With boundary condition a = 0, at the time of projectile arrival, t_b, integration of equation 33 yields

$$\pm\sqrt{A^2 - a^2} = A - B(t - t_b) \tag{34}$$

where, according to equation 32

$$\zeta = 1/2\left[BA - B^2(t - t_b)\right] \tag{35}$$

The cavity behavior reaches a maximum radius when da/dt = 0. From equation 33, this radius is A, and from equation 34, the maximum radius occurs at time, t_m, at

$$t_m = t_b + \frac{A}{B} \tag{36}$$

The effects of the walls were neglected, so equations 30 and 31 give only the upper bounds

for A and B; hence the source strength, equation 35, will be increasingly inaccurate as the cavity approaches its maximum inside an actual fuel cell.

Now, the pressure field resulting from the line of sources can be calculated. Substituting equation 35 for the source strength in equation 21 yields

$$\phi(x,\omega,t) = -1/2B \int_0^{X_b(\tau)} \frac{1}{r}\left\{A(\xi) - B\left[t - \frac{r}{c} - t_b(\xi)\right]\right\} d\xi \tag{37}$$

Note that the retarded time τ in equation 21 was replaced by t - r/c.

To compute the pressure, the terms in Bernoulli's equation (equation 20) must be evaluated. The term, $\partial\phi/\partial t$, in Bernoulli's equation can be expressed in a simple form by using Leibnitz's rule for the differentiation of integrals. Equation 37 becomes (see Appendix A)

$$\frac{\partial\phi}{\partial t} = -1/2\left[\frac{BA_b}{R_b}\frac{\partial X_b(\tau)}{\partial t}\right] + 1/2\,B^2 \int_0^{X_b(\tau)} \frac{d\xi}{r} \tag{38}$$

where R_b is the distance between the bullet and the point (x,ω) and A_b denotes the value of A, evaluated at X_b. The chain rule for differentiation gives

$$\frac{\partial X_b(\tau)}{\partial t} = \frac{\partial X_b(\tau)}{\partial \tau}\frac{\partial \tau}{\partial t} \tag{39}$$

where

$$\frac{\partial X_b}{\partial \tau} = V \tag{40}$$

where V is the bullet velocity evaluated at X_b, and since

$$\frac{\partial \tau}{\partial t} = 1 - \frac{1}{c}\frac{\partial R_b(\tau)}{\partial t} = 1 + \frac{1}{c}\frac{x - X_b}{R_b}\frac{\partial X_b(\tau)}{\partial t} \tag{41}$$

equation 39 becomes

$$\frac{\partial X_b(\tau)}{\partial t} = V\left[1 + \frac{1}{c}\frac{x - X_b}{R_b}\frac{\partial X_b(\tau)}{\partial t}\right] \tag{42}$$

Solving for $\partial X_b(\tau)/\partial t$ gives

$$\frac{\partial X_b(\tau)}{\partial t} = \frac{V}{1 - \frac{V}{c}\frac{x - X_b}{R_b}} \tag{43}$$

With equation 43 and solving the integral, equation 38 becomes

$$\frac{\partial \phi}{\partial t} = -1/2 \frac{BA_b}{R_b} \frac{V}{1 - \frac{V}{c} \frac{x - X_b}{R_b}} + 1/2 B^2 \ell n \left[\frac{x + R_o}{x - X_b + R_b} \right] \tag{44}$$

where R_o is the distance between the impact point and the point (x,ω). In the same manner the fluid velocity components, u_x in the x direction and u_ω in the ω direction, can be derived as

$$u_x = \frac{\partial \phi}{\partial x} = 1/2 \frac{BA_b}{R_b} \frac{\frac{V}{c} \frac{x - X_b}{R_b}}{1 - \frac{V}{c} \frac{x - X_b}{R_b}}$$

$$+ 1/2B \int_o^{X_b(\tau)} \left\{ A(\xi) - B\left[t - t_b(\xi) \right] \frac{x - \xi}{r^3} \right\} d\xi \tag{45}$$

$$u_\omega = \frac{\partial \phi}{\partial \omega} = 1/2 \frac{BA_b}{R_b} \frac{\frac{V}{c} \frac{\omega}{R_b}}{1 - \frac{V}{c} \frac{x - X_b}{R_b}}$$

$$+ 1/2B\omega \int_o^{X_b} \left\{ A(\xi) - B\left[t - t_b(\xi) \right] \right\} \frac{1}{r^3} \, d\xi \tag{46}$$

It should be noted that functions $A(\xi)$ and $t_b(\xi)$ depend on the tumbling behavior of the bullet. Hence, the integrals in equations 45 and 46 cannot be evaluated explicitly. Noting the reaction that

$$u^2 = u_x^2 + u_\omega^2 \tag{47}$$

the pressure field can be obtained by substituting equations 44, 45, 46, and 47 into Bernoulli's equation 20.

Waves reflected from rigid plane walls can be calculated exactly by means of the method of images. The boundary condition for a rigid wall is that the normal component of the fluid velocity, u_n, vanishes at the wall. Pressure generated by the bullet has been approximated by a line of sources (or sinks). The boundary condition at the wall can be satisfied by adding the pressure due to a mirror image line of sources (or sinks) as illustrated in Figure 5.

The boundary condition for a free surface is P = 0 at the surface. A negative mirror image satisfies this condition to the extent that

$$\left|\frac{\partial \phi}{\partial t} + 1/2 u_t^2\right| >> \left|1/2 u_n^2\right| \tag{48}$$

where u_t and u_n are the tangential and normal fluid velocity components at the surface. Equation 48 is satisfied for most conditions during the initial phase of hydraulic ram.

The method of images is easily extended to calculate reflections from the walls of rectangular volumes. The result is a three-dimensional rectangular array of images. The number of images in the array is determined by the number of wave reflections to be included in the calculation. A method for automatic generation of the image array coordinates was developed, and its use is discussed in Appendix B.

The walls of aircraft fuel cells are neither free nor rigid. However, due to their typically light construction, waves reflected from these walls can be approximated by means of the method of images for free surfaces. The effect of the inertial properties of the fuel cell walls on wave reflections is discussed in the Lundstrom report (Footnote 1).

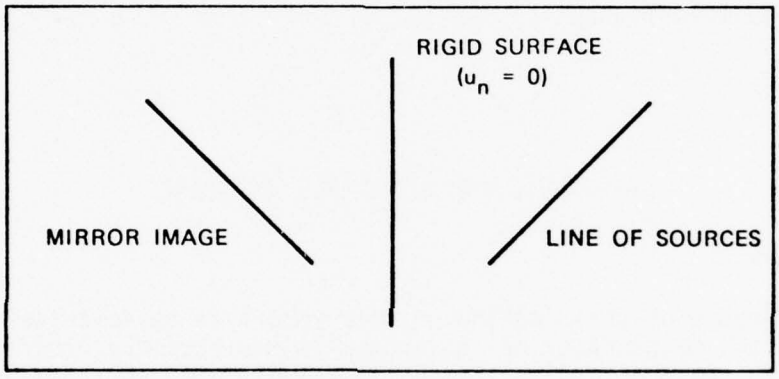

Figure 5. Geometry of Method of Images for a Single Rigid Surface.

SUMMARY

The pressure is calculated according to Bernoulli's equation

$$P - P_o = -\rho \frac{\partial \phi}{\partial t} - 1/2 \rho u^2$$

The first term is dominant far from the bullet, while the second term is important closer to the bullet. The boundary condition P = 0 at the surface is satisfied by the method of images for the $\rho\ \partial\phi/\partial t$ term only. It is suggested that the full equation be used to calculate incident pressure waves on the wall.

Although the action of the cavity behind the bullet is accounted for in the fluid model, the absence of fluid within the cavity is ignored. Therefore, in the absence of external surfaces, the calculated pressure will be positive outside the cavity, zero on the cavity surface, and negative within the cavity. Indeed, the pressure will go to minus infinity as the cavity axis is approached. In addition, the cavity presents an additional surface for reflecting

pressure waves. Thus, waves arising from the bullet, reflecting from the fluid volume surface, and then *reflecting from the cavity surface* are not accounted for.

The presence of the bounding free surfaces of the fluid volume often produces large negative pressures within the fluid, thus producing bulk cavitation. These phenomena are not included in the fluid model.

It is suggested that the pressure calculated by the program be truncated at negative pressures; that is, if

$$P \leq O$$

then

$$P = 0$$

This process assumed that bulk cavitation always occurred and also automatically accounted for the absence of fluid in the cavity.

Since the bullet is modeled by a line of sources, the pressure goes to infinity at the bullet. It is suggested that the pressure calculated by the program be truncated at the stagnation pressure of the bullet.

HYDRAULIC RAM STRUCTURAL RESPONSE

INTRODUCTION

The purpose of this section of this report is to describe modifications to the methodology of the Hydraulic Ram Pressure Program discussed in the previous section. These modifications allow for the determination of the wall deflections that result from projectile interaction with a fluid-filled rectangular tank. The theory and example discussed are for the exit tank wall. However, the theory should be easily extended to the other tank walls as required.

In the development of the theory for Hydraulic Ram Pressure Prediction, the time variation of the pressure can be calculated at various points internal to a fuel tank that has been impacted by a projectile. The pressure prediction theory stipulated that wall reflections could be modeled by line sources which were negative mirror images (sinks) of the sources modeling the original projectile penetration. Under these conditions, the sides of the tank are represented as free surfaces, and hence, by definition, the tank wall pressure is zero at all times. The hydraulic ram structural response theory, now to be described, modifies this so as to allow calculation of wall response by the so-called "variable image" theory.

STRUCTURAL RESPONSE THEORY

The specific response model that is used replaces the mirror image from the exit wall used in version one of the code with an infinite void.

Consequently, a pressure distribution $p_z(xyt)$ and a fluid velocity $u_z(xyt)$ can be calculated at the position of the exit wall. The structural response of the exit wall which acts against this pressure is based on Foppls' calculation.[4] The assumption is that the total response pressure, q, generated by the wall is such that

$$q = q_1 + q_2$$

where q_1 is due to the load resisted by bending (theory of small deflections) and q_2 is due to the load resisted by membrane stress. For a given displacement, z_o, one can calculate the total strain energy, U, which is given by the expression

$$U = U_1 + U_2$$

where

U_1 = bending strain energy

U_2 = membrane strain energy

Timoshenko et al[4, 5] have determined the analytical forms for the membrane and bending strain energies under uniform pressure for a plate of horizontal length, a, and vertical length, b. The wall deflection is assumed to have the form

$$z = z_o \cos\left(\frac{\pi x}{a}\right)\cos\left(\frac{\pi y}{b}\right)$$

where x, y are the transverse coordinates on the wall; a, b are the associated widths; and z_o is the center deflection.

The resulting energy expressions are given by

$$U_1 = \frac{\pi^4(ab)(Eh^3)(z_o^2)}{8(12)(1-\nu^2)}\left(\frac{1}{a^2}+\frac{1}{b^2}\right)^2 \qquad (49)$$

---

[4] S. Timoshenko and S. Woinowsky-Krieger. *Theory of Plates and Shells*, 2nd Ed. New York, McGraw-Hill Book Company, Inc., 1959, pp. 415–420.

[5] S. Timoshenko, et al . *Vibration Problems in Engineering*, 4th Ed. New York, Wiley and Company, 1974, p. 443.

$$U_2 = \frac{Eh}{2(1-\nu^2)}\left\{\frac{\pi^4 z_o^4}{256}\left[9\left(\frac{b}{a^3}+\frac{a}{b^3}\right)+\frac{2}{ab}\right]\right.$$

$$-\frac{\pi^2 C z_o^2}{3}\left[\frac{1}{2}\left(\frac{1}{a}+\frac{1}{b}\right)+2\left(\frac{a}{b^2}+\frac{b}{a^2}\right)\right]$$

$$+\frac{9}{8}\pi^2 C^2\left(\frac{a}{b}+\frac{b}{a}\right)+\frac{16}{9}C^2$$

$$\left.+\nu\left[\frac{\pi^2 C z_o^2}{2}\left(\frac{1}{a}+\frac{1}{b}\right)-\frac{\pi^2 C^2}{8}\left(\frac{a}{b}+\frac{b}{a}\right)+\frac{16}{9}C^2\right]\right\} \tag{50}$$

where

ν = Poisson's ratio

E = modulus of elasticity

h = plate thickness

and

$$C = \pi^2 z_o^2\left\{\frac{(6-18\nu)\left(\frac{1}{a}+\frac{1}{b}\right)+24\left(\frac{a}{b^2}+\frac{b}{a^2}\right)}{4(32)(1+\nu)+9(9-\nu)\pi^2\left(\frac{a}{b}+\frac{b}{a}\right)}\right\} \tag{51}$$

for

$$\frac{\partial U_2}{\partial C} = 0$$

The kinetic energy term for the wall deflection is given by

$$T = \frac{\gamma h}{2g}\frac{ab}{4}\dot{z}_o^2$$

where

$\frac{\gamma h}{g}$ = mass/unit area of plate

This allows the establishment of the Lagrangian L = T - U and its associated differential equation so that

$$\left(\frac{\partial}{\partial t}\right)\left(\frac{\partial L}{\partial \dot{z}_o}\right) - \left(\frac{\partial L}{\partial z_o}\right) - Q = 0$$

where Q represents the pressure forcing function due to the projectile-fluid interaction and is related to the total weighted average pressure at the wall such that

$$Q = \left(\frac{2}{\pi}\right)^2 ab\bar{p}_T$$

where

$$\bar{p}_T = \left(\frac{\pi}{2}\right)^2 \frac{1}{ab} \int_{-b/2}^{b/2} \int_{-a/2}^{a/2} p_T(xyt) \cos\left(\frac{\pi x}{a}\right) \cos\left(\frac{\pi y}{b}\right) dxdy \qquad (52)$$

From the Lagrangian formulation,

$$\ddot{z}_o + \frac{g}{\gamma h} \frac{\pi^4 Eh^3}{12(1-\gamma^2)} \left(\frac{1}{a^2} + \frac{1}{b^2}\right)^2 z_o$$

$$+ \frac{Eh}{(1-\nu^2)} \frac{2g}{\gamma h} \frac{1}{ab} \left\{ \frac{\pi 4}{64} \left[9\left(\frac{b}{a^3} + \frac{a}{b^3}\right) + \frac{2}{ab} \right] \right.$$

$$- \frac{4}{3}\pi^2 \, coe \left[\frac{1}{2}\left(\frac{1}{a} + \frac{1}{b}\right) + 2\left(\frac{a}{b^2} + \frac{b}{a^2}\right) \right]$$

$$+ \frac{9}{2}\pi^2 (coe)^2 \left(\frac{a}{b} + \frac{b}{a}\right) + \frac{64}{9}(coe)^2$$

$$+ \nu \left[2\pi^2 \, coe \left(\frac{1}{a} + \frac{1}{b}\right) - \frac{\pi^2}{2}(coe)^2 \left(\frac{a}{b} + \frac{b}{a}\right) \right.$$

$$+ \frac{64}{9} (coe)^2 \Bigg] \Bigg\} z_o^3 - \frac{g}{\gamma h} \frac{16}{\pi^2} \bar{p} = 0 \tag{53}$$

where

$$coe = \pi^2 \left\{ \frac{(6 - 18\nu)\left(\frac{1}{a} + \frac{1}{b}\right) + 24\left(\frac{a}{b^2} + \frac{b}{a^2}\right)}{4(32)(1 + \nu) + 9(9 - \nu)\pi^2\left(\frac{a}{b} + \frac{b}{a}\right)} \right\} \tag{53a}$$

The pressure distribution is calculated from the pressures due to the fluid-bullet interaction evaluated at the exit surface. A problem with this formulation is that values are generated for the wall velocity which exceed the particle velocity of the fluid. To correct this deficiency, a variable image technique is employed. This allows the interaction to be modified through the fluid potential function in such a manner as to preserve the continuity between the plate velocity and particle velocity of the fluid.

Using the potential function, ϕ_i, associated with the incident pressure wave and Bernoulli's equation, then

$$p_i = -\rho \frac{\partial \phi_i}{\partial t} - \frac{1}{2} \rho u_1^2 \tag{54}$$

where ϕ_i includes the potential produced by the projectile and by the waves reflected from the walls of the container exclusive of the exit wall. p_i is the incident pressure, ρ is the density of the fluid and u_i is the fluid velocity where $u_i = \nabla \phi_i$. Now assume that the potential of the reflected wave from the exit wall has the form $\phi_r = k\tilde{\phi}_i$ where k varies in time and space and $\tilde{\phi}_i$ is the mirror image of ϕ_i.

Bernoulli's equation for the reflected wave gives

$$p_r = -\rho \frac{\partial \phi_r}{\partial t} = - k\tilde{p}_i - \tilde{\rho}\tilde{\phi}_i \left(\frac{\partial k}{\partial t}\right) \tag{55}$$

and with similar substitution

$$u_{rn} = \frac{\partial \phi_r}{\partial n} = k\tilde{u}_{ni} + \tilde{\phi}_i\left(\frac{\partial k}{\partial n}\right) \tag{56}$$

where n indicates the normal at the exit surface. Since the u^2 term in equation 2 can be considered small relative to the potential term, it will be ignored in these and subsequent equations. At the wall, $\tilde{\phi}_i$ equals ϕ_i and $\partial\phi_i/\partial n$ equals $-\partial\tilde{\phi}_i/\partial n$. From piston theory, a plane reflected wave is assumed, propagating parallel to the wall normal such that

$$p_r = -\rho c u_{rn} \text{ and } p_i = \rho c u_{in} \tag{57}$$

where c is the velocity of sound in the fluid.

Substituting equation 56 into equation 57,

$$p_r = +\rho c k u_{ni} - \rho c \phi_i \left(\frac{\partial k}{\partial n}\right) = k p_i - \rho c \phi_i \left(\frac{\partial k}{\partial n}\right) \tag{58}$$

but from equation 55,

$$p_r = k p_i - \rho \phi_i \left(\frac{\partial k}{\partial t}\right) \tag{59}$$

Comparing equations 58 and 59,

$$\frac{\partial k}{\partial n} = \left(\frac{1}{c}\right)\left(\frac{\partial k}{\partial t}\right) \tag{60}$$

Thus the total pressure at the wall is

$$p_T = p_i + p_r = (1 + k)p_i - \rho \phi_i \left(\frac{\partial k}{\partial t}\right) \tag{61}$$

Similarly, if equation 56 is substituted into an expression that equates the wall and fluid velocities at the wall,

$$\dot{z} = u_{in} + u_{rn} = (1 - k)u_{ni} + \left(\frac{\phi_i}{c}\right)\left(\frac{\partial k}{\partial t}\right)$$

or

$$\frac{\partial k}{\partial t} = - \frac{c}{\phi_i} \left[(1 - k) u_{ni} - \dot{z} \right]$$

Eliminating the derivative from p_T,

$$p_T = (1 + k) p_i + \rho c \left[(1 - k) u_{ni} - \dot{z} \right]$$

To derive an expression equivalent to the weighted average pressure at the exit wall, this equation must be integrated by substituting into the expression for the forcing function. This gives

$$\bar{p}_T = (1 + k) \bar{p}_i + \rho c (1 - k) \bar{u}_{ni} - \rho c \left(\frac{\pi}{4} \right)^2 \dot{z}_o \tag{62}$$

and, equivalently,

$$\frac{\partial k}{\partial t} = - \frac{c}{\bar{\phi}_i} \left[(1 - k) \bar{u}_{ni} - \left(\frac{\pi}{4} \right)^2 \dot{z}_o \right] \tag{63}$$

where k is assumed uniform at the exit wall. Given the initial pressures and fluid velocities at specific time increments, one can then calculate the pressure $\bar{p}_T$ and the time variation of k, z_o, and $\dot{z}_o$. These values are then used to predict a new set of variables at the next time increment which are finally averaged with the initial set to yield the final parameters for the given time interval. The pressures used in the calculations are gauge pressures and are allowed to go negative. For time intervals exceeding the time for maximum deflection, this formulation occasionally generates unrealistic results. However, experimental data and data obtained from these calculations tend to be reasonably consistent for the time intervals of interest.

The magnitude of the stress on the exit plate due to these deflections can also be estimated. From Hooks Law, an empirical relation is established between the components of stress and strain in a given body. For a thin plate,[6] the equations relating the unit elongations ε_x and ε_y and the normal stresses σ_x and σ_y become

---

[6] S. Timoshenko and J. N. Goodier. *Theory of Elasticity*. New York, McGraw-Hill Book Company, Inc., 1951, p. 24.

$$\varepsilon_x = \frac{1}{E}(\sigma_x - \nu\,\sigma_y) \qquad \varepsilon_y = \frac{1}{E}(\sigma_y - \nu\,\sigma_x) \tag{64}$$

where E is the modulus of elasticity and ν is Poisson's ratio. Using the equations for the plate displacements and the basic relations for the unit elongations (ε_x and ε_y) given by Timoshenko,[4] at the center of the exit plate,

$$\varepsilon_x = (\text{coe})\,\frac{2\pi}{a}\,z_o^2 \quad \text{and} \quad \varepsilon_y = (\text{coe})\,\frac{2\pi}{b}\,z_o^2 \tag{65}$$

where coe is determined in equation 53a. Solving equation 64 for σ_x and σ_y and substituting equation 65,

$$\sigma_x = \frac{E}{1-\nu^2}\,2\pi\,(\text{coe})\left(\frac{1}{a} + \frac{\nu}{b}\right) z_o^2$$

$$\sigma_y = \frac{E}{1-\nu^2}\,2\pi\,(\text{coe})\left(\frac{1}{b} + \frac{\nu}{a}\right) z_o^2$$

These are the expressions for the stress used in the code.

All these relations apply to the special case of a planar wave normally incident on a planar wall and are assumed to be adequate for all situations input to the code. The more general expression for the pressure introduced in this section reduces to the piston theory expressions for the pressure for transmissive, rigid, and free surfaces when the parameter, k, has the values of 0, 1, and -1, respectively. The parameter, k, is listed in the output and its variation models these various wall response conditions.

EXPERIMENTS

Experiments were performed with a 5-ft-high by 5-ft-wide by 2-ft-thick water-filled test cell. A number of 12.7-mm API rounds were fired through the 2-ft thickness. The exit wall was a 20-inch-square, 0.125-inch-thick aluminum sheet that was rigidly clamped at the edges. Deflection of the exit wall was measured by two high-speed camera viewing the exit wall profile from the top and from the side. Details of the experiment are described in a paper by Ankeney.[7]

---

[7] D. P. Ankeney, "Hydraulic Ram Structural Response," presented at the Hydrodynamic Ram Seminar, Dayton, Ohio, 20–22 October 1976.

An equation of motion for the exit wall deflection is previously derived in this report. The derivation assumes a wall deformation in the form

$$Z = Z_0 \cos \frac{\pi x}{\ell} \cos \frac{\pi y}{\ell} \tag{66}$$

where x and y are transverse coordinates on the wall, ℓ is the width of the square panel, and Z_0 is the panel center deflection.

Using the Lagrange equation, a second-order, nonlinear, ordinary differential equation for Z_0 was obtained. The effects of plate mass, and elastic bending and membrane stresses are included. The forcing function for this equation is the weighted average pressure at the wall

$$\bar{p}_T = \left(\frac{\pi}{2\ell}\right)^2 \int_{-\ell/2}^{\ell/2} \int_{-\ell/2}^{\ell/2} p_T(x,y,t) \cos\left(\frac{\pi x}{\ell}\right) \cos\left(\frac{\pi y}{\ell}\right) dxdy \tag{67}$$

Assuming k is uniform across the plate, repeating equation 62 gives

$$\bar{p}_T = (1 + k)\, \bar{p}_i + \rho\, c(1 - k)\, \bar{u}_{ni} - \rho\, c\left(\frac{\pi}{4}\right)^2 \dot{Z}_0 \tag{68}$$

Similarly, an equation for k is obtained by integrating equation 63

$$\frac{\partial k}{\partial t} = \frac{c}{\bar{\phi}_i} \left[(1 - k)\, \bar{u}_{ni} - \rho\, c\left(\frac{\pi}{4}\right)^2 \dot{Z}_0\right] \tag{69}$$

The weighted average incident pressure $\bar{p}_i$ and normal fluid velocity $\bar{u}_{ni}$ are obtained from the previously discussed theory. In practice, the integrals for $\bar{p}_i$ and $\bar{u}_{ni}$ were evaluated by calculating p_i and u_{ni} at 400 equally spaced points on the exit wall. Within the bullet cavity $p_i = -13.8$ psi and $u_{in} = 0$. The weighted potential is most easily obtained by integrating $\bar{p}_i = \rho\, \partial\bar{\phi}_i/\partial t$.

One shot from the experiments of Reference 7 was analyzed. The impact velocity of the round was 1,354 ft/sec. Inspection of the high-speed motion pictures of the bullet cavity showed that the bullet had just attained a fully tumbled attitude on exiting the test cell. No permanent deformation of the exit wall was observed, so the assumption of elastic strain in the analysis is justified.

The incident pressure, $\bar{p}_i$, and the quantity, $\rho\, c\, \bar{u}_{ni}$, are plotted in Figure 6 as a function of time. The bullet exits the test cell at 1.6 milliseconds. As a consequence of the diverging flow produced by the bullet, $\bar{p}_i \neq \rho\, c\, \bar{u}_{ni}$. Problems with piston theory are anticipated.

The exit wall deflection was then calculated by the variable image

method as expressed in equation 15. The results are plotted in Figure 7, together with the two sets of experimental points. The experimental error is estimated at ±0.25 cm. The variable image method clearly gives reasonable agreement with experiment. The rise time of the experimental wall deflection is much faster than expected from theory. This discrepancy is not yet understood.

The total pressure at the wall, p, and the source strength, k, are plotted as a function of time in Figure 8. The incident pressure, $\bar{p}_i$, is included for reference. During the first part of the panel deflection, the dominant characteristic of the plate motion is inertia. The mass of the plate is so low, however, that the plate acts very much like a free surface. This is clear from Figure 8 where $\bar{p} << p_i$. The source strength, k, responds to this situation by dropping very rapidly from its initial value of 1 to approximately -0.9. This is consistent with the previous observation that the variable image method is exact for free surfaces when k = -1.

As the wall approaches its maximum deflection, the bending and membrane stresses begin to dominate the wall motion. The inward acceleration of the wall is resisted by the fluid, producing a large net pressure at the wall. The image strength, k, responds to this by increasing gradually up to a value of 3 or 4. In a sense, the wall might be called "super rigid" at this point.

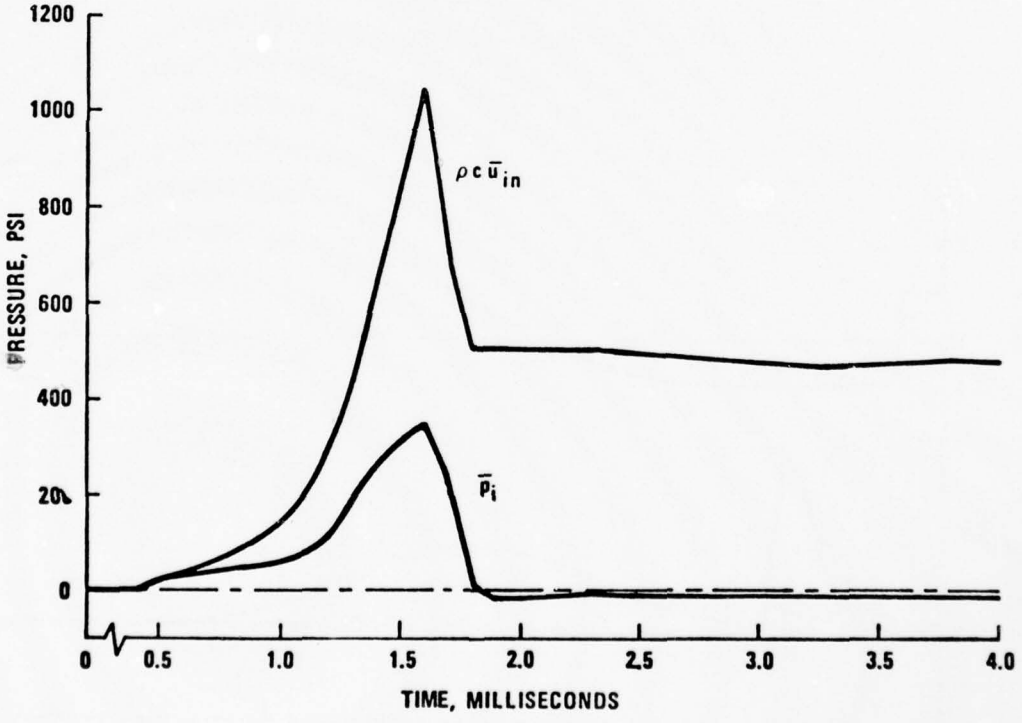

FIGURE 6. Weighted Average Incident Pressure and Normal Velocity.

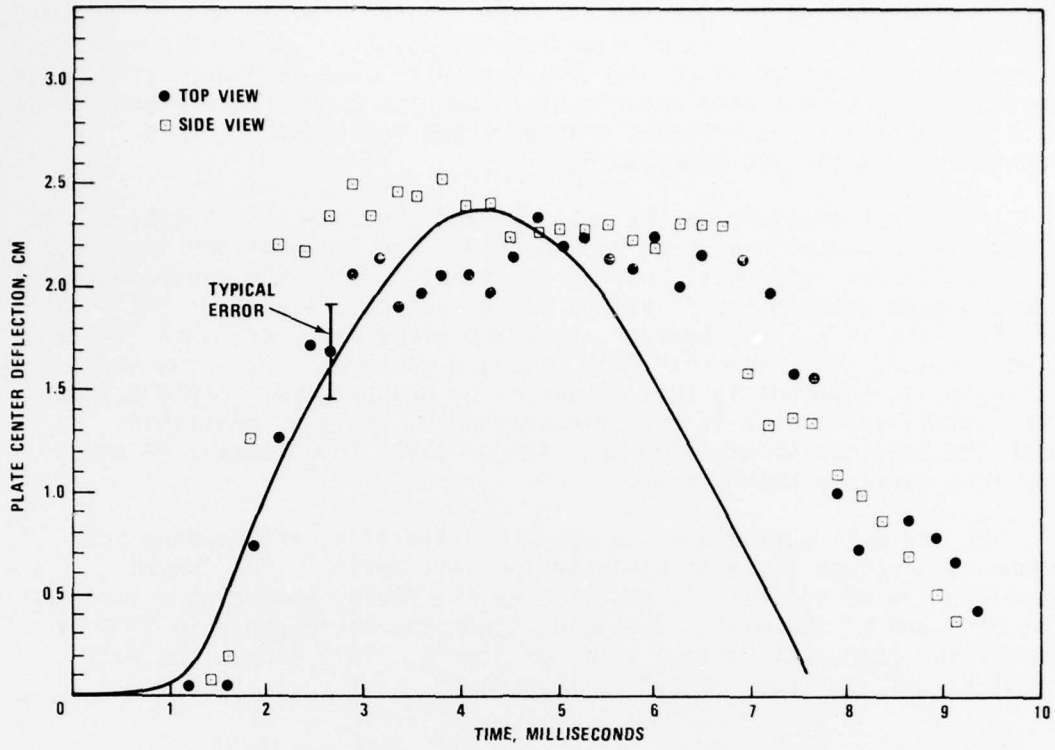

FIGURE 7. Results of Experiment Versus Theory.

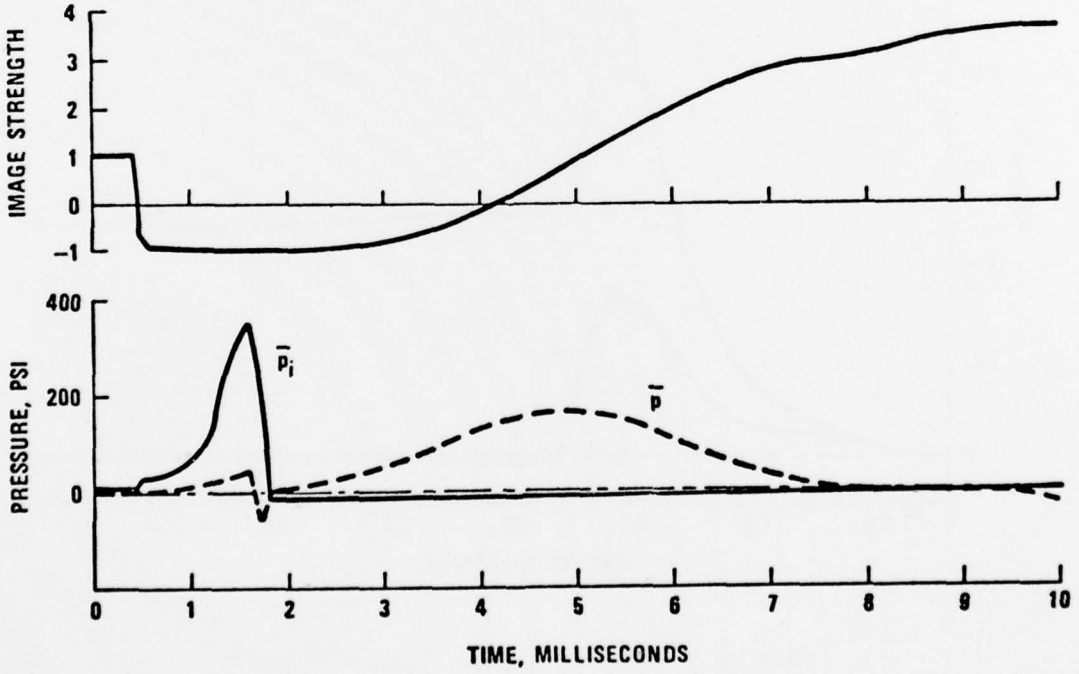

FIGURE 8. Image Strength and Pressure as a Function of Time.

The variable image method was applied here assuming a prescribed deflection profile of the exit wall and a uniform image strength, k. Equations 59 and 60 can also be applied when using more sophisticated techniques of structural analysis by allowing k to be nonuniform over the wall.

Appendix A

DERIVATIVES OF POTENTIAL

POTENTIAL

$$\phi = -\frac{B}{2} \int_{o}^{X_b(\tau)} \frac{1}{r} \left\{ A(\xi) - B\left[t - \frac{r}{c} - t_b(\xi) \right] \right\} d\xi$$

LEIBNITZ'S RULE

$$\frac{\partial \phi}{\partial t} = -\frac{BA_b}{2R_b} \left[\frac{\partial X_b(\tau)}{\partial t} \right] + \frac{B^2}{2} \int_{o}^{X_b(\tau)} \frac{d\xi}{r}$$

$$\frac{\partial \phi}{\partial \omega} = -\frac{BA_b}{2R_b} \left[\frac{\partial X_b(\tau)}{\partial \omega} \right] - \frac{B}{2} \int_{o}^{X_b(\tau)} \frac{\partial 1/r}{\partial \omega} \left\{ A(\xi) - B\left[t - t_b(\xi) \right] \right\} d\xi$$

$$\frac{\partial \phi}{\partial x} = -\frac{BA_b}{2R_b} \left[\frac{\partial X_b(\tau)}{\partial x} \right] - \frac{B}{2} \int_{o}^{X_b(\tau)} \frac{\partial 1/r}{\partial x} \left\{ A(\xi) - B\left[t - t_b(\xi) \right] \right\} d\xi$$

DERIVATIVES OF $X_b(\tau)$

$$\frac{\partial X_b(\tau)}{\partial t} = \frac{\partial X_b(\tau)}{\partial \tau} \frac{\partial \tau}{\partial t} = V \frac{\partial \tau}{\partial t}$$

Similarly,

$$\frac{\partial X_b(\tau)}{\partial \omega} = V \frac{\partial \tau}{\partial \omega}$$

$$\frac{\partial X_b(\tau)}{\partial x} = V \frac{\partial \tau}{\partial x}$$

Since $\tau = t - \frac{R_b}{c}$; $R_b = \sqrt{\omega^2 + (x - X_b)^2}$

$$\frac{\partial \tau}{\partial t} = 1 - \frac{1}{c} \frac{\partial R_b}{\partial t} = 1 + \frac{1}{c} \frac{x - X_b}{R_b} \frac{\partial X_b(\tau)}{\partial t}$$

$$\therefore \frac{\partial X_b(\tau)}{\partial t} = V\left[1 + \frac{1}{c}\frac{x - X_b}{R_b}\frac{\partial X_b(\tau)}{\partial t}\right]$$

$$\bigstar\ \therefore \frac{\partial X_b(\tau)}{\partial t} = \frac{V}{1 - \frac{V}{c}\frac{x - X_b}{R_b}}$$

$$\frac{\partial \tau}{\partial \omega} = -\frac{1}{c}\frac{\partial R_b}{\partial \omega} = -\frac{1}{cR_b}\left[\omega - (x - X_b)\frac{\partial X_b(\tau)}{\partial \omega}\right]$$

$$\therefore \frac{\partial X_b(\tau)}{\partial \omega} = -\frac{V}{cR_b}\left[\omega - (x - X_b)\frac{\partial X_b(\tau)}{\partial \omega}\right]$$

$$\bigstar\ \therefore \frac{\partial X_b(\tau)}{\partial \omega} = \frac{-\frac{V}{c}\frac{\omega}{R_b}}{1 - \frac{V}{c}\frac{x - X_b}{R_b}}$$

$$\frac{\partial \tau}{\partial x} = -\frac{1}{c}\frac{\partial R_b}{\partial x} = -\frac{1}{cR_b}(x - X_b)\left[1 - \frac{\partial X_b(\tau)}{\partial x}\right]$$

$$\therefore \frac{\partial X_b(\tau)}{\partial x} = -\frac{V}{c}\frac{x - X_b}{R_b}\left[1 - \frac{\partial X_b(\tau)}{\partial x}\right]$$

$$\bigstar\ \therefore \frac{\partial X_b(\tau)}{\partial x} = \frac{-\frac{V}{c}\frac{x - X_b}{R_b}}{1 - \frac{V}{c}\frac{x - X_b}{R_b}}$$

Integral in $\partial\phi/\partial t$ expression

$$I \equiv \int_0^{X_b} \frac{d\xi}{r} = \int_0^{X_b} \frac{d\xi}{\sqrt{\omega^2 + (x - \xi)^2}}$$

$$y \equiv x - \xi \qquad \xi = x - y \qquad d\xi = -dy$$

$$I = -\int_{x}^{x - X_b} \frac{dy}{\sqrt{\omega^2 + y^2}}$$

From tables

$$I = -\left[\ell n\left(y + \sqrt{\omega^2 + y^2}\right)\right]_{x}^{x - X_b}$$

$$= \ell n \frac{x + \sqrt{\omega^2 + x^2}}{x - X_b + \sqrt{\omega^2 + (x - X_b)^2}}$$

$$I = \ell n \frac{x + R_o}{x - X_b + R_b}$$

Derivatives within integrals of $\partial\phi/\partial x$, $\partial\phi/\partial\omega$ expressions

$$\frac{\partial 1/r}{\partial\omega} = -\frac{1}{r^2}\frac{\partial r}{\partial\omega} = -\frac{1}{r^2}\frac{\partial}{\partial\omega}\sqrt{\omega^2 + (x - \xi)^2} = -\frac{\omega}{r^3}$$

$$\frac{\partial 1/r}{\partial x} = -\frac{1}{r^2}\frac{\partial r}{\partial x} = -\frac{1}{r^2}\frac{\partial}{\partial x}\sqrt{\omega^2 + (x - \xi)^2} = -\frac{x - \xi}{r^3}$$

Combining terms

$$\frac{\partial\phi}{\partial t} = -\frac{BA_b}{2R_b}\frac{V}{1 - \frac{V}{c}\frac{x - X_b}{R_b}} + \frac{B^2}{2}\ell n\left(\frac{x + R_o}{x - X_b + R_b}\right)$$

$$\frac{\partial\phi}{\partial\omega} = +\frac{BA_b}{2R_b}\frac{\frac{V}{c}\frac{\omega}{R_b}}{1 - \frac{V}{c}\frac{x - X_b}{R_b}} + \frac{B\omega}{2}\int_{o}^{X_b(\tau)}\left[A(\xi) - B(t - t_b)\right]\frac{1}{r^3}\,d\xi$$

$$\frac{\partial\phi}{\partial x} = +\frac{BA_b}{2R_b}\frac{\frac{V}{c}\frac{x - X_b}{R_b}}{1 - \frac{V}{c}\frac{x - X_b}{R_b}} + \frac{B}{2}\int_{o}^{X_b(\tau)}\left\{A(\xi) - B\left[t - t_b(\xi)\right]\right\}\frac{x - \xi}{r^3}\,d\xi$$

PROGRAMMING NOTE

The remaining integrals are difficult to evaluate numerically. For example, for x term define

$$I_x \equiv \int_o^{X_b(\tau)} \left\{A(\xi) - B\left[t - t_b(\xi)\right]\right\} \frac{x - \xi}{r^3}\, d\xi$$

Find an expression for $\partial I/\partial t$ and calculate I as a function of time by integrating $\partial I/\partial t$.

Leibnitz's Rule

$$\frac{\partial I_x}{\partial t} = \left(A_b - B\,\frac{R_b}{c}\right)\frac{x - X_b}{R_b^3}\left[\frac{\partial X_b(\tau)}{\partial t}\right] - B\int_o^{X_b(\tau)} \frac{x - \xi}{r^3}\, d\xi$$

but

$$\int_o^{X_b(\tau)} \frac{x - \xi}{r^3}\, d\xi = -\int_x^{x - X_b} \frac{y}{(\omega^2 + y^2)^{3/2}}\, dy = \left(\frac{1}{\sqrt{\omega^2 + y^2}}\right)_x^{x - X_b}$$

$$= \left(\frac{1}{R_b} - \frac{1}{R_o}\right)$$

and

$$\frac{\partial X_b(\tau)}{\partial t} = \frac{V}{1 - \frac{V}{c}\,\frac{x - X_b}{R_b}}$$

$$\therefore \frac{\partial I_x}{\partial t} = \left(A_b - B\,\frac{R_b}{c}\right)\frac{x - X_b}{R_b^3}\,\frac{V}{1 - \frac{V}{c}\,\frac{x - X_b}{R_b}} + B\left(\frac{1}{R_o} - \frac{1}{R_b}\right)$$

Similarly, for the ω term

$$I_\omega \equiv \omega \int_o^{X_b(\tau)} \left[A - B(t - t_b)\right]\frac{1}{r^3}\, d\xi$$

Leibnitz's Rule

$$\frac{\partial I_\omega}{\partial t} = \left(A_b - B\frac{R_b}{c}\right)\frac{\omega}{{R_b}^3}\left[\frac{\partial X_b(\tau)}{\partial t}\right] - B\omega\int_o^{X_b(\tau)}\frac{1}{r^3}\,d\xi$$

but

$$\int_o^{X_b(\tau)}\frac{d\xi}{r^3} = -\int_x^{x - X_b}\frac{dy}{(\omega^2 + y^2)^{3/2}} = -\frac{1}{\omega^2}\left(\frac{y}{\sqrt{\omega^2 + y^2}}\right)_x^{x - X_b}$$

$$= \frac{1}{\omega^2}\left(\frac{x}{R_o} - \frac{x - X_b}{R_b}\right)$$

$$\frac{\partial X_b(\tau)}{\partial t} = \frac{V}{1 - \frac{V}{c}\frac{x - X_b}{R_b}}$$

$$\star\ \therefore \frac{\partial I_\omega}{\partial t} = \left(A_b - B\frac{R_b}{c}\right)\frac{\omega}{{R_b}^3}\,\frac{V}{1 - \frac{V}{c}\frac{x - X_b}{R_b}} - \frac{B}{\omega}\left(\frac{x}{R_o}\,\frac{x - X_b}{R_b}\right)$$

Appendix B

RECOMMENDED BULLET CONSTANTS

Constants	.30 caliber	.50 caliber	12.7 mm	14.5 mm
Bullet weight	165.7 grains	622-649 grains	746 grains	963 grains
Bullet dimensions	Diameter: 0.308 in. Length: 1.39 in.	Diameter: 0.510 → 0.511 in. Length: 2.31 in.	Diameter: 0.510 → 0.511 in. Length: 2.5 in.	Diameter: 0.586 → 0.587 in. Length: 2.6 in.
Penetrator weight	80 → 81.2 grains	375 grains	448/449 grains	655 grains
Penetrator dimensions	Diameter: 0.244 → 0.245 in. Length: 1.08 in.	Diameter: 0.426 → 0.427 in. Length: 1.8 in.	Diameter: 0.427 in. Length: 2.07 in.	Diameter: 0.4889 in. Length: 2.075 in.
Jacket weight	84.5 → 85.7 grains	247 → 274 grains includes incendiary	297 → 298 grains includes incendiary	293.21 grains excludes incendiary
Jacket dimensions	Same as bullet dimensions	Same as bullet dimensions	Same as bullet dimensions	Same as bullet dimensions
Bullet/jacket projected area, untumbled	0.0745 in^2	0.2042 → 0.2050 in.	0.2042 → 0.2050 in.	0.2697 → 0.2906 in.
Bullet/jacket projected area, untumbled	0.31732 in^2	0.73625 in^2	1.03772 in^2	1.322 in^2
Penetrator projected area, untumbled	0.0468 → 0.0471 in^2	0.1425 → 0.1432 in^2	0.1432 in^2	0.18773 in^2
Penetrator projected area, tumbled	0.2601 in^2	0.59830 in^2	0.700214 in^2	1.05 in^2
Bullet projected area, stern-first	0.0314 in^2	0.1121 in^2	0.0855 in^2	0.12566 in^2
C_D of bullet, normal attitude	0.10	0.05	0.05	0.10
C_D of bullet, tumbled attitude	0.60	0.30	0.30	0.30
C_D of penetrator, normal attitude	0.10	0.05	0.05	0.10
C_D of penetrator, tumbled attitude	0.60	0.30	0.30	0.30
C_D of jacket, tumbled attitude	1.0	1.0	1.0	1.0
C_D of bullet, stern-first attitude	0.82	0.82	0.82	0.82

Appendix C

TUMBLING BEHAVIOR OF 12.7 AND 14.5 MM API FROM FOOTNOTE 2

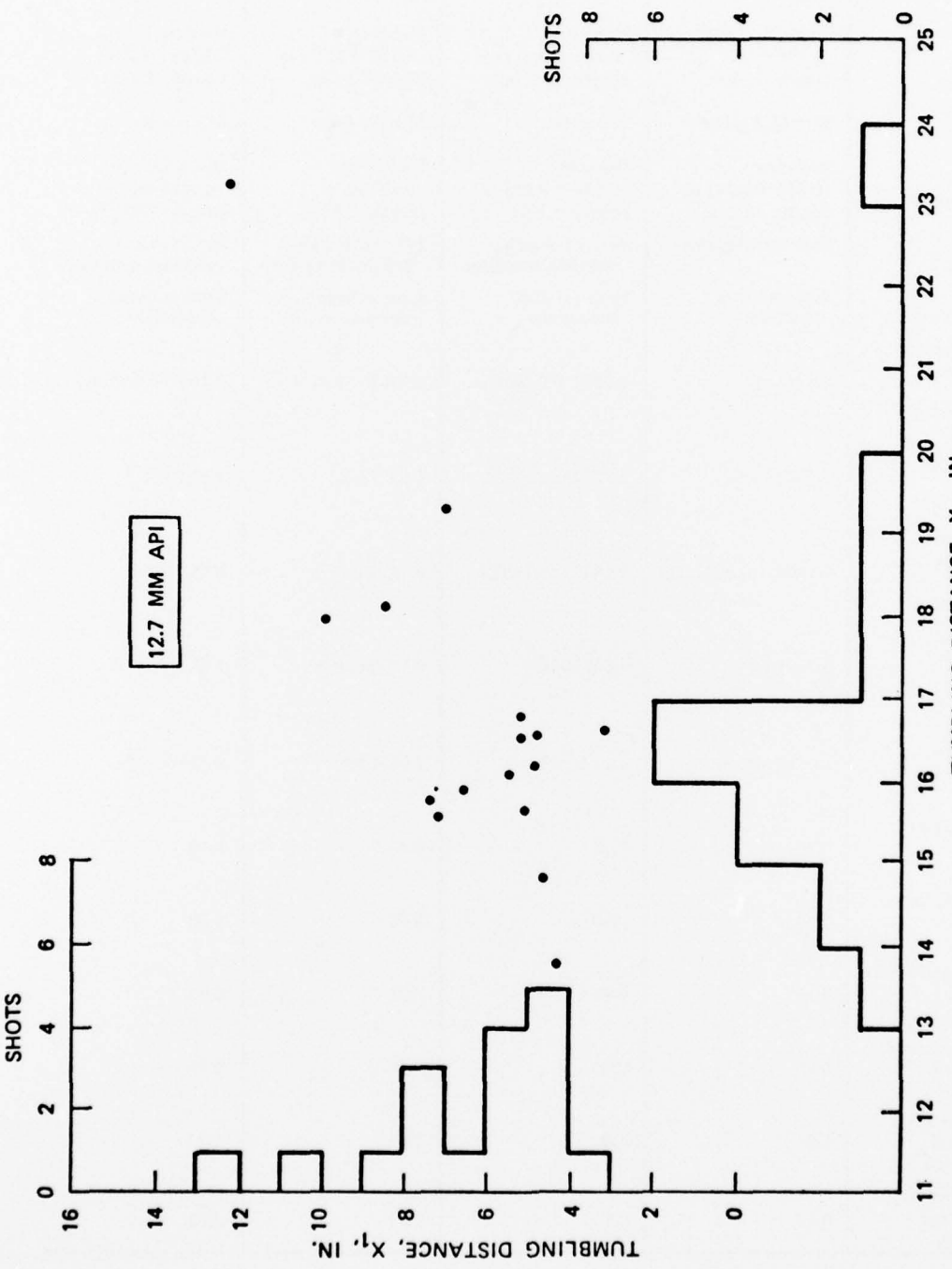

FIGURE 9. Tumbling Distance Distribution; 0 Degree Obliquity, 0 Degree Yaw.

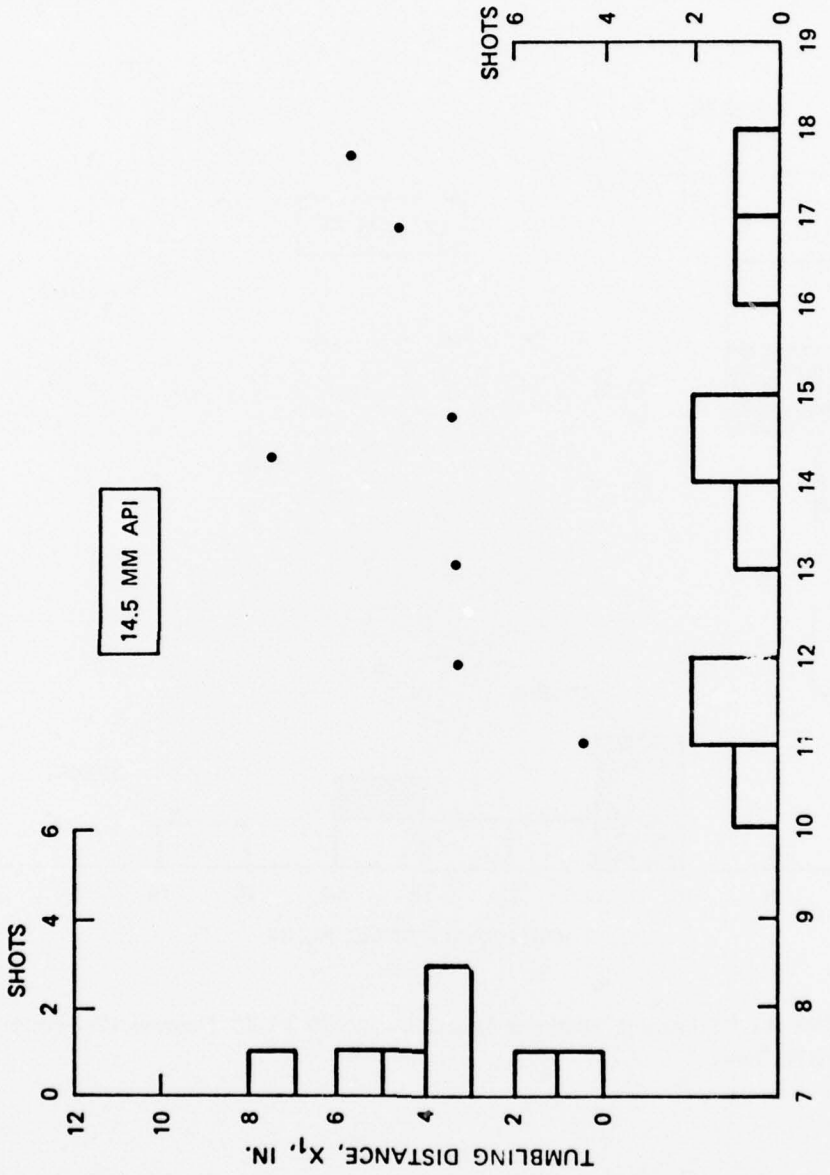

FIGURE 10. Tumbling Distance Distribution; 0 Degree Obliquity, 0 Degree Yaw.

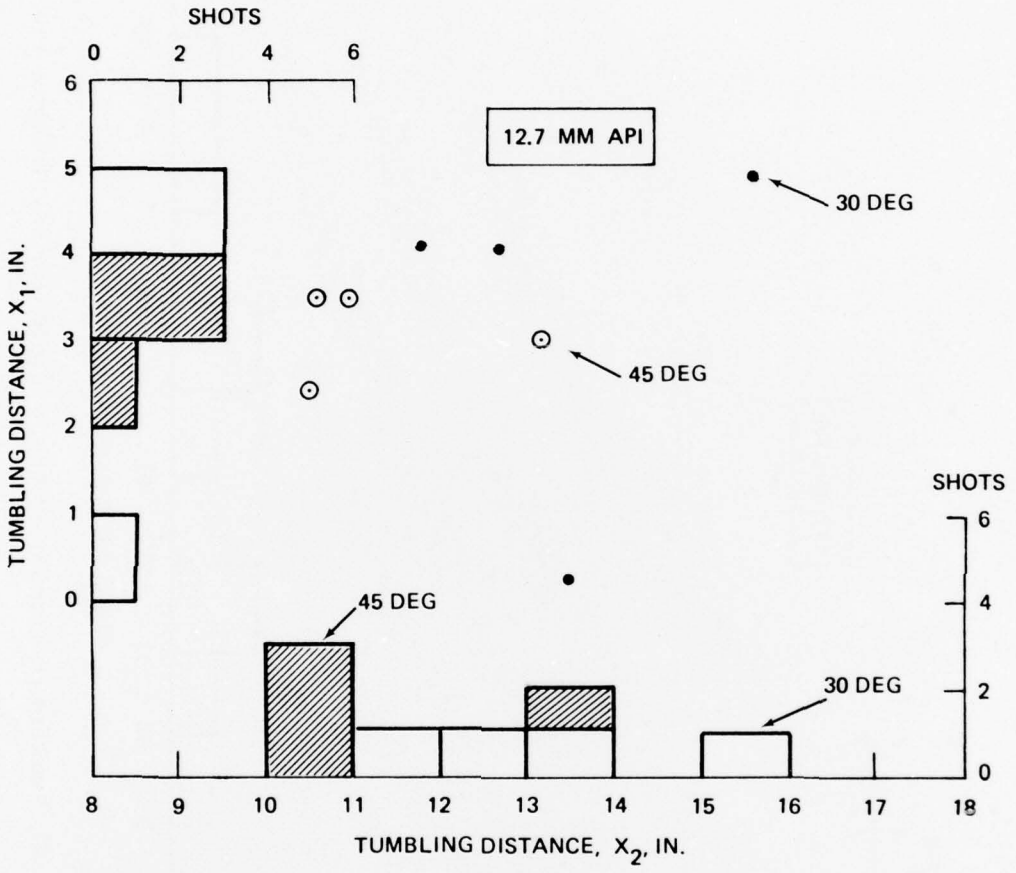

FIGURE 11. Tumbling Distance Distribution; 30 to 45 Degrees Obliquity, 0 Degree Yaw.

REPORT DOCUMENTATION PAGE

1. Recipient's Reference	2. Originator's Reference	3. Further Reference	4. Security Classification of Document
	AGARD-AR-106	ISBN 92-835-1249-9	UNCLASSIFIED

5. Originator Advisory Group for Aerospace Research and Development
North Atlantic Treaty Organization
7 rue Ancelle, 92200 Neuilly sur Seine, France

6. Title PHYSICAL VULNERABILITY OF AIRCRAFT DUE TO FLUID DYNAMIC EFFECTS

7. Presented at

8. Author(s) D.B.Ankeney

9. Date July 1977

10. Author's Address Naval Weapons Center
China Lake, California 93555, USA

11. Pages 82

12. Distribution Statement This document is distributed in accordance with AGARD policies and regulations, which are outlined on the Outside Back Covers of all AGARD publications.

13. Keywords/Descriptors

Explosion effects	Predictions	Hydraulic pressure pumps
Vulnerability	Loads (forces)	Fluid dynamics
Aircraft	Dynamic structural analysis	

14. Abstract

The material in this Report is intended to supplement and provide a more detailed fluid dynamic input to AGARD Advisory Report No. 47, *The Physical Vulnerability of Aircraft*, (3 volumes, September 1972, May 1973 and May 1973, NATO Classified). Readers with a general interest in the subject of aircraft physical vulnerability are referred to AR-47.

The present report consists of two Papers: (1) Techniques for Predicting Structural Response due to Explosive Air Blast; and (2) Hydraulic Ram Pressure Prediction and Structural Response.

This Advisory Report has been prepared at the request of the Fluid Dynamics Panel of AGARD.

AGARD Advisory Report No.106
Advisory Group for Aerospace Research and Development, NATO
PHYSICAL VULNERABILITY OF AIRCRAFT DUE TO FLUID DYNAMIC EFFECTS
D.B.Ankeney
Published July 1977
82 pages

The material in this Report is intended to supplement and provide a more detailed fluid dynamic input to AGARD Advisory Report No.47, *The Physical Vulnerability of Aircraft*, (3 volumes, September 1972, May 1973 and May 1973, NATO Classified). Readers with a general interest in the subject of aircraft physical vulnerability are referred to AR-47.

P.T.O.

AGARD-AR-106

Explosion effects
Vulnerability
Aircraft
Predictions
Loads (forces)
Dynamic structural analysis
Hydraulic pressure pumps
Fluid dynamics

The present report consists of two Papers: (1) Techniques for Predicting Structural Response due to Explosive Air Blast; and (2) Hydraulic Ram Pressure Prediction and Structural Response.

This Advisory Report has been prepared at the request of the Fluid Dynamics Panel of AGARD.

ISBN 92-835-1249-9

The present report consists of two Papers: (1) Techniques for Predicting Structural Response due to Explosive Air Blast; and (2) Hydraulic Ram Pressure Prediction and Structural Response.

This Advisory Report has been prepared at the request of the Fluid Dynamics Panel of AGARD.

ISBN 92-835-1249-9

The present report consists of two Papers: (1) Techniques for Predicting Structural Response due to Explosive Air Blast; and (2) Hydraulic Ram Pressure Prediction and Structural Response.

This Advisory Report has been prepared at the request of the Fluid Dynamics Panel of AGARD.

ISBN 92-835-1249-9

The present report consists of two Papers: (1) Techniques for Predicting Structural Response due to Explosive Air Blast; and (2) Hydraulic Ram Pressure Prediction and Structural Response.

This Advisory Report has been prepared at the request of the Fluid Dynamics Panel of AGARD.

ISBN 92-835-1249-9